REPORT DOCUMENTATION PAGE

AFRL-SR-BL-TR-99-

0238

1. AGENCY USE ONLY (Leave blank)	2. REPORT DATE	3. REPORT TYPE AND DATES COVERED
	Sept. 20, 1999	Final Technical Report 7/1/96—6/30/99

4. TITLE AND SUBTITLE
Development of a Micromechanic Theory of Crack Initiation Under High-Cycle Fatigue

5. FUNDING NUMBERS
Grant No. F4962-~~96-I-350~~ 96-I-0350

6. AUTHOR(S)
T. H. Lin

7. PERFORMING ORGANIZATION NAME(S) AND ADDRESS(ES)
University of California, Las Angeles
405 Hilgard Avenue
Los Angeles, CA. 90095-1593

8. PERFORMING ORGANIZATION REPORT NUMBER

9. SPONSORING/MONITORING AGENCY NAME(S) AND ADDRESS(ES)
AFOSR/PK4
110 Duncan Avenue Room B115
Bolling AFB DC20332-8050

10. SPONSORING/MONITORING AGENCY REPORT NUMBER

11. SUPPLEMENTARY NOTES

12a. DISTRIBUTION/AVAILABILITY STATEMENT
DISTRIBUTION STATEMENT A
Approved for Public Release
~~Distribution Unlimited~~

12b. DISTRIBUTION CODE

19991006 139

13. ABSTRACT (Maximum 200 words)

From the hint provided by extrusion and intrusion in fatigue specimen, a micromechanic model consisting of a thin slice R sandwiched in two thin slices P and Q is developed. P with positive initial shear stress slides forward in the forward loading, while the other Q with negative initial shear stress slides backward during the reversed loading.

Micromechanic analysis shows that the positive slip in P relieves the positive shear stress not only in P, but also in Q. This helps Q to slide in the reversed loading. Similarly the negative slip in Q helps P to slide during the next forward loading. The micro stress fields generated by the alternate sliding in P and Q gives the ratchet mechanism in fatigue.

Extrusion causes a tensile stress in R. This stress combining with other stress can activate a second slip systems of an aluminum single crystal. The macroscopic deformation & hysteresis loop are thus computed. The computed microstructures check amazingly well with the experimental fatigue data of aluminum single crystals by Zhai et al of Oxford University.

14. SUBJECT TERMS			15. NUMBER OF PAGES
			16. PRICE CODE
17. SECURITY CLASSIFICATION OF REPORT	18. SECURITY CLASSIFICATION OF THIS PAGE	19. SECURITY CLASSIFICATION OF ABSTRACT	20. LIMITATION OF ABSTRACT
UNCLASSIFIED	UNCLASSIFIED	UNCLASSIFIED	

TABLE OF CONTENTS

Development of a Micromechanic Theory of Crack Initiation Under High-Cycle Fatigue

I. Introduction

More than 90% of catastrophic failures of airplane structures and engine parts occurring in practice are caused by fatigue of materials. Fatigue deformation proceeds in two stages: fatigue crack initiation and crack propagation. Crack propagation dominates the life of low cycle fatigue and crack initiation occupies about 80% of the life in high-cycle fatigue (HCF). Both low cycle and high cycle fatigue loadings commonly occur in practice. Initiation always proceeds propagation. Crack initiation has been studied by a number of distinguished scientists without complete success. Both crack initiation & propagation are important for the reduction of fatigue failures. Present study gives a development of a physics model of fatigue crack initiation and is of both scientific and practical importance.

Single crystal tests (Taylor, 1938) have shown that under stress, slip occurs along certain crystal directions on certain crystal planes. This shear stress along the crystal direction on this crystal plane is called the resolved shear stress. Slip depends on this resolved shear stress and is independent of the normal stress on the sliding plane. This shear stress to initiate or cause the continuation of slip is called the critical shear stress. This dependency of slip on this resolved shear stress is known as the Schmid's law and has been shown to hold also for cyclic loading (Parker, 1961).

Since 1950's, many metallurgical researches on fatigue were undertaken. A formidable amount of experimental information is available. As indicated by Kennedy (1963), the difficulty seems to see these multitudinous facts as a related and connected whole, largely because of the lack of a sound general theory and also because of the very great complexity of metallurgical effects. With the development of dislocation theory since about 1940, new explanations of the fatigue theory have been proposed. Dislocation explains the characteristics of metals at the atomic level, which of course is very important. However, dislocations may be too fine to correlate even the macroscopic phenomena observed under optical microscope, such as

fatigue bands. Plastic strain represents a large number of dislocations (Mura, 1982). Hence plastic strain is here used to explain the macroscopic phenomena.

Forsyth & Stubbington (1954) made an important discovery of extrusions in slip bands during fatigue tests of some aluminum alloys. Since then, a number of distinguished investigators (Thompson et al (1955), Hull (1958) Mughrabi (1990), Mecke & Blockwitz (1980) etc) also reported detection of extrusion & intrusion in different metals. Following the clue provided by the observations of extrusions & intrusions in slip bands, a number of theories of fatigue crack initiation have been proposed (Mott (1958), Cuttrell & Hull (1957), Wood 1956, etc). For a dislocation to glide, first it has to glide in a crystal slip system and second the slip system must subject to a resolved shear stress equal or greater than the critical shear stress. The above mentioned and most of other theories mainly show the possible paths of dislocation movement to satisfy the first condition, but this resolved shear stress field caused by the dislocation movement was not adequately considered. In the micromechanic theory proposed by the writer and his associates, the effect of this stress field, which provides a natural gating mechanism is quantitatively shown.

II-1. A Micromechanic Model of Shear Bands and Fatigue Bands

When a piece of metal is uniformly loaded, slip lines appear on the surface. These slip lines are the results of highly localized plastic deformation. This raises the question of why under a uniform loading, the plastic strain is so heterogeneous. To explain the heterogeneous plastic deformation, the micromechanic shear stress field due to a uniform $e_{12}^{"}$ in a thin slice, Fig.1a in a infinite isotropic medium is analyzed (Lin, 1992). Imagine that we cut the slice out and apply a uniform shear stress -2G$e_{12}^{"}$, where G is the shear modulus, to restore the slice back to its original shape and size before the occurrence of the plastic strain as shown in Fig. 1c and then welded back to the medium. Since there is no such applied stress, it is relaxed by applying an equal and opposite force of $2Ge_{12}"$ per unit area of the boundary. Denoting the stress field caused by this boundary force by τ_{ij}^{s}, the residual shear stress field τ_{ij}^{r} due to this plastic strain is

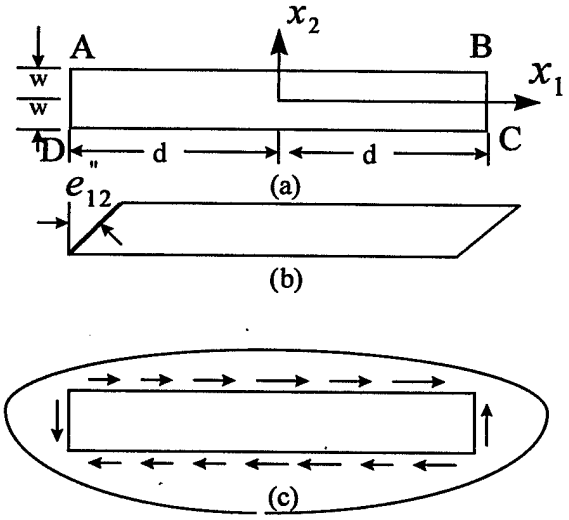

Figure 1 Shear Band model

$$\tau_{ij}^{r} = \tau_{ij}^{s} - 2Ge_{12}^{"} \tag{1}$$

and has been found to be, writing $e_{12}^{"}$ as $e^{"}$,

$$\tau^{r} = \frac{2\mu e^{"} w}{\pi(1-\nu)}\left\{\frac{(x_1-d)[(x_1-d)^2-x_2^2]}{(x_1-d)^2+x_2^2} - \frac{(x_1+d)[(x_1+d)^2-x_2^2]}{(x_1+d)^2+x_2^2}\right\} \tag{2}$$

This model was ingeniously given by Eshelby (1951) in his paper on the determination of the elastic field of an ellipsoidal inclusion. The resolved shear stress due to an edge dislocation along x_3-axis with its Burger's vector along x_1-direction is given by Hirth & Lothe(1968) as

$$\tau = \frac{\mu b}{2\pi(1-\nu)} \frac{x_1(x_1^2 - x_2^2)}{x_1^2 + x_2^2} \tag{3}$$

Substituting $2we^{"}$ in Eq.2 by the magnitude of the Burger's vector b, it is seen that the resolved shear stress caused by this displacement of the edge dislocation of the Burger's vector from (-d,0) to (d,0) is exactly the same as given by Eq.3. Hence the plastic strain in this slice can be provided by the displacement of dislocations. The equivalence of plastic strain and dislocation distribution has been shown by Mura (1981) and others. Hence a plastic strain distribution in a solid can also be represented by a distribution of dislocations.

Along x_1-axis, Eq.2 gives $\tau^r = \frac{4\mu e^{"} w}{\pi(1-\nu)(x_1+d))(x_1-d)}$. When $x_1 > d$ or $x < -d$, τ^r is positive. This increases the resolved shear stress and causes the length of the sliding rectangle to increases.

Along x_2-axis, the shear stress τ^r, relieved by $e^{"}$ reduces to

$$\tau^r = \frac{4Ge^{"}w}{\pi(1-\nu)d} \left\{ \frac{\left(\frac{x_2}{d}\right)^2 - 1}{\left[\left(\frac{x_2}{d}\right)^2 + 1\right]^2} \right\} \tag{4}$$

The relief of stress τ^r is proportional to $e^{"}(\frac{w}{d})$. To relieve a finite value of shear stress τ^r, $e^{"}$ has to be large since $(\frac{w}{d})$ is very small. This explains the formation of the localized plastic strain to give a shear band under a monotonic loading. This equation also gives a negligible variation of this relief of shear stress across the thickness. This provides a natural gating

mechanism as shown later. The above plastic deformation behavior applies to polycrystals as well as single crystals

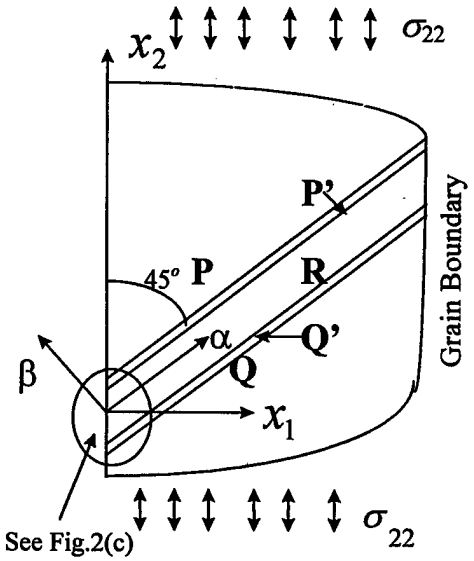

(a) Most Favorable Oriented Crystal

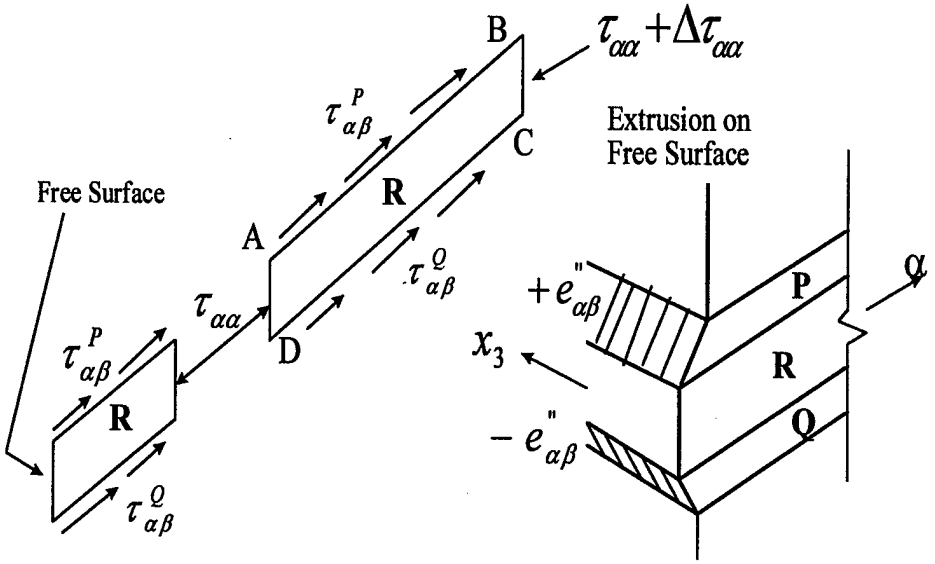

Fig.2 Fatigue Band Model of an Extrusion

Forsyth and Stubbington (1955) discovered that thin ribbons protruding out of the surface of fatigue specimens. These protruding ribbons are known as extrusions. Negative extrusion, called intrusion was also observed. Based on these observations, a physical model of fatigue crack initiation was proposed. This model for a polycrystal (Lin, 1992) is shown in Fig.2. The formation of an extrusion requires a positive shear strain $e''_{\alpha\beta}$ in P on the top and a negative shear strain in Q on the bottom of the extrusion R, Fig.2c. This can be caused by a positive initial resolved shear stress τ^i in P and a negative initial stress in Q. This system of initial resolved shear stress in a segment can be caused by a variation of compressive stress in R, as shown in Fig.2(b).

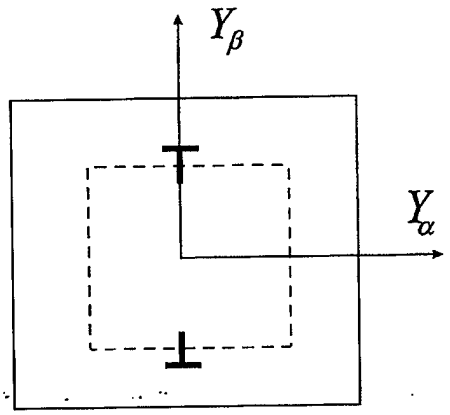

Fig.3 A Dislocation Interstitial Dipole

If we cut a slit through a perfect crystal and force a sheet of metal of one atom thick into the slit, a pair of parallel edge dislocations of opposite signs, forming an interstitial dipole, is produced as shown in Fig.3, where Y_α denotes the gliding direction and Y_β denotes the normal to the slip plane. If we cut a rectangular block along the dotted line, the free length of this block will be one atomic spacing more than the corresponding length of the hole. If there are n such dipoles in a length of N atomic spacing, this will give an initial strain $e^i_{\alpha\alpha}$ of n/N. Hence, this initial strain can be caused by an array of dislocation dipoles. This array of dipoles was suggested by Lin and Ito (1969) as a possible way of providing the initial strain to cause the

favorable initial stress field. Recently, Mughrabi et al.(1979) have shown that the ladder structure in a persistent slip band (Fig.4) can be represented by such an array of dislocation dipoles.

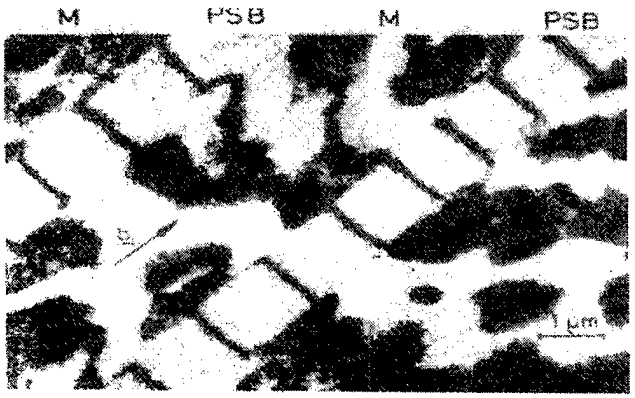

Fig.4 Dislocation arrangement in fatigued copper single Crystal (121)-section showing matrix(M) and persistent slip bands (PSB). Reproduced from ASTM STP675, 1975 .

Hence, this system of initial shear stress can be caused by an array of dislocation dipoles (Lin, 1992).

II-2. Gating Mechanism Provided by Stress Field

With an initial tensile strain in R (Figure 2), the initial shear stress τ_P^i in P, is positive and that in Q, τ_Q^i, is negative. The shear stress due to the applied load σ_{22} is the same in the whole crystal, thus $\tau_P^a = \tau_Q^a = \tau^a$. Consider the following sequence of loadings :

1. First Cyclic Forward Loading $(\tau^a > 0)$: P slides. The residual shear stress in P during the first forward loading $\tau_{1f}^r < 0$. Therefore,

$$\tau_P = \tau_p^i + \tau^a + \tau_{1fP}^r = \tau^c \qquad (5a)$$

$$\tau_Q = \tau_Q^i + \tau^a + \tau_{1fQ}^r > -\tau^c \qquad (5b)$$

2. First Cyclic Reverse Loading $(\tau^a < 0)$: Q slides, $\tau_{1rQ}^r > 0$. Therefore,

$$\tau_P = \tau_p^i + \tau^a + \tau_{1fP}^r + \tau_{1rP}^r < \tau^c \tag{6a}$$

$$\tau_Q = \tau_Q^i + \tau^a + \tau_{1fQ}^r + \tau_{1rQ}^r = -\tau^c \tag{6b}$$

3. Second Cyclic Forward Loading $(\tau^a > 0)$: P slides, $\tau_{2fP}^r < 0$. Therefore,

$$\tau_P = \tau_p^i + \tau^a + \tau_{1fP}^r + \tau_{1rP}^r + \tau_{2fP}^r = \tau^c \tag{7a}$$

$$\tau_Q = \tau_Q^i + \tau^a + \tau_{1fQ}^r + \tau_{1rQ}^r + \tau_{2fQ}^r > -\tau^c \tag{7b}$$

4. Second Cyclic Reverse Loading $(\tau^a < 0)$: Q slides, $\tau_{1rQ}^r > 0$. Therefore,

$$\tau_P = \tau_p^i + \tau^a + \tau_{1fP}^r + \tau_{1rQ}^r + \tau_{2fP}^r + \tau_{2rQ}^r < \tau^c \tag{8a}$$

$$\tau_Q = \tau_Q^i + \tau^a + \tau_{1fP}^r + \tau_{1rQ}^r + \tau_{2fP}^r + \tau_{2rQ}^r = -\tau^c \tag{8b}$$

This process is repeated. In the above τ^c is constant. This represents zero strain hardening. For the cases with strain hardening or softenning, τ^c increases or decreases with plastic strain.

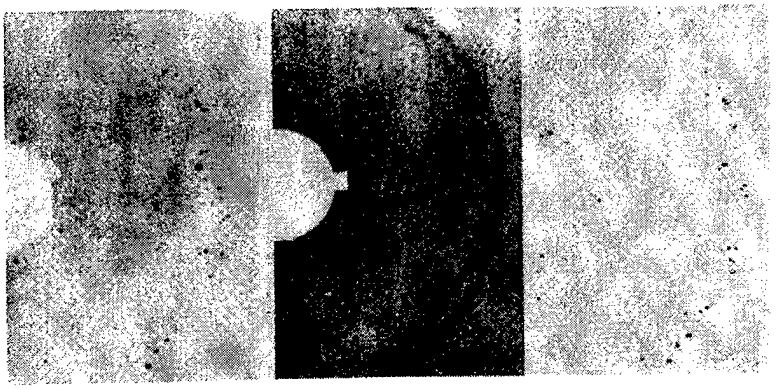

Fig.5. (a) Sharp X-ray reflection from annealed α -brass. (b) From same specimen as (a) after a unidirectional strain 150x0.5° twist. (c) From same specimen as (a) after 1500 reversals of plastic strain 0.5° twist and showing same reflections as (a). Reproduced from the book "Fracture," 1959, courtesy of Technological Press, MIT.

The residual shear stress occurred during forward loading is negative and occurred in the

negative loading is positive. Considering the incremental plastic strain $\Delta e^{"}$ in P, $x_2 = 0$ in P and $x_2 = t$ in Q, where t is the thickness of R. Eq.4 gives a residual stress in P to be more than that in Q by a very small amount. In the reversed loading, negative slip occurs in Q. This gives a residual stress τ^r in Q to be numerically a very small amount more than τ^r in P. The build-up of the slip strain $e^i_{\alpha\beta}$ in P and Q is caused by $e^i_{\alpha\alpha}$ in R. If R were cut out, the free length of R would be longer than the slot by an amount referred to as the static extrusion by Mughrabi et al. (1983). This $e^i_{\alpha\alpha}$ causes an initial compression $\tau^i_{\alpha\alpha}$ in R. Under cyclic loading, the extrusion grows and the thin slice R increases in length. This elongation causes the compression to decrease. The change of the direct stress $\tau_{\alpha\alpha}$ in R causes changes of resolved shear stress in all slip systems in a f.c.c.-crystal. When the decrease of compression in R becomes large after millions of cycle, its

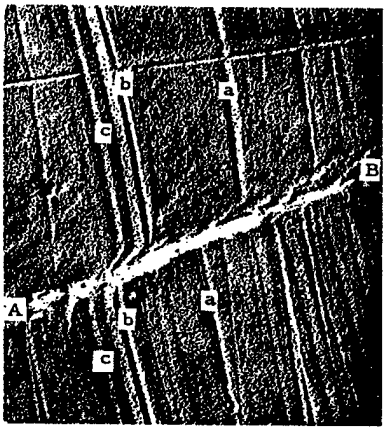

Fig.6(a) Initially straight scratches a, b, c are displaced unidirectionally by Static slip band AB. Reproduced from Trans. Metal Soc. AIME,1992, courtesy of AIME.

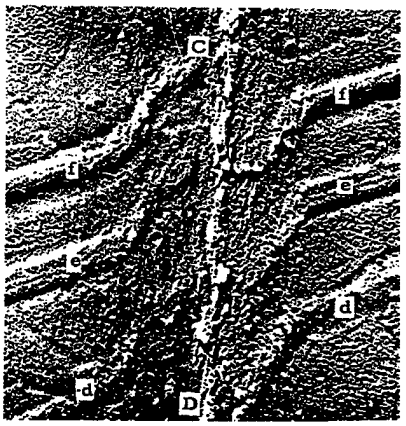

Fig.6(b) Cyclic slip band CD produces no overall displacement of scratches d, e, f within the slip band; the scratches are displaced equally backward and forward. The same as Fig.6(a), courtesy of AIME.

resulting residual stresses combined with the applied stress can cause a second slip system to have shear stress reaching the critical and slides. Let this second system be denoted by $\xi\eta$. The plastic strain $e^{"}_{\xi\eta}$ caused by this slip has a tensor component $e^{"}_{\alpha\alpha}$, just like $e^i_{\alpha\alpha}$ in causing the

positive and negative $\tau^{i}_{\alpha\beta}$ in P and Q, respectively. Hence, with secondary slip the extrusion can grow considerably beyond the static extrusion as shown in Fig.23 in (Lin, 1992).

Now R is subject to a static axial loading due to $\tau_{\alpha\alpha}$ superposed on a cyclic axial stress due to $\pm\sigma_{22}$. It has been found that this region of the secondary slip grows with cycles of loading.

II-3. Experimental Verifications

The preceding theory has extensive experimental evidences. Some of these are briefly shown in the following. Tests on single aluminum crystals under cyclic loading in tension and compression by Buckley & Entwistle (1956) and Charsley & Thompson (1965) on an aluminum crystal show that slip lines formed during compression lie between those formed in the prior tensile loading. Many other tests also show the occurrence of slip lines in the reversed loading to be very close, but distinct from those formed in forward loading like P and Q in the proposed model. Wood (1956) has shown the X-ray reflection patterns of monotonically and cyclically loaded specimens to be quite different as shown in Fig.5. The latter retain the discrete spots like that of an annealed metal while the former do not. This shows that at some distance from the fatigue band, the stress field caused by the positive slip in P is balanced by that of the negative slip in Q. Under the monotonic loading, the slips in all slip lines are of the same sign and causes a significant lattice strain in the bulk of the metal. This is explained by the proposed model. Wood & Bender tested copper crystal rod under torsion. Some specimens were subject to single torsion and some are subject to cyclic torsion. They found that under a monotonic loading, scratches are discontinuous across this shear band, while under a cyclic loading, scratches have no relative displacement across this fatigue band except in the small region near the band, Fig.6. These observations clearly verify the proposed model. The detail of these tests are given in the reference (Lin, 1992).

This model shows that P slides only in forward loading and Q only slides in reversed loadings. The macroscopic positive shear strain $e^{''}_{\alpha\beta}$ in the specimen caused by P sliding is balanced by the negative shear strain in Q. This gives a macroscopic reversed strain as observed.

The highly local positive shear strain $e''_{\alpha\beta}$ in P and negative shear strain in Q causes the formation of fatigue band. This shear strain at the free surface causes the monotonic growth of extrusion. If the interstitial dipoles were replaced by vacancy ones, intrusion instead of extrusions would occur. The mechanism of shear band and fatigue band developed for polycrystals under HCF is presently applied to single crystals.

III. Micromechanic Analysis of Fatigue Band of Single Crystal

Mecke and Blockwitz (1980) observed the subgrain displacement in a single nickel crystal under cyclic loading. Their experiments were carried out under constant plastic strain amplitude at room temperature. It is seen that the PSBs have penetrated across the whole crystal and extruded out on both sides as shown in Fig.7.

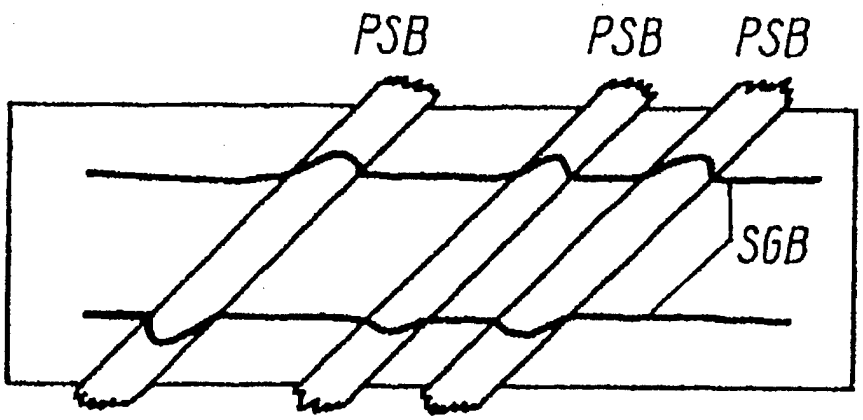

Fig.7 Extrusions observed in single crystal. (Meke and Blochwitz, 1980)

As shown previously, the length of a rectangular slice with a uniform plastic shear strain tends to increase. This increases the lengths of both P and Q. Hence this present model of P, Q and R can give the fatigue band to extend the extrusion out of the two surfaces of the single crystal. Copper single crystal test data are much more abundant than those of aluminum (Ma & Laird, 1989; Basinski & Basinski, 1992; Mughrabi et al., 1983). The anisotropy of elastic constants of aluminum is much less than that of copper. The micromechanic analysis of fatigue

band in a crystal with anisotropic constant is much more complex than that with isotropic one (Teng and Lin, 1995). In our present analysis, the crystal is taken to be elastically isotropic. As the loading cycles increases, the number of fatigue bands increases. These bands interact with each other. This interaction needs to be considered. Hence in the present study, the micromechanic analysis of an aluminum single crystal with multiple fatigue bands is performed. The microstress-strain fields vary along three axes. The elasto-plastic 3-dimensional analysis is very complicated. And Boundary Element Method is chosen for the computation.

III-1. Method of Numerical Analysis

Elasto-plastic Boundary Element Method is applied to the elasto-plastic 3-dimensional solid of heterogeneous isotropic elastic constants. Consider a body under equilibrium with two sets of stresses and strains. Referring to a set of rectangular coordinates, the stress is denoted by σ_{ij} and strain by e_{ij}. The displacement along the x_i-axis is denoted by u_i. The equilibrium condition is expressed as $\sigma_{ij,j} + f_i = 0$, where f_i is the body force per unit volume along x_i-direction. The comma after j denotes differentiation along j-axis and the repetition of the subscript denotes summation from one to three.

$$e_{ij} = \frac{1}{2}\left(\frac{\partial u_i}{\partial x_j} + \frac{\partial u_j}{\partial x_i}\right) = e_{ij}^{'} + e_{ij}^{''} \tag{9}$$

The strain is composed of the elastic $e_{ij}^{'}$ and the plastic $e_{ij}^{''}$. The stress is related to the elastic strain by

$$\sigma_{ij} = C_{ijkl} e_{kl}^{'} \tag{10}$$

where C_{ijkl}'s are the elastic constants.

The other set of stresses and strains are denoted by subscript *

$$\sigma_{ij,j}^{*} + f_i^{*} = 0, \qquad e_{ij}^{*} = \frac{1}{2}\left(\frac{\partial u_i^{*}}{\partial x_j} + \frac{\partial u_j^{*}}{\partial x_i}\right), \qquad \sigma_{ij}^{*} = C_{ijkl} e_{kl}^{*} \tag{11}$$

For a homogeneous isotropic medium

$$C_{ijkl} = \lambda\delta_{ij}\delta_{kl} + \mu(\delta_{ik}\delta_{ji} + \delta_{il}\delta_{jk}) \tag{12}$$

where δ_{ij} is the Kronecker delta. λ and μ are Lame's constants.

From the above, we can write

$$\int_{\Omega}\sigma_{ij}^{*}e_{ij}^{'}d\Omega = \int_{\Omega}C_{ijkl}e_{kl}^{*}e_{ij}^{'}d\Omega = \int_{\Omega}C_{ijkl}e_{ij}^{'}e_{kl}^{*}d\Omega = \int_{\Omega}\sigma_{kl}e_{kl}^{*}d\Omega \tag{13}$$

where Ω denotes volume of the solid. This gives the reciprocal relation for elastic bodies.

Replacing $e_{ij}^{'}$ by $e_{ij} - e_{ij}^{'}$ and using divergence theorem, we obtain

$$\int_{\Omega}f_i^{*}u_i d\Omega + \int_{\Gamma}S_i^{*}u_i d\Gamma - \int_{\Omega}\sigma_{ij}^{*}e_{ij}^{''}d\Omega = \int_{\Omega}f_i u_i^{*}d\Omega + \int_{\Gamma}S_i u_i^{*}d\Gamma \tag{14}$$

where Γ denotes the surface.

Let f_n^{*} be a unit delta function in the x_n-direction at point $x^{'}$,

$$f_n^{*} = \delta_n(x,x^{'}) \qquad \text{i.e.: } \int_{\Omega}\delta_n(x,x^{'})d\Omega = 1 \tag{15}$$

From Kelvin's solution of a constant force along x_n-direction applied in an infinite homogeneous isotropic medium

$$u_i^{*}(\vec{x},x_k^{'}) = A\Big[\ \underset{\sim}{B}\delta_{ik}\left(\frac{1}{r}\right) - \left(\frac{1}{r}\right)_{,i}(x_k - x_k^{'})\ \Big] \tag{16}$$

where $A=\dfrac{\lambda+\mu}{8\pi(\lambda+2\mu)}$, $B=\dfrac{\lambda+3\mu}{\lambda+\mu}$, $r=\sqrt{(x_1-x_1')^2+(x_2-x_2')^2+(x_3-x_3')^2}$ (17)

From the expression of displacement u_i^* we obtain strain e_{ij}^* and the stress σ_{ij}^*. Noting the surface traction on the surface with normal η_j, we obtain

$$C_{kj}u_j(\vec{x},e'')+\int_\Gamma S_i^*(\vec{x},x')u_i(x,e'')d\Gamma=\int_\Omega \sigma_{ij}^*(\vec{x},x_k')e_{ij}''d\Omega+\int_\Gamma S_i(\vec{x},e'')u_i^*d\Gamma \tag{18}$$

where $C_{kj}=\begin{cases}1 & \text{for } k=j \text{ and } \delta_k(\mathbf{x}') \text{ applied inside body}\\ 0.5 & \text{for } k=j \text{ and } \delta_k(\mathbf{x}') \text{ applied on smooth surface}\\ 0 & \text{for } k\neq j\end{cases}$ (19)

The above shows the method to calculate the microscopic stress and strain fields, the average of which give the macroscopic stress and strain, and hence the hysteresis loops of the crystal.

III-2. Recent Aluminum Single Crystal Data

Recently, Zhai et al (1992,1996) have shown a set of excellent fatigue data of aluminum single crystals under stress-controlled loadings. The specimen has two special surfaces: One is the side surface containing the active Burger's vector, the other is the front surface perpendicular to the side surface and having the largest slip steps under fatigue. The specimen was loaded in equal cyclic tension and compression. The preferred slip system is $[0\,\bar{1}\,1](111)$. The PSB's on the front surface were of the same size and distribution as those on the side surface. Many PSB's on the side surface were concave. The extrusion on the front surface was found to be continuous with the intrusion on the side surface as shown in Fig.8. The present model predicts these experimental observations. This micromechanic model is verified to such detail. Hence the validity of this theory is reassured.

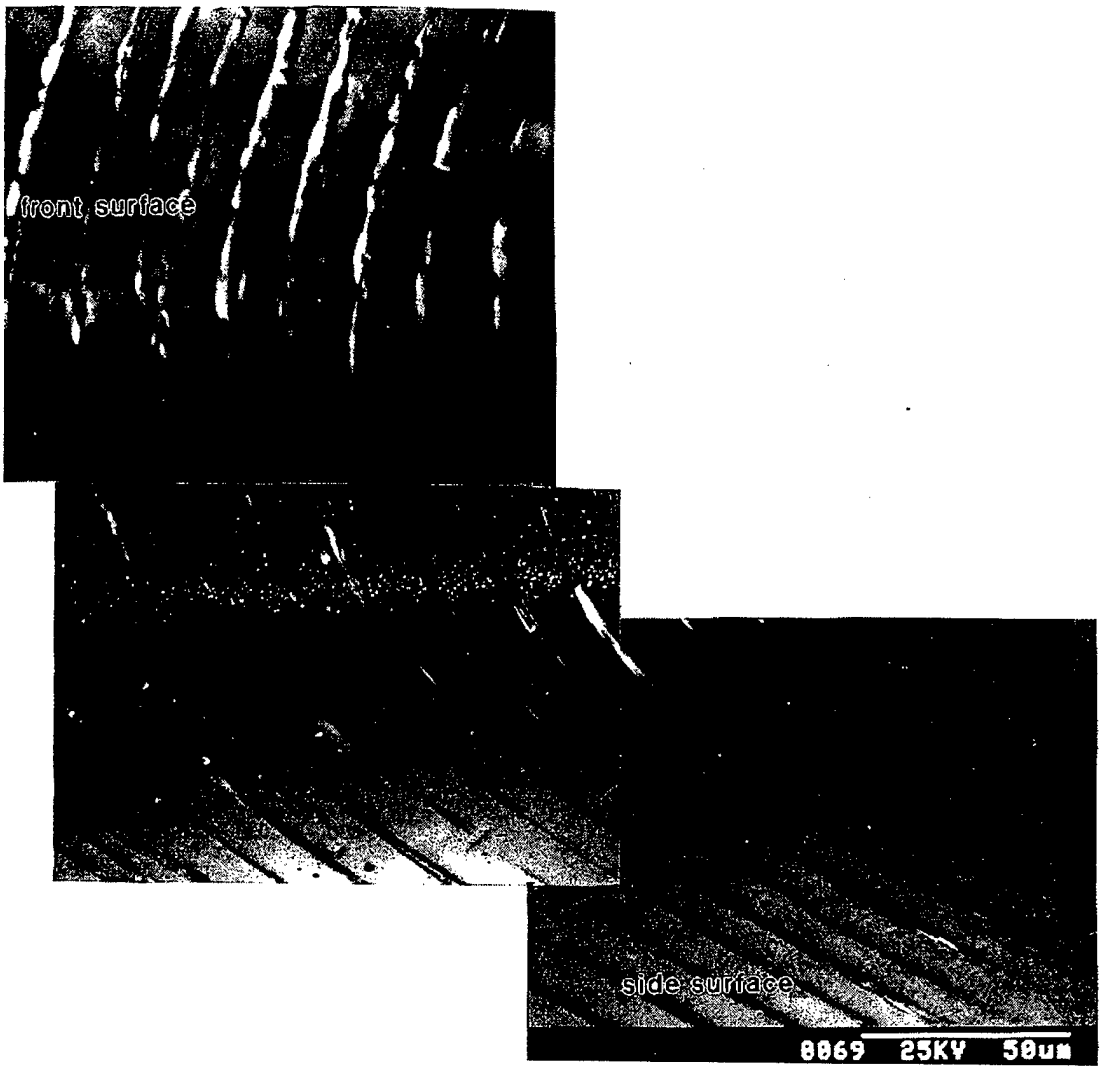

Fig.8 SEM micrograph showing the topographies of the area around the common edge of the front-surface(in the top) and side-surface(in the bottom) in specimen 1 at 1.2×10^6 cycles. The dark bands on the side-surface and the PSBs on the front-surface meet at the edge, including that the drak bands on the side-suface correspond to the PSBs.

III-3 Numerical Results

The dimensions of the specimen to be analyzed are shown in Fig.9. The specimen is taken to be of pure aluminum with a critical shear stress τ^c of 0.369 MPa(53 p.s.i) and is loaded under uniform tensile and compressive stress of 0.9x0.369 MPa.

In the present analysis, the multiple fatigue bands were assumed to be 1 μm across each band and have 5 μm spacing. These are similar to those in Zhai et al.'s.

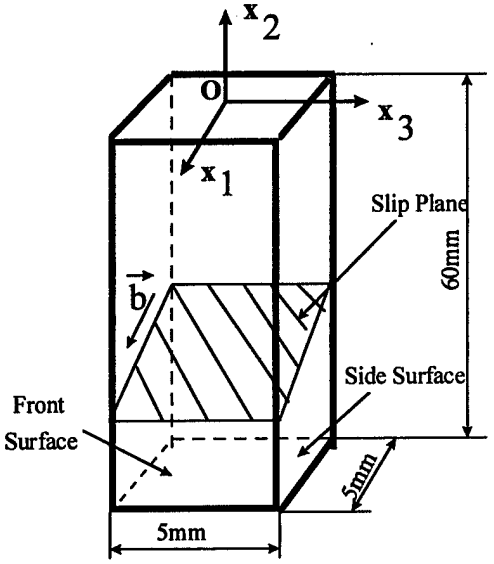

Fig.9 Dimensions of the specimen to be analyzed

From Eq.5 to Eq.8, the residual stress τ^r depends on the initial stress τ^i. Two sets of initial stresses of the same average values in each of the four segments P, P', Q and Q' (Fig. 2) were calculated under the same cyclic loading: one with a linear initial stress giving hysteresis loops shown in Fig.10 and the other with a uniform distributed one giving hysteresis loops shown in Fig.11. It is seen that one with uniform initial shear stress reaches the saturation value of cumulating plastic strain much sooner than the one with linear initial stress. The initial shear stress τ^i is generally heterogeneous. Let $\tau^i_{P\max}$ denote the maximum initial stress. During the forward loading, when this $\tau^i_{P\max} + \tau^a = \tau^c$ in some region, this region slides and yields plastic strain. This loading give the elastic limit of the specimen. As the forward loading increases, more

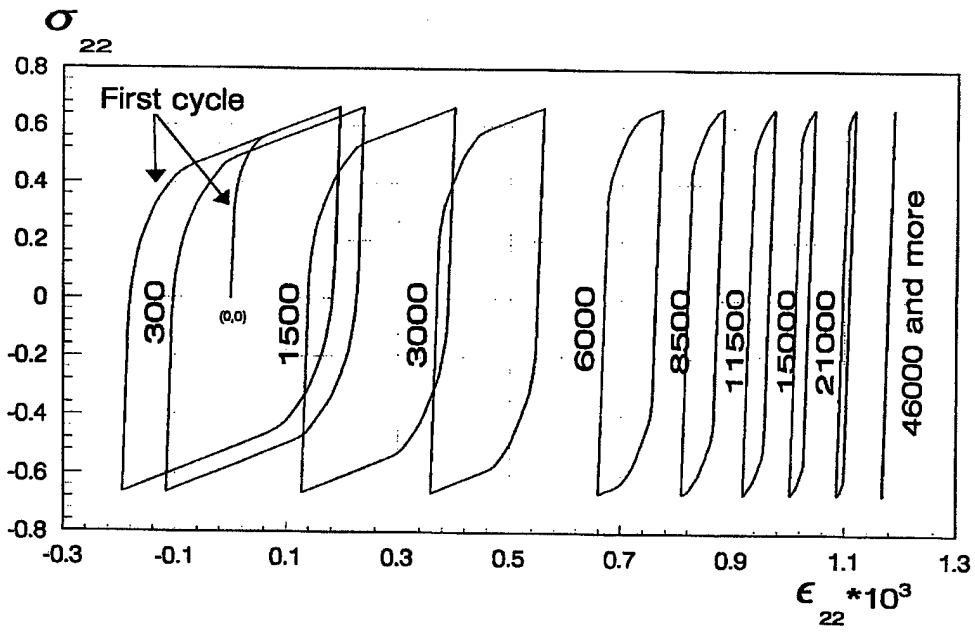

Fig.10 Hysteresis Loops of a Crystal with linear distributed initial shear stress

regions slide. This gives the curved part of the stress-strain curve. The residual stress in P and Q are negative to relieve the shear stress in P, but increases the negative shear stress in Q. Thus negative shear stress causes Q to slides easier in the reverses loading. This is known as the Bauchinger Effect. Further negative loading gives the curved part of the negative stress-strain curve until the maximum negative loading is reached. Then the forward loading gives the linear stress-strain curve followed by a curved part of the hysteresis loop until the maximum forward loading is reached. As explained before, the negative residual stress τ_P^r is built-up in P and the positive residual stress τ_Q^r in Q. These residual stresses tend to cancel the initial shear stress τ^i in P and Q. This process produces an extrusion, which causes a steady tensile stress $\tau_{\alpha\alpha}^r$ combining with the cyclic axial stress caused by $\pm\sigma_{22}$ in R. This causes R to be under a cyclic loading with a mean stress.

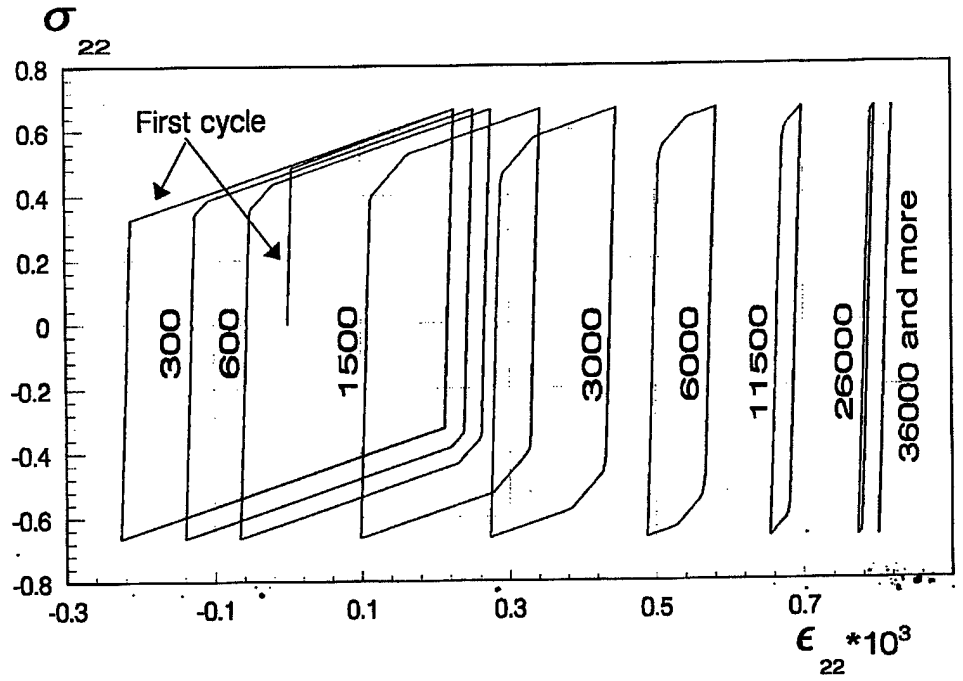

Fig.11 Hysteresis Loops of a Crystal with uniform initial shear stress

The calculated extrusion height in the present analysis exceeds 0.7μm, which agrees with that observed by Zhai et al. This is taken as the extrusion height in saturation. The present model seems to be able to explain a number of experimental observations. ~~The above analysis is for a constant cyclic axial loading. Experimentally it is known that a pre-tension or an overload increases the fatigue life. These two effects are to be analyzed.~~

In the present project, ending on 6/30/99, based on some previous work of the writer on micromechanics of HCF, we have developed the quantitave physical theory of HCF of f.c.c. polycrystal, as described in section II-2. We have also developed the micromechanic analysis of the hysteresis loops of single crystals. This fatigue theory satisfies the conditions of stress equilibrium and displacement continuity throughout the metal. This model clearly represents much more realistically the actual deformation of the single and the polycrystals.

IV. Suggested Future Studies

The basic variables in HCF have been identified as shown in the previous sections. We have been considering the fatigue at very low loading amplitude and have assumed that fatigue band occurs only in the most favorably oriented crystal in a polycrystal. Higher loading amplitude often occurs in practice and causing fatigue bands to occur in other crystals. The interaction of fatigue bands in few crystals needs to be considered. This needs a micromechanic

analysis of polycrystal stress and strain fields in the early stage of plastic deformation. A physical model of this analysis was proposed by the writer (Lin, 1971). This analysis is to be further developed for fatigue bands developed beyond the most favorably oriented crystals.

High temperature strength of some ordered superalloys has made them attractive for use in structures subject to high temperature such as rockets and gas turbines. When these alloys are in polycrystal form, intergranular cracks frequently develop under loading. In order to avoid these brittle intercrystalline cracks, these alloys, such as GE's Rene N-4 and Pratt-whitney's PWA-1450, in single crystal form have been used in gas turbines. The design of these requires the constitutive relation of this single crystal alloy. At low and intermediate temperatures, these nickel-based superalloys generally are in disordered form and plastically deformed through $\frac{1}{2}$<110>{111} slip. If this slip occurs in superalloys in ordered form, this slip will leave a plane of anti-plane boundary APB in the wake (Pope and Ess, 1984). The energy required to create such a fault is high. This causes large resistance to this slip and causes cross-slip or multiple slip to be difficult. The APB energy is anisotropic, being smaller on the cube-plane than on an octahedral plane. These screw dislocations tend to cross-slip from the octahedral plane, where the APB energy is high to the cube planes where it is low. The pinning of the screw dislocations on the cube planes impedes the motion of the primary octahedral screw dislocations and raises the flow stress in the octahedral system (Walker and Jordan, 1989). The rate at which the screw dislocations cross-slip and become pinned is governed by a diffusives process, which is dependent on temperature. Hence the octahedral flow stress increases with temperature. This property is highly desirable for those parts subject to high temperature and hence is used in turbine parts. The active slip system changes with temperature. To design such parts, the stress-strain relationship with variation in temperature is needed.

Walker and Jordan(1989) developed a constitutive relation of a superalloy single crystal assuming a relation similar to the unified isotropic viscoplastic model (Lindholm et al, 1994,1995). They have made good progress to this very difficult problem. However their model did not consider the heterogeneity of stress and strain in the single crystal described in Section III and did not give the stress-strain relations under non-proportional loading. The present micromechanic model of fatigue band considering the heterogeneity of plastic deformation

based on the experimental observations and is clearly much more realistic than the phenomenological model based on the unified viscoplastic constitutive model. This constitutive relation to be derived will be compared to the experimental data. It is expected that the agreement between these analytical and experimental results will be much better than the previous models. This present theory satisfies the stress equilibrium, displacement continuity and numerous experimental observations of fatigued single crystals and polycrystals. This research should give significant benefits to our industry and contribute greatly to the advance of science in the fatigue models.

V. References

Basinski,Z.S. and Bainski,S.T.,1992"Fundamental aspets of Low Amplitude Cyclic Deformation in Face-centreted Cubic Crystals" Progress in Materials Scince, Vol 36, pp89-148.

Brebbia,C.A. and Domingues,J., 1992, Boundary Elements, An Introductory Course, Chap.3, Computation Mechanics Publishing, McGrawn Hall Book Company.

Buckley,S.N. and Entwistle,K.M.(1956). The Bauschinger effect in super pure aluminum single crystal and polycrystals. Acta Metallurgica 4, 352.

Charsley,P. and Thompson,N.(1965). The behavior of slip lines on aluminum crystal under reversed stresses in tension and compression. Phil. Mag. 8, 77.

Cottrell,A.H., and Hull,D.(1957).Extrusions and intrusions by cyclic slip in copper. Proc. Roy. Soc. London A. **242,** 211.

Eshelby,J.D.(1957). The determination of the elastic field of an ellipsoidal inclusion and related Problems. Proc. Roy. Soc. A. **241,** 369.

Forsyth,P.J.E. and Stubbington,C.A.(1955). The slip band extrusion effect observed in some aluminum alloys subjected to cyclic stresses. J. Inst. Metals 83, 395.

Hirth,J.P. and Lothe,J.,1968, Theory of Dislocations, McGraw Hill Book Company, New York, Chap.3.

Lin,T.H. and Ito,Y.M.,(1969). Fatigue crack nucleation in metals. Proc. U.S. Nat. Academy of Sciences 62, 631-780.

Lin,T.H.,1977"Micromechanics of Deformation of Slip Bands under Monotonic and Cyclic Loadings" Reviews on the Deformation Behavior of Materials, Freund Publishing House Ltd, Tel-avir Isreal.

Lin,T.H.,1992 "Micromechanics of Crack Initiation in High-cyclic Fatigue," Advances in Applied Mechanics, Vol.29, pp1-62.

Lindholm,U.S., Chan,K.S., Bodner,S.R.,Weber,R.M.,Walker,K.P. and Cassenti,B.M.(1984) Constitutive modelling for isotropic materials(HOST), NASA CR174718, pp.1.1-A-68.

Lindholm,U.S., Chan,K.S., Bodner,S.R.,Weber,R.M.,Walker,K.P. and Cassenti,B.M.(1985) Constitutive modelling for isotropic materials(HOST), NASA CR174980, pp.1-173.

Ma, B.T. and Laird,C.,1998, Overview of Fatigue Behavior in Cooper Single Crystals" ACTA Metall & Mater, Vol.37,No.2.

Mecke,K. and Blockwitz,C.,1980 "Internal Displacement of Persistent Slip Bands in Cyclically Deformed Nickle Single Crystals" Phys. Stat. Sol. Vol(A) 64, K5.

Mughrabi,H. Ackermann,F. and Herz,K.,1979,"Persistent Slip Band in Fatigue Face-centered and Body centreted Cubic Crystals", ASTM ST675, pp69-105.

Mura,T,1982,Micromechanics of Defects in Metals, Matinus Nijhoff Publishers, The Hague/Boston/London

Pope, D.P. and Ezz, S.S.,1984,"Mechanical Properties of Ni3Al and Nickel-based alloys with high volume fraction of γ'," Int.Met.Rev. 29, pp136-166.

Puskar,A. and Golovin,S.A.,1985, Fatigue in Materials, Cumulative Damage Processes. p13 Elsevier Science Publishing Company Inc, New York, Amsterdam.

Walker, K.P. and Jordan, E.M., 1989,"Biaxial Constitutive Modelling and Testing of single crystal superalloy at Elevated Temperatures," Biaxial and Multiaxial Fatigue. EGF3(Edited by M.W.Brown and J.K.Miller), Mechanical Engineering Publications, London, pp145-170.

Wood, W.A.(1956). Mechanisms of fatigue. In "Fatigue in Aircraft Structure" (A.M.Freundental, ed.), Academic Press, New York, pp.1-19.

Wood, W.A., and Bender,A.M.(1962). The fatigue process in copper as studies by electron metallography. Trans. Metallurgical Society AIME 244, 180-186.

Zhai,T., Matin,J.W. and Briggs,G.A.D., 1995-6, "Fatigue Damage in Aluminum Single Crystals. ACTA Metall-Mater.,Vol. 43, pp3813-3825, Vol. 49, pp1279-1739,3477-3496.

VI. List of Publications sponsored by this grant

1. T.H. Lin, K.K.F. Wong & N.J. Teng, " Micromechanics of High-Cycle Fatigue in Single and Polycrystals", published in Analysis and Design Issuses For Modem Aerospace Vehicles, Edited by G.J.Simifses, published by ASME, New York, N.Y. 1997.
2. T.H. Lin, K.K.F. Wong,, N.J. Teng, S.R. Lin, "Micromechanic Analysis of Fatigue Band Crossing Grain Boundary," published in Material Science and Engineering, Vol.A246, pp169-179, 1998.
3. W. Zhong, T.H. Lin & S.R. Lin, "An Elastic-plastic Micromechanical Analysis of A Cross-ply Composite," published in Composites Science and Technology, Vol.58, pp527-537, 1998.
4. T.H. Lin, K.K.F. Wong & N.J. Teng, " Micromechanics of Fatigue Crack Initiation of Single Crystal Under Plane Strain", published in Damage Mechanics in Engineering Materials, Edited by G.Z. Voyiadjis, J.W. Ju & J.L. Chonache, Studies in Applied Mechanics 46, by Elsevier, Amsterdam, pp115-124, 1998.
5. T.H. Lin, N.G. Liang K.K.F. Wong & N.J. Teng, " A Physical Method of Fatigue Crack Initiation in Single Crystal", Proc. of the 7th Int. Fatigue Congress held in Beijing, China, Fatigue'99, Vol.1/4, pp265-270, 1999.
6. T.H. Lin, K.K.F. Wong & N.J. Teng, "Micromechanics of Hysteresis Loops of Fatigue in Single Crystal" to be published in the Journal of Applied Mechanics, 1999 or 2000.
7. T.H. Lin, N.G. Liang, K.K.F. Wong & N.J. Teng, "Micromechanic Analysis of Crack Initiation and Hysteresis Loops of Aluminum Single Crystal" to be published in Philosophical Magazine A, 1999 or 2000.

VII. Appendixes: Copies of Publications

T.H. Lin, K.K.F. Wong,, N.J. Teng, S.R. Lin, "Micromechanic Analysis of Fatigue Band Crossing Grain Boundary," published in Material Science and Engineering, Vol.A246, pp169-179, 1998.

W. Zhong, T.H. Lin & S.R. Lin, "An Elastic-plastic Micromechanical Analysis of A Cross-ply Composite," published in Composites Science and Technology, Vol.58, pp527-537, 1998.

T.H. Lin, K.K.F. Wong & N.J. Teng, " Micromechanics of Fatigue Crack Initiation of Single Crystal Under Plane Strain", published in Damage Mechanics in Engineering Materials, Edited by G.Z. Voyiadjis, J.W. Ju & J.L. Chonache, Studies in Applied Mechanics 46, by Elsevier, Amsterdam, pp115-124, 1998.

T.H. Lin, N.G. Liang K.K.F. Wong & N.J. Teng, " A Physical Method of Fatigue Crack Initiation in Single Crystal", Proc. of the 7th Int. Fatigue Congress held in Beijing, China, Fatigue'99, Vol.1/4, pp265-270, 1999.

T.H. Lin, K.K.F. Wong & N.J. Teng, "Micromechanics of Hysteresis Loops of Fatigue in Single Crystal" to be published in the Journal of Applied Mechanics, 1999 or 2000.

T.H. Lin, N.G. Liang, K.K.F. Wong & N.J. Teng, "Micromechanic Analysis of Crack Initiation and Hysteresis Loops of Aluminum Single Crystal" to be published in Philosophical Magazine A, 1999 or 2000.

ELSEVIER

PII: S0266-3538(97)00160-7

Composites Science and Technology **58** (1998) 527–537

Printed in Great Britain
0266-3538/98 $19.00

AN ELASTIC–PLASTIC MICROMECHANICAL ANALYSIS OF A CROSS-PLY COMPOSITE

W. Zhong,[a] T. H. Lin[a]* & S. R. Lin[b]

[a]*Department of Civil and Environmental Engineering, University of California, PO Box 951953, 5731/5732 Boelter Hall, Los Angeles, CA 900095-1593, USA*

[b]*Structure Technology Department, The Aerospace Corporation, El Segundo, CA, USA*

(Received 10 February 1997; revised 24 July 1997; accepted 6 August 1997)

Abstract

Multi-directional fiber-reinforced composites are often used in aerospace structures. The design of such structures needs a realistic macroscopic stress/strain relationship for the composite material. In this paper an analytical approach for determining this stress/strain relationship is developed which is based on detailed analysis of the microscopic stress/strain fields, which govern the spread of plastic strain and the amount of material damage. In this approach, the heterogeneous composite is transformed into a homogeneous solid by Eshelby's equivalent-inclusion method (Mura, T., Micromechanics of Defects in Solids. *Martinus Nijhoff, The Hague, 1982).*[1] *The microstresses and strains are then analyzed by using Lin's method of analyzing the microstress fields of elastically homogeneous polycrystals of periodic crystal orientations based on Green's functions of an infinite solid (Lin, T. H.,* Adv. Appl. Mech., *1971, 11, 255–311).*[2] *The major advantage of the present approach is that it does not need to isolate a representative volume (or 'unit cell') and specify the unknown boundary conditions. A numerical example for a cross-plied boron/aluminum composite is given.* © *1998 Elsevier Science Ltd. All rights reserved*

Keywords: C. residual stress, equivalent inclusion method, micromechanics, boundary conditions, Green's function

1 INTRODUCTION

Fiber-reinforced composites are used in aerospace structures where high strength and stiffness to weight ratios are needed. In designing structures with these composite materials, the macroscopic incremental stress/strain relationship and the macroscopic stiffness are required. Structural analyses give the macroscopic stress distributions in the structure. Material yielding generally starts at some localized high-stress region. However, local yielding does not cause failure. Failure occurs mostly when plastic strain spreads over a major part of the cross-section. To analyze this spread of plastic zone, the microscopic stress/strain is to be obtained at the regions of high macrostresses. This requires a macroscopic stress/strain relationship derived from microscopic stress/strain fields.

Evaluation of the overall elastic stiffness properties of composites have been shown by Hashin and Shtrikman[4] and Hashin and Rosen[5] and from the self-consistent approach by Hill,[6] Budiansky,[7] Walpole,[8] Willis,[9] and Weng[10] to give the bounds of the elastic stiffness. Teply and Dvorak[11] applied the minimum principles of plasticity[12,13] to evaluate the upper and lower bound properties of elastic–plastic composites aggregates subjected to macroscopically uniform incremental stress and strain histories. Numerical calculations can be greatly reduced if the composite can be considered to have a periodic microstructure. The periodic microstructure would require the fibers to be uniformly spaced. Scheirer and Toth[14] have shown that such composites can be produced at high cost. For important structures such as hypersonic planes, such high cost may be justified. Considering a composite of periodic microstructure, Walker *et al.*[15] and Nemat-Nasser and Hori[16] have elegantly shown the mathematics of the micromechanic analysis of such composites.

Fiber and matrix have different elastic moduli, and the finite-element method (FEM) can handle these different moduli in different grids. Hence, the FEM is applicable to the stress analysis of composites in the same way as that of a single-phase material. Recently, Dvorak and his associates have made many important contributions to the understanding of the elastic–plastic behavior of composites. In 1985, Dvorak and Teply[17] have used the FEM to obtain estimates of local stress and strain fields as well as the bounds on the instantaneous moduli of elastic–plastic

*To whom correspondence should be addressed.

uniaxial fiber reinforced composites. In 1994, Dvorak *et al.*[18] applied Eshelby's equivalent inclusion method[1] to a unit cell subject to the boundary condition of uniform macroscopic strain. In their analysis, the representative volume of the heterogenenous medium is divided into a number of phases, each of which can have a different elastic moduli and different eigenstrains. They assumed a macroscopically homogeneous response under macroscopically uniform overall stress or uniform overall strains, prescribed through surface tractions or displacements specified on the surface of the representative volume. When the phase eigenstrains are present, they further assume that if the surface is free of tractions, the displacements on the surface are consistent with a macroscopically uniform overall strain. Their results agree with those obtained by FEM. As will be shown later, these assumptions are removed in the present model.

Referring to the analysis of a periodic composite, in 1990, Adams[3] indicated 'a major problem in currently modeling composite material behavior is adequately representing the complex boundary condition that are introduced when a local material region is isolated for analysis'. This seems to indicate some difficulty in specifying the boundary conditions in analyzing the unit cell, especially for composites of cross-ply fibers under combined shear and biaxial loadings.

Lin[2] considered a polycrystal composed of innumerous identical cubic blocks embedded in an infinite elastic medium subject to loadings applied at infinity. The stress/strain relationship of the center block was taken to represent the macroscopic stress/strain relationship of the polycrystal. Since there are innumerable identical cubic blocks, the plastic-strain distribution in the crystals surrounding the center block are taken to be the same as that in the center block. The interaction of the plastic strain in the surrounding blocks on the stresses in the center block is readily calculated using Kelvin's solution of stress field caused by a concentrated force in an infinite isotropic elastic medium.[19] For a polycrystal of repeated cubic blocks, i.e. of a periodic microstructure, Wu[20] and Hill[21] have shown that the macroscopic strain equal to the volume average of the microscopic strain and the macroscopic stress equals the volume average of the microscopic stress. This derivation of the macroscopic stress/strain curve for the polycrystal does not need to know the boundary conditions of the center block. This approach is applied to the analysis of composite of periodic microstructure. The heterogenous composite is here transformed into a homogenous solid, similar to that used by Dvorak *et al.*[18] Then the macroscopic stress/strain relation of the composite is similarly derived by considering the composite to be composed of repeated unit cells embedded in an infinite medium. In this way, no local region or unit cell needs to be isolated and the problem of specifying the boundary condition on the unit cell is eliminated.

2 ELASTIC–PLASTIC ANALYSIS OF SINGLE-PHASE PERIODIC MATERIALS

The equilibrium conditions with plastic strain e''_{ij} within a region Ω and on the boundary Γ have been found by Lin and co-workers:[22,23]

$$C_{ijkl}e_{kl,j} + (-C_{ijkl}e''_{kl,j}) + F_i = O \text{ in } \Omega \tag{1}$$

$$S^n_i + (C_{ijkl}e''_{kl}\eta_j) = C_{ijkl}e_{kl}\eta_j \text{ on } \Gamma \tag{2}$$

where the subscript after comma denotes differentiation, the repetition of the subscript denotes summation from 1 to 3, F_i denotes the body force per unit volume along the x_i axis, S^n_i is the surface traction per unit area of the surface with normal $\mathbf{n}$, and η_i is the i-component of normal $\mathbf{n}$. The parenthesis terms in eqns (1) and (2) are here denoted by $\bar{F}_i$ and $\bar{S}^n_{ij}$, respectively. For isotropic elastic materials:

$$C_{ijkl} = \lambda\delta_{ij}\delta_{kl} + \mu(\delta_{ik}\delta_{jl} + \delta_{il}\delta_{jk}) \tag{3}$$

where δ_{ij} is the Kronecker Delta, and λ and μ are Lame's constants. Assuming plastic dilatation to be zero, $\bar{F}_i$ and $\bar{S}^n_i$ reduce to

$$\bar{F}_i = -2\mu e''_{ij,j} \text{ in } \Omega,\ \bar{S}^n_i = 2\mu e''_{ij}\eta_j \text{ on } \Gamma \tag{4}$$

Denoting the stress at point $\mathbf{x}$ caused by $\bar{F}_i$ and $\bar{S}^n_i$ by $\tau^s_{ij}(\mathbf{x})$, the residual stress at point $\mathbf{x}$, $\tau^R_{ij}(\mathbf{x})$, caused by the plastic strain is

$$\tau^R_{ij}(\mathbf{x}) = \tau^S_{ij}(\mathbf{x}) - 2\mu e''_{ij}(\mathbf{x}) \tag{5}$$

Since this solid is considered to be embedded in an infinite elastic solid of the same elastic constants, the equivalent body force due to plastic strain can be considered to be applied in an infinite elastic medium.The elastic solution due to a concentrated force in an infinite isotropic medium has been given by Kelvin,[20] from which the stress τ_{ij} at point $\mathbf{x}$ caused by a unit concentrated force at point $\mathbf{x}'$ along the x_k direction is given by

$$K_{ijk}(\mathbf{x},\mathbf{x}') = -\frac{3}{8\pi(1-\nu)}\frac{(x_i-x'_i)(x_j-x'_j)(x_k-x'_k)}{r^5} + \frac{1-2\nu}{8\pi(1-\nu)}\frac{\delta_{ij}(x_k-x'_k)-\delta_{ik}(x_j-x'_j)-\delta_{jk}(x_i-x'_i)}{r^3} \tag{6}$$

where ν is Poisson's ratio and $r^2 = (x_i-x'_i)^2 + (x_j-x'_j)^2 + (x_k-x'_k)^2$. From eqns (1) and (5), the residual stress field due to the plastic strain is

$$\tau^R_{ij}(\mathbf{x}) = -\int_\Omega K_{ijk}(\mathbf{x},\mathbf{x}')C_{klrs}e''_{rs,l}(\mathbf{x}')\mathrm{d}V - C_{ijkl}e''_{kl}(\mathbf{x}) \tag{7}$$

The distribution of plastic strain in the blocks near the center block is taken to be identical to that in the center block. The residual stress $\tau_{ij}^R(\mathbf{x})$ at $\mathbf{x}$ due to $e_{ij}''(\mathbf{x}')$ of all blocks can be written as

$$\tau_{ij}^R(\mathbf{x}) = Q_{ijkl}(\mathbf{x}, \mathbf{x}')e_{kl}''(\mathbf{x}') \tag{8}$$

where $Q_{ijkl}(\mathbf{x}, \mathbf{x}')$ is the influence coefficient of the residual stress $\tau_{ij}^R(\mathbf{x})$ due to a unit plastic strain of a unit volume at $\mathbf{x}'$.

Under a uniform stress τ_{ij}^o applied to the infinite medium, the stress τ_{ij} of the element with center at $\mathbf{x}$ is given by

$$\tau_{ij}(\mathbf{x}) = \tau_{ij}^o + \tau_{ij}^R(\mathbf{x}) = \tau_{ij}^o + Q_{ijkl}(\mathbf{x}, \mathbf{x}')e_{kl}''(\mathbf{x}') \tag{9}$$

The average stress over the region Ω denoted by T_{ij} is given by

$$T_{ij} = \bar{\tau}_{ij} = \tau_{ij}^o + \bar{Q}_{ijkl}(\mathbf{x}')e_{kl}''(\mathbf{x}') \tag{10}$$

where the bar denotes the average over the region. Equations (8) and (10) give

$$\tau_{ij}(\mathbf{x}) = T_{ij} + \left(Q_{ijkl}(\mathbf{x}, \mathbf{x}') - \bar{Q}_{ijkl}(\mathbf{x}')\right)e_{kl}''(\mathbf{x}') \tag{11}$$

Let $\tilde{Q}_{ijkl}(\mathbf{x}, \mathbf{x}') = Q_{ijkl}(\mathbf{x}, \mathbf{x}') - \bar{Q}_{ijkl}(\mathbf{x}')$ and writing eqn (11) in incremental form, we have

$$\Delta\tau_{ij}(\mathbf{x}) = \Delta T_{ij} + \tilde{Q}_{ijkl}(\mathbf{x}, \mathbf{x}')\Delta e_{kl}''(\mathbf{x}') \tag{12}$$

Here, $\tilde{Q}_{ijkl}(\mathbf{x}, \mathbf{x}')$ is the influence coefficient of the average residual stress of the element with center at $\mathbf{x}$ caused by a unit plastic strain in the element with center at $\mathbf{x}'$. These influence coefficients satisfy the reciprocal relation and form a symmetric matrix. This formulation greatly simplifies the numerical calculations of the stress and strain increments in the different elements. This approach is to be used in the analysis of composites.

3 ELASTO-PLASTIC STRESS AND STRAIN FIELDS OF COMPOSITES

A solid with uniform elastic moduli is referred to as a homogeneous solid. If a solid has one or more inclusions with elastic moduli different from the rest, like a composite, this solid is referred to a heterogeneous (or inhomogeneous) solid.

3.1 Equivalent inclusion method

If a homogeneous solid with elastic moduli C_{ijkl} is uniformly loaded, i.e. the boundary traction is $S_i^n = \tau_{ij}^o\eta_j$ on Γ, the strain e_{ij}^o is uniform throughout the solid. However, if this solid Ω has an inclusion Ω^* with different elastic moduli C_{ijkl}^* as shown in Fig. 1, the stress and strain in the solid would vary from point to point. The stress in the solid is expressed as

$$\tau_{ij} = \tau_{ij}^o + \tilde{\tau}_{ij} = C_{ijkl}^*\left(e_{kl}^o + \tilde{e}_{kl}\right) \text{ in } \Omega^* \tag{13}$$

$$\tau_{ij} = \tau_{ij}^o + \tilde{\tau}_{ij} = C_{ijkl}\left(e_{kl}^o + \tilde{e}_{kl}\right) \text{ in } \Omega - \Omega^* \tag{14}$$

where $\tilde{\tau}_{ij}$ and $\tilde{e}_{kl}$, are disturbance stress and strain, respectively. They are due to the inhomogeneity of the solid and vary from point to point. If the inclusion Ω^* with C_{ijkl}^* is replaced by one with C_{ijkl} and with extra inelastic strain e_{ij}^*, then

$$\tau_{ij} = C_{ijkl}^*\left(e_{kl}^o + \tilde{e}_{kl}\right) = C_{ijkl}\left(e_{kl}^o + \tilde{e}_{kl} - e_{kl}^*\right) \text{ in } \Omega^* \tag{15}$$

these two inclusions will have the same stress/strain relations and their stress distributions will be identical. This gives the equivalency of these two inclusions, a concept which was first ingeniously introduced by Eshelby.[24] Eshelby has found stress in an ellipsoidal inclusion in an infinite isotropic medium to be uniform. But the relation given by eqn (15) is valid for inclusions of all shapes and is not restricted to ellipsoidal inclusions.

Now that the actual inclusion with C_{ijkl}^* is replaced by one with C_{ijkl}, the solid becomes homogeneous and the elastic–plastic analysis of a homogeneous solid as given in Section 2 can be applied. This inelastic strain e_{ij}^* will be referred to as eigenstrain by Mura to differentiate it from the inelastic strain commonly denoting plastic or creep strains.

3.2 Elastic stress and strain fields of composites

After replacing the inclusion with C_{ijkl}^* by one with C_{ijkl}, the heterogeneous solid becomes homogeneous. The effect of eigenstrain e_{ij}^* in the homogeneous solid is the same as that of plastic strain e_{ij}''. Therefore, replacing $e_{ij}''(\mathbf{x}')$ by e_{ij}^* in eqn (9), it follows that

$$\tau_{ij}(\mathbf{x}) = \tau_{ij}^o + Q_{ijkl}(\mathbf{x}, \mathbf{x}')e_{kl}^*(\mathbf{x}') \tag{16}$$

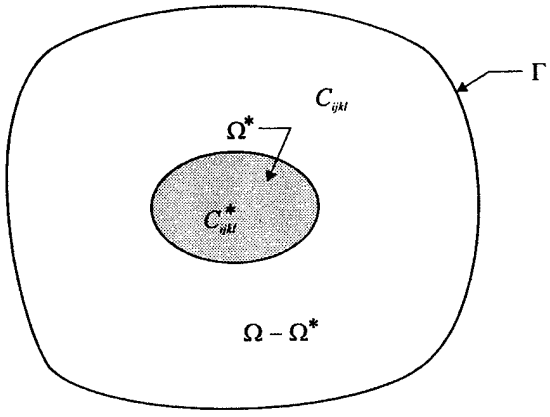

Fig. 1. An inhomogeneous solid with an inclusion Ω*.

and eqn (11) becomes

$$\tau_{ij}(\mathbf{x}) = T_{ij} + \tilde{Q}_{ijkl}(\mathbf{x}, \mathbf{x}')e^*_{kl}(\mathbf{x}') \tag{17}$$

where T_{ij} is the average stress over the region Ω. Let S_{ijkl} be the compliance tensor of C_{ijkl}, where $S_{ijkl}\tau^o_{kl} = e^o_{ij}$, it follows from eqn (10) that

$$e^o_{ij} = S_{ijkl}T_{kl} - S_{ijkl}\bar{Q}_{klmn}(\mathbf{x}')e^*_{mn}(\mathbf{x}) \tag{18}$$

Similarly, eqn (2) can be rewritten as

$$e^o_{ij} + \bar{e}_{ij} - e^*_{ij} = S_{ijkl}\tau_{kl} \tag{19}$$

Substituting τ_{ij} in eqn (17) and e^o_{ij} in eqn (18) to eqn (19), it follows that

$$\bar{e}_{ij}(\mathbf{x}) = e^*_{ij}(\mathbf{x}) + S_{ijkl}Q_{klmn}(\mathbf{x}, \mathbf{x}')e^*_{mn}(\mathbf{x}') \tag{20}$$

while recalling that $\tilde{Q}_{ijkl}(\mathbf{x}, \mathbf{x}') = Q_{ijkl}(\mathbf{x}, \mathbf{x}') - \bar{Q}_{ijkl}(\mathbf{x}')$. Substituting eqns (18) and (20) into eqn (15), it follows that

$$Q^*_{ijkl}(\mathbf{x}, \mathbf{x}')e^*_{kl}(\mathbf{x}') = T_{ij} - C^*_{ijkl}S_{ijkl}T_{mn} \tag{21}$$

where

$$\begin{aligned} Q^*_{ijkl}(\mathbf{x}, \mathbf{x}') = {} & C^*_{ijmn}S_{mnrs}\tilde{Q}_{rskl}(\mathbf{x}, \mathbf{x}') \\ & + C^*_{ijkl}\delta(\mathbf{x}, \mathbf{x}') - \tilde{Q}_{ijkl}(\mathbf{x}, \mathbf{x}') \end{aligned} \tag{22}$$

Equation (21) gives the solution of the eigenstrain e^*_{ij} under given T_{ij}:

$$e^*_{ij}(\mathbf{x}') = {Q^*_{ijkl}}^{-1}(\mathbf{x}, \mathbf{x}')\left(T_{kl} - C^*_{klmn}S_{mnrs}T_{rs}\right) \tag{23}$$

Substituting eqn (23) into eqn (17), it follows that

$$\begin{aligned} \tau_{ij}(\mathbf{x}) = {} & T_{ij} + \tilde{Q}_{ijkl}(\mathbf{x}, \mathbf{x}'){Q^*_{klmn}}^{-1}(\mathbf{x}, \mathbf{x}') \\ & \times \left(T_{mn} - C^*_{mnrs}S_{rspq}T_{pq}\right) \end{aligned} \tag{24}$$

Equation (24) represents the elastic stress field of the heterogeneous solid. The macroscopic stress T_{ij} is defined as the volume average stress over the block. Following eqn (16),

$$T_{ij} = \tau^o_{ij} + \bar{Q}_{ijkl}(\mathbf{x}')e^*_{kl}(\mathbf{x}') \tag{25}$$

where the bar on the top denotes the volume average. Solving for τ^o_{ij} in eqn (25) and substituting the result into eqn (16) gives

$$\tau_{ij}(\mathbf{x}) = T_{ij} + \tilde{Q}_{ijkl}(\mathbf{x}, \mathbf{x}')e^*_{kl}(\mathbf{x}') \tag{26}$$

Structures often have high stress concentrations, which will cause high elastic local stresses. However, the high stresses are relieved through plastic deformation. Most materials can allow some developments of plastic deformation before they reach their ultimate strengths.

3.3 Elasto-plastic stress and strain fields

If plastic strain e''_{ij} occurs in the heterogeneous solid, eqns (13) and (14) become

$$\tau_{ij} = \tau^o_{ij} + \bar{\tau}_{ij} = C^*_{ijkl}(e^o_{kl} + \bar{e}_{kl} - e''_{kl}) \text{ in } \Omega^* \tag{27}$$

$$\tau_{ij} = \tau^o_{ij} + \bar{\tau}_{ij} = C_{ijkl}(e^o_{kl} + \bar{e}_{kl} - e''_{kl}) \text{ in } \Omega - \Omega^* \tag{28}$$

Using Eshelby's equivalent inclusion concept, eqn (27) becomes

$$\begin{aligned} \tau_{ij} &= C^*_{ijkl}(e^o_{kl} + \bar{e}_{kl} - e''_{kl}) \\ &= C_{ijkl}(e^o_{kl} + \bar{e}_{kl} - e''_{kl} - e^*_{kl}) \text{ in } \Omega^* \end{aligned} \tag{29}$$

The right side of eqn (29) reduces to eqn (27) in $\Omega - \Omega^*$ and hence the right side holds for both Ω^* and $\Omega - \Omega^*$. Equation (26) can be rewritten as

$$\tau_{ij}(\mathbf{x}) = T_{ij} + \tilde{Q}_{ijkl}(\mathbf{x}, \mathbf{x}')e^*_{kl}(\mathbf{x}') + \tilde{Q}_{ijkl}(\mathbf{x}, \mathbf{x}'')e''_{kl}(\mathbf{x}'') \tag{30}$$

where $\mathbf{x}'$ covers Ω^* and $\mathbf{x}''$ covers Ω. The same process of deriving eqns (18) to (16) can be used with the presence of plastic strain. Including the plastic strain term in eqn (18) gives

$$e^o_{ij} = S_{ijkl}T_{kl} - S_{ijkl}\bar{Q}_{ijkl}(\mathbf{x}')e^*_{kl}(\mathbf{x}') - S_{ijkl}\bar{Q}_{ijkl}(\mathbf{x}'')e''_{kl}(\mathbf{x}'') \tag{31}$$

Combining eqns (29) to (31) and noting $\tilde{Q}_{ijkl}(\mathbf{x}, \mathbf{x}') = Q_{ijkl}(\mathbf{x}, \mathbf{x}') - \bar{Q}_{ijkl}(\mathbf{x}')$, it follows that

$$\begin{aligned} \bar{e}_{ij}(\mathbf{x}) = {} & e^*_{ij}(\mathbf{x}) + e''_{ij}(\mathbf{x}) + S_{ijkl}Q_{klmn}(\mathbf{x}, \mathbf{x}'')e^*_{mn}(\mathbf{x}'') \\ & + S_{ijkl}Q_{klmn}(\mathbf{x}, \mathbf{x}'')e''_{mn}(\mathbf{x}'') \end{aligned} \tag{32}$$

Substituting eqns (31) and (32) into eqn (28) gives

$$\begin{aligned} & [C^*_{ijmn}S_{mnrs}\tilde{Q}_{rskl}(\mathbf{x}, \mathbf{x}') - \tilde{Q}_{ijkl}(\mathbf{x}, \mathbf{x}') + C^*_{ijkl}\delta(\mathbf{x}, \mathbf{x}')]e^*_{kl}(\mathbf{x}') \\ & = \left(T_{ij} - C^*_{ijmn}S_{mnkl}T_{kl}\right) \\ & \quad + \left[\tilde{Q}_{ijkl}(\mathbf{x}, \mathbf{x}'') - C^*_{ijmn}S_{mnrs}\tilde{Q}_{rskl}(\mathbf{x}, \mathbf{x}'')\right]e''_{kl}(\mathbf{x}'') \end{aligned} \tag{33}$$

where $\mathbf{x} \in \Omega^*$, $\mathbf{x}'$ covers Ω and $\mathbf{x}''$ denotes the point where $e''_{kl}(\mathbf{x}'')$ occurs. Let the terms in the bracket of the

left side of eqn (33) be $Q^*_{ijkl}(\mathbf{x}, \mathbf{x}')$, and the terms in the bracket of the right side of eqn (37) be $Q^p_{ijkl}(\mathbf{x}, \mathbf{x}')$. Then eqn (33) becomes

$$Q^*_{ijkl}(\mathbf{x}, \mathbf{x}')e^*_{kl}(\mathbf{x}') = (T_{ij} - C^*_{ijmn}S_{mnkl}T_{kl}) + Q^p_{ijkl}(\mathbf{x}, \mathbf{x}')e''_{kl}(\mathbf{x}'') \tag{34}$$

Solving for the eigenstrain e^*_{ij} in eqn (34) in terms of T_{ij} and e''_{ij}, it follows that

$$e^*_{ij}(\mathbf{x}') = Q^{*-1}_{ijkl}(\mathbf{x}', \mathbf{x})(T_{kl} - C^*_{klmn}S_{mnrs}T_{rs}) + Q^{*-1}_{ijmn}(\mathbf{x}', \mathbf{x})Q^p_{mnkl}(\mathbf{x}, \mathbf{x}'')e''_{kl}(\mathbf{x}'') \tag{35}$$

where $Q^{*-1}_{ijkl}(\mathbf{x}', \mathbf{x})$ is the inverse of $Q^*_{ijkl}(\mathbf{x}, \mathbf{x}')$. Note that eqn (35) reduces to eqn (23) when the plastic strain vanishes. Substituting eqn (35) into eqn (30), it follows that

$$\tau_{ij}(\mathbf{x}) = \hat{T}_{ij}(\mathbf{x}) + \hat{Q}_{ijkl}(\mathbf{x}, \mathbf{x}')e''_{kl}(\mathbf{x}) \quad \mathbf{x} \in \Omega \tag{36}$$

where

$$\hat{T}_{ij}(\mathbf{x}) = T_{ij}(\mathbf{x}) + \tilde{Q}_{ijkl}(\mathbf{x}, \mathbf{x}')Q^{*-1}_{klmn}(\mathbf{x}', \mathbf{x}'')(T_{mn} - C^*_{mnpq}S_{pqnrs}T_{rs}) \tag{37}$$

$$\hat{Q}_{ijkl}(\mathbf{x}, \mathbf{x},') = \tilde{Q}_{ijkl}(\mathbf{x}, \mathbf{x}') + \tilde{Q}_{ijmn}(\mathbf{x}, \mathbf{x}'')Q^{*-1}_{mnrs}(\mathbf{x}'', \mathbf{x}''')Q^p_{rskl}(\mathbf{x}''', \mathbf{x}') \tag{38}$$

Expressing eqn (36) in incremental form gives

$$\Delta\tau_{ij}(\mathbf{x}) = \Delta\hat{T}_{ij}(\mathbf{x}) + \hat{Q}_{ijkl}(\mathbf{x}, \mathbf{x}')\Delta e''_{kl}(\mathbf{x}') \quad \mathbf{x} \in \Omega \tag{39}$$

This equation is used to determine the incremental plastic strain $\Delta e''_{kl}(\mathbf{x}')$ as the loading progresses.

4 NUMERICAL CALCULATION OF A CROSS-PLY FIBER REINFORCED COMPOSITE

This section is to show how the method presented is applied to multi-directional fiber-reinforced composite subject to elastic–plastic radial and non-radial loadings. The numerical calculations were carried out on a (0°/90°) long fiber reinforced composite. The fiber is made of boron and the matrix is made of aluminum alloy 6061-T6. The method given is applicable to polymer matrix as well. The fiber volume in this study is taken to be 0·5. The geometric arrangement of the composite is shown in Fig. 2. Both the fiber and the matrix are assumed to be elastically isotropic and to follow von Mises criterion of plasticity. The tensile strength of Boron is 3·6 GPa (520·0 ksi) and is assumed to have no plastic strain. Its Poisson's ratio is 0·20. The mechanical properties of aluminum alloy 6061-T6 are taken from the *Military Handbook (5F) Metallic Materials and Elements for Flight Vehicle Structures* published in June 1988. The ultimate tensile strength is about 280 MPa (40·0 ksi) and Poisson's ratio is 0·3.

4.1 Von Mises criterion of plasticity

We assume the fiber and matrix to be elastically isotropic and to follow the von Mises criterion of plasticity. The effective stress and strain[22] are taken to be

$$\sigma_E = \sqrt{\frac{3}{2}\tau'_{ij}\tau'_{ij}} = \frac{1}{\sqrt{2}}[(\tau_{11} - \tau_{22})^2 + (\tau_{22} - \tau_{33})^2 + (\tau_{33} - \tau_{11})^2 + 6(\tau^2_{12} + \tau^2_{23} + \tau^2_{31})]^{1/2} \tag{40}$$

$$e''_E = \frac{\sqrt{2}}{3}[(e''_{11} - e''_{22})^2 + (e''_{22} - e''_{33})^2 + (e''_{33} - e''_{11})^2 + 6(e''^2_{12} + e''^2_{23} + e''^2_{31})]^{1/2} \tag{41}$$

where τ'_{ij} is the deviatoric stress component, i.e. $\tau'_{ij} = \tau_{ij} - \frac{1}{3}\delta_{ij}\tau_{kk}$. The yield stress is assumed to be a function of the effective plastic strain, where

$$\sigma^s(\mathbf{x}) = f(e''_E(\mathbf{x})) \; \mathbf{x} \in \Omega \tag{42}$$

The condition of loading and unloading is expressed as the following three cases:

(a) If $\sigma_E(\mathbf{x}) = \sigma^s(\mathbf{x})$ and $\Delta\sigma_E(\mathbf{x}) = \Delta\sigma^s(\mathbf{x})$, then

$$\frac{\Delta e''_{ij}}{\tau'_{ij}} = \frac{3\Delta e''_E}{2\sigma_E} = \Delta\kappa, \; \Delta\kappa > 0 \tag{43}$$

(b) If $\sigma_E(\mathbf{x}) = \sigma^s(\mathbf{x})$ but $\Delta\sigma_E(\mathbf{x}) < \Delta\sigma^s(\mathbf{x})$, then

$$\Delta\kappa = 0 \tag{44}$$

(c) If $\sigma_E(\mathbf{x}) < \sigma^s(\mathbf{x})$, then

$$\Delta\kappa = 0 \tag{45}$$

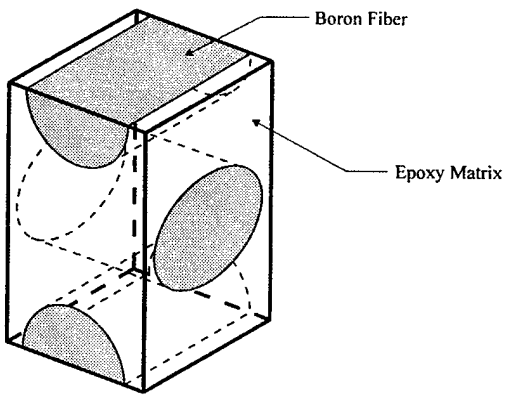

Fig. 2. Unit cell, $V_f = 50\%$.

Writing eqn (42) in incremental form,

$$\Delta\sigma^s(\mathbf{x}) = f'(e''_E(\mathbf{x}))\Delta e''_E(\mathbf{x}) \quad \mathbf{x} \in \Omega \tag{46}$$

where $f'(\cdot)$ denotes differentiation with respect to the argument. Rewriting eqn (40) in incremental form, it follows that

$$\Delta\sigma_E(\mathbf{x}) = \frac{3}{2\sigma_E(\mathbf{x})}\tau'_{ij}\Delta\tau'_{ij} \quad \mathbf{x} \in \Omega \tag{47}$$

Substituting eqns (46) and (47) into the equation $\Delta\sigma_E(\mathbf{x}) = \Delta\sigma^s(\mathbf{x}$ yields

$$\tau'_{ij}(\mathbf{x})\Delta\tau'_{ij}(\mathbf{x}) = \frac{2}{3}\sigma_E(\mathbf{x})f'(e''_E(\mathbf{x}))\Delta e''_E(\mathbf{x}) \tag{48}$$

From eqn (37), the deviatoric stress is given by

$$\tau'_{ij}(\mathbf{x}) = \hat{T}'_{ij}(\mathbf{x}) + \hat{Q}'_{ijkl}(\mathbf{x}, \mathbf{x}')e''_{kl}(\mathbf{x}') \quad \mathbf{x} \in \Omega \tag{49}$$

where prime denotes the deviatoric components, i.e.

$$\hat{T}'_{ij}(\mathbf{x}) = \hat{T}_{ij}(\mathbf{x}) - \frac{1}{3}\delta_{ij}\hat{T}_{kk}(\mathbf{x}) \tag{50}$$

$$\hat{Q}'_{ijkl}(\mathbf{x}, \mathbf{x}') = \hat{Q}_{ijkl}(\mathbf{x}, \mathbf{x}') - \frac{1}{3}\delta_{ij}\hat{Q}_{mmkl}(\mathbf{x}, \mathbf{x}') \tag{51}$$

Rewriting eqn (49) in incremental form gives

$$\Delta\tau'_{ij}(\mathbf{x}) = \Delta\hat{T}'_{ij}(\mathbf{x}) + \hat{Q}'_{ijkl}(\mathbf{x}, \mathbf{x}')\Delta e''_{kl}(\mathbf{x}') \quad \mathbf{x} \in \Omega \tag{52}$$

Substituting eqn (43) into eqn (52), it follows that

$$\Delta\tau'_{ij}(\mathbf{x}) = \Delta\hat{T}'_{ij}(\mathbf{x}) + \hat{Q}'_{ijkl}(\mathbf{x}, \mathbf{x}')\tau'_{kl}(\mathbf{x}')\Delta\kappa(\mathbf{x}'), \quad \Delta\kappa > 0 \tag{53}$$

Substituting eqns (43) and (53) into eqn (48), for $\sigma_E(\mathbf{x}) = \sigma^s(\mathbf{x})$, condition (a) above becomes: If

$$\tau'_{ij}(\mathbf{x})\Delta\hat{T}'_{ij}(\mathbf{x}) + \tau'_{ij}(\mathbf{x})\hat{Q}'_{ijkl}(\mathbf{x}, \mathbf{x}')\tau'_{kl}(\mathbf{x})\Delta\kappa(\mathbf{x}) = \left[\frac{2}{3}\sigma_E(\mathbf{x})\right]^2 f'(e''_E(\mathbf{x}))\Delta\kappa(\mathbf{x}) \tag{54}$$

then

$$\Delta\kappa(\mathbf{x}) > 0$$

Following a similar procedure using eqn (44) in place of eqn (43), for $\sigma_E(\mathbf{x}) = \sigma^s(\mathbf{x})$, condition (b) above becomes: If

$$\tau'_{ij}(\mathbf{x})\Delta\hat{T}'_{ij}(\mathbf{x}) + \tau'_{ij}(\mathbf{x})\hat{Q}'_{ijkl}(\mathbf{x}, \mathbf{x}')\tau'_{kl}(\mathbf{x})\Delta\kappa(\mathbf{x}) < \left[\frac{2}{3}\sigma_E(\mathbf{x})\right]^2 f'(e''_E(\mathbf{x}))\Delta\kappa(\mathbf{x}) \tag{55}$$

then

$$\Delta\kappa(\mathbf{x}) = 0$$

4.2 Numerical integration of influence coefficients

For numerical calculation, the basic block (i.e. unit cell) is divided into elements as shown in (Fig. 3). These elements are quadrilateral prism elements, and each element is made of two triangular prism elements (Fig. 4). These elements are used for numerical integrations of eqn (12). They are not for finite element analysis, hence they do not need to satisfy the requirements of the elements in FEM analysis.[26] Since the heterogeneous solid is transformed into a homogeneous one using Eshelby's method of equivalent inclusion,[1] the residual stress field in the composite is calculated by using the influence coefficients $Q_{ijkl}(p, q)$ caused by $e''_{kl}(q)$ or $e^*_{kl}(q)$.

Including the eigenstrain $e^*_{kl}(q)$ in eqn (11) yields

$$\tau^R_{ij}(p) = Q_{ijkl}(p, q)[e''_{kl}(q) + e^*_{kl}(q)] \tag{56}$$

There is a discontinuous change of C_{ijkl} to C^*_{ijkl} at the interface of matrix and fiber. This jump of elastic con-

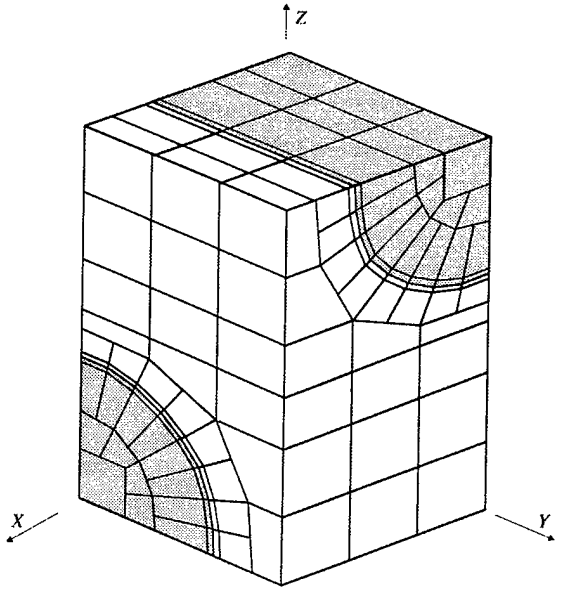

Fig. 3. Mesh of one-eighth of unit cell.

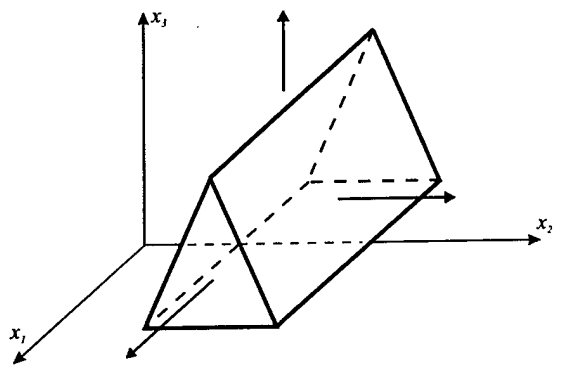

Fig. 4. Triangular prism parallel to the x_i-axis, one of fiber orientation.

stants will induce the eigenstrains, which cause equivalent surface forces at the interfaces. To represent the surface force accurately, thin elements are used. From eqn (12), the influence coefficients are represented as

$$Q_{ijkl}(p, q) = \Phi_{ijmn}(p, q)C_{mnkl} - \frac{1}{V_p}(V_p \cap V_q)C_{ijkl} \quad (57)$$

where

$$\Phi_{ijkl}(p, q) = -\frac{1}{V_p}\int_{\Omega_p}\left[\int_{\Gamma_q} K_{ijk}(\mathbf{x}, \mathbf{x}')C_{mnkl}\eta_n(\mathbf{x}')d\Gamma(\mathbf{x}')\right]dV(\mathbf{x})$$

$$V_p \cap V_q = \begin{cases} 1, & p = q \\ 0, & p \neq q \end{cases}$$

For isotropic elastic solids, the elastic constants C_{ijkl} are given in eqn (5). Substituting eqn (5) into eqn (57) gives

$$Q_{ijkl}(p, q) = \lambda\Phi_{ijmn}\delta_{kl} + \mu(\Phi_{ijkl} + \Phi_{ijlk}) - \frac{1}{V_p}(V_p \cap V_q)[\lambda\delta_{ij}\delta_{kl} + \mu(\delta_{ik}\delta_{jl} + \delta_{il}\delta_{jk})] \quad (58)$$

Substituting eqn (8) into eqn (57)

$$\Phi_{ijkl} = \frac{3}{8\pi(1-\nu)}\varphi_{ijkl} - \frac{1-2\nu}{8\pi(1-\nu)}(\delta_{ij}\psi_{kl} - \delta_{jk}\psi_{il} - \delta_{ik}\psi_{jl}) \quad (59)$$

where

$$\varphi_{ijkl}(p, q) = -\frac{1}{V_p}\int_{\Gamma_q}\left[\int_{\Omega_p}\frac{(x_i - x_i')(x_j - x_j')(x_k - x_k')}{r^5}dV(\mathbf{x})\right]\eta_l(\mathbf{x}')d\Gamma(\mathbf{x}')$$

$$\psi_{kl}(p, q) = \frac{1}{V_p}\int_{\Gamma_q}\left[\int_{\Omega_p}\frac{(x_k - x_k')}{r^3}dV(\mathbf{x})\right]\eta_l(\mathbf{x})d\Gamma(\mathbf{x}')$$

Let

$$A(p, x') = \frac{1}{V_p}\int_{\Omega_p}\frac{(x_k - x_k')}{r^3}dV(\mathbf{x}), \quad k = 1, 2, 3 \quad (60)$$

$$B_{ijk}(p, \mathbf{x}') = \frac{1}{V_p}\int_{\Omega_p}\frac{(x_i - x_i')(x_j - x_j')(x_k - x_k')}{r^5}dV(\mathbf{x}), \quad i, j, k = 1, 2, 3 \quad (61)$$

Expressing eqns (60) and (61) in cylindrical co-ordinates, $A(p, x')$ and $B_{ijk}(p, \mathbf{x}')$ are integrated over the

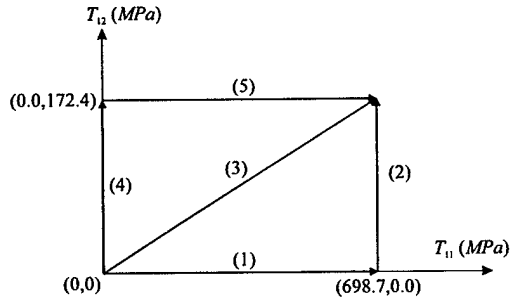

(1) Pure Tension.

(2) Shear after tension up to $T_{11} = 698.7$ *MPa* giving shear strain and additional plastic strain.

(3) Combined tension and shear loading $T_{12}/T_{11} = 25/100$.

(4) Pure Shear.

(5) Tension after shear up to $T_{12} = 172.4$ *MPa* giving tensile strain and additional plastic strain.

Fig. 5. Loading paths.

triangular prism element as shown in Fig. 4.[27] By this way, the influence coefficients $Q_{ijkl}(p, q)$ are calculated. With the assumption that identical basic blocks are repeated in the composite, the incremental plastic strain $\Delta e''_{ij}(\mathbf{x})$ and eigenstrain $\Delta e^*_{ij}(\mathbf{x})$ in the neighboring blocks are taken to be the same as those in the center block. The sum of the residual stresses due to plastic strains and eigenstrains in all those neighboring blocks is given in eqn (30), and the incremental stress $\Delta\tau_{ij}$ is given by eqn (39). This approach satisfies both the equilibrium and compatibility conditions.

As the loading, T_{ij}, increased, the number of elements with stress reaching the yielding stress increases. These elements are known as the potential active elements. Among these elements, the element that yields $\Delta\kappa > O$ slides and develops plastic strains (Condition (a)) and other elements that give $\Delta\kappa = 0$ will not reach yield point (Condition (b)). To find this set of yielding elements, the Simplex Method[28,29] is used. This method is especially useful in the calculations under non-proportional loadings by the above described method. The isolation of an unit cell and specifying its boundary conditions for stress analysis is not required.

4.3 Numerical results

The fibers and matrix are assumed to have perfect bonding. The unit cell of the composite is divided into grids for numerical calculations, as shown in Fig. 3. The variation of the microstress and microstrain

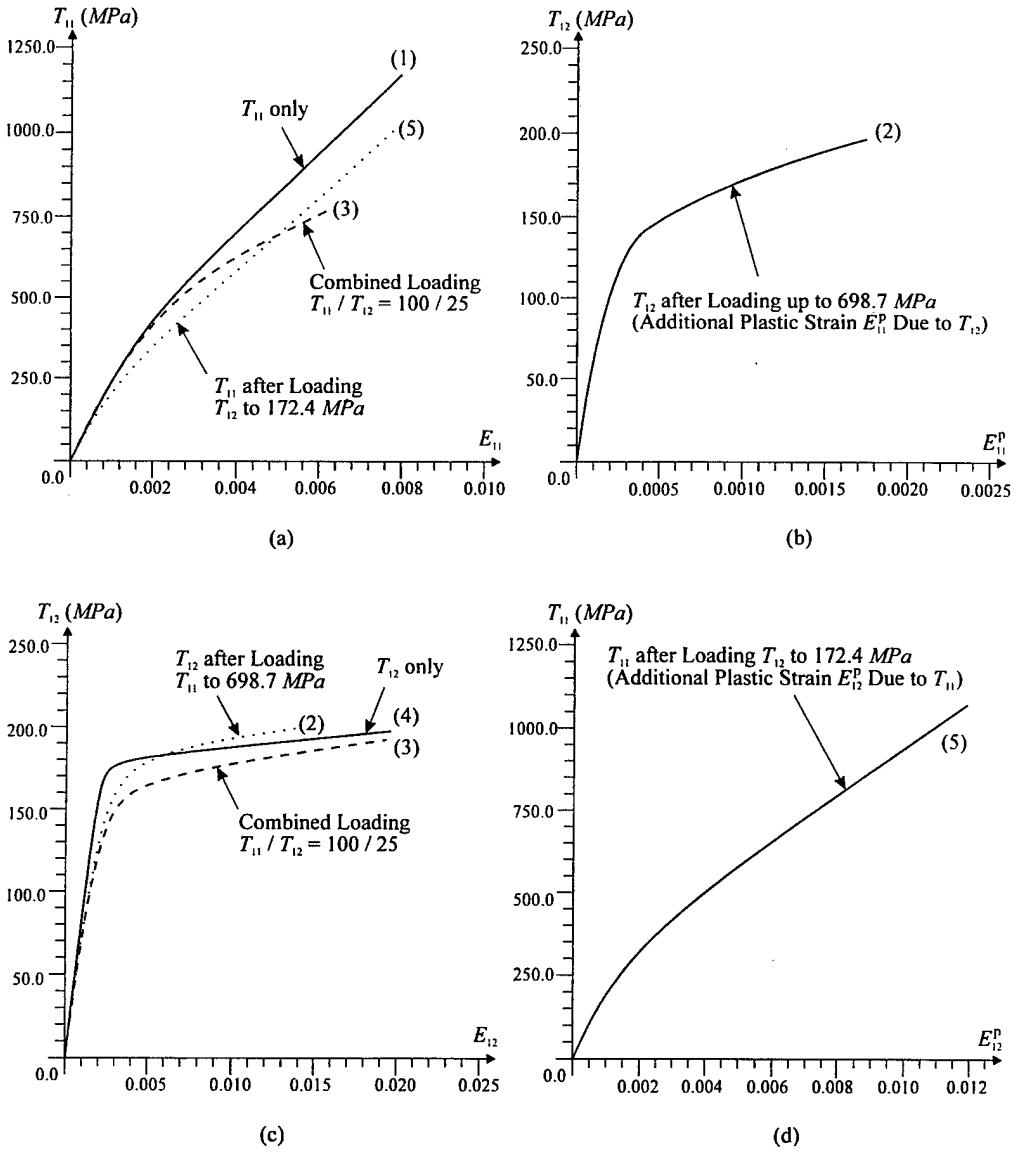

Fig. 6. Macroscopic stress/strain relationship under different loadings.

components in the fibers and matrix under five different proportional and non-proportional loadings as indicated in Fig. 5 are evaluated. These stress and strain components are used to calculate the effective stress and the effective plastic strain from which the first failure mode can be identified.

Under these five loading conditions, the macroscopic stress, T_{ij}, and strain, E_{ij}, are calculated from the corresponding microscopic stress and strain fields and are plotted in Fig. 6. For the cases with small strain-hardening, the variation of the effective stress is much less than that of the effective plastic strain. Hence, the effective plastic strain instead of the effective stress are plotted. Figure 7 shows the case of pure tension loading $T_{11} = 906{\cdot}3\,\text{MPa}$ and Fig. 8 shows the case of pure shear loading $T_{12} = 180{\cdot}8\,\text{MPa}$.

5 CONCLUSIONS AND DISCUSSIONS

This paper provides a micromechanical analysis of fibre-reinforced cross-ply composite under incremental combined axial and shear non-proportional loadings. In the present method, the inhomogenous composites are transformed into homogenous solids using Eshelby's equivalent inclusion method, i.e. an extra eigenstrain's e^*_{ij} is introduced. This transformation was used by Dvorak *et al.*[18] in their analysis of unidirectionally reinforced composites. After the transformation, the stress fields caused by plastic strain and the eigenstrain are calculated using Kelvin's solution of the displacement field caused by a body force F_i in an infinite elastic solid. There is no need to isolate a "unit cell" from the bulk of the periodic composite and the difficulty of

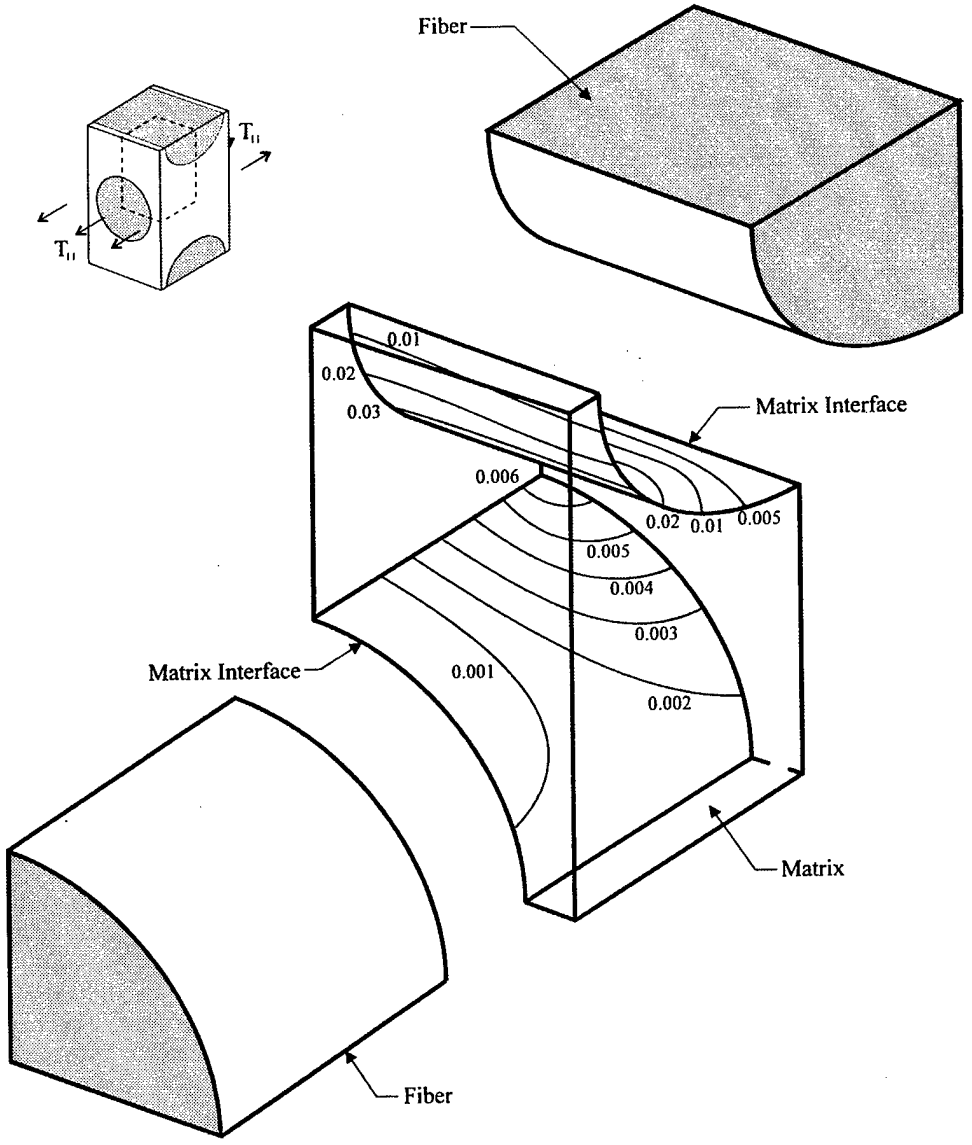

Fig. 7. Effective plastic strain distribution at interfaces under tension $T_{11} = 906{\cdot}3\,\text{Mpa}$ and $E_{11} = 0{\cdot}0059$.

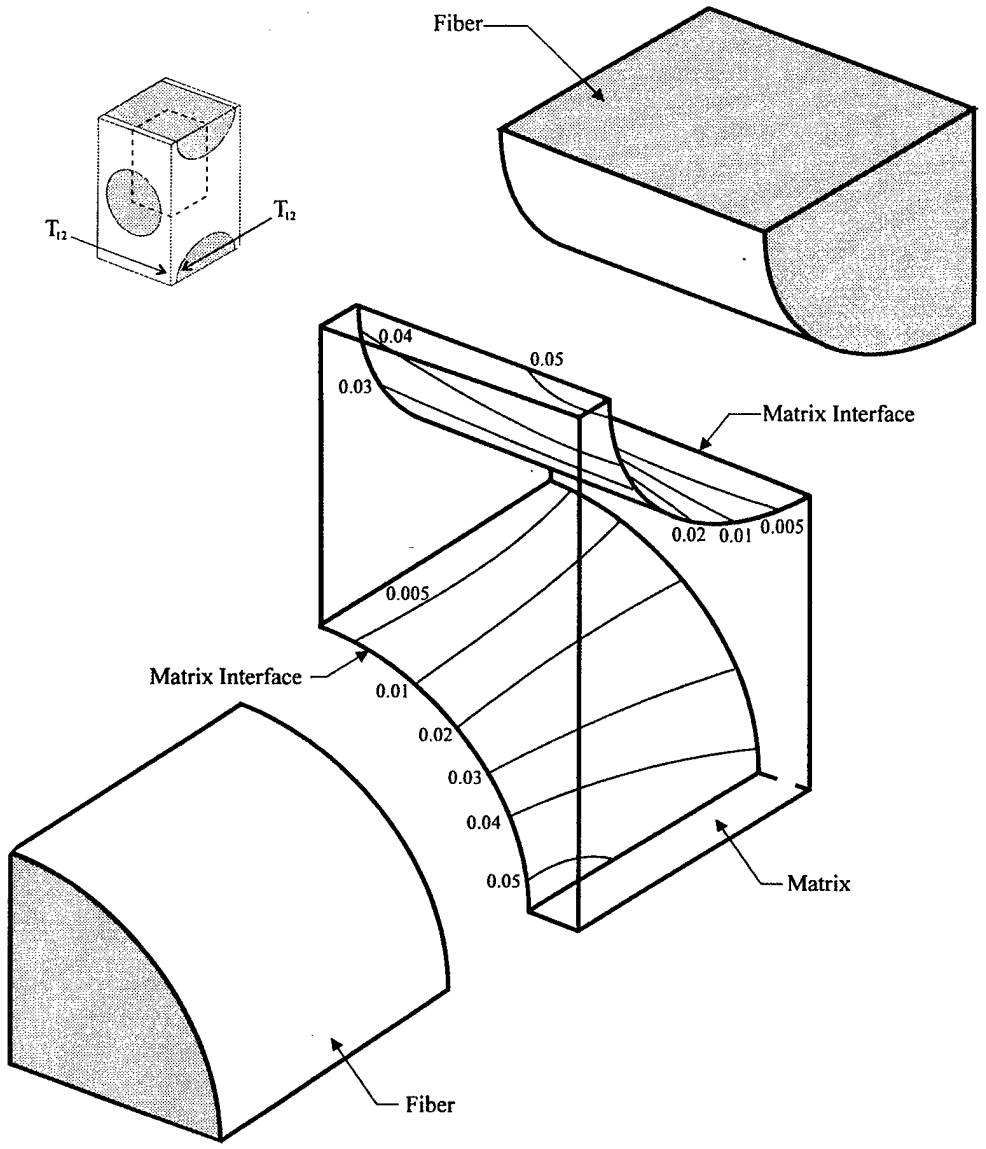

Fig. 8. Effective plastic strain distribution at interfaces under shear $T_{12} = 180{\cdot}8$ Mpa and $E_{12} = 0{\cdot}0049$.

defining appropriate boundary conditions on the unit cell commonly required in the micromechanics finite-element method is eliminated.

Fibre reinforced composites have many possible failure modes such as fibre breakage, matrix cracking, fiber/matrix debonding, compression buckling in fibres, etc. The analysis presented here is mainly for the composites before any of these failures occurs. However, from the microscopic stress and strain fields, we can determine the loading, at which the first failure mode starts. The numerical results leading to the first failure mode should guide us in preventing or delaying the failure.

Highly localized plastic strain generally does not cause global failure. As pointed out by Clyne and Withers[30] that the overall yield stresss of composite is governed not so much by localized yielding, but rather by the attainment of an average plastic deformation sufficient for the global yielding. The approach presented in this study is to calculate the load to cause the spread of the plastic zone to a greater area. The global yielding will indicate the start of a failure mode. The plastic strain intensity and the extent of the plastic zones at different stages of loading will show the damage levels as well as the residual strength of the composite. Since structures are generally designed for final (global) failure, these damage levels in composite materials can be used in design of the composite structures. This approach can also be applied to the analysis of composites with thermal strains, as shown by Bigelow[31] and other inelastic strains.

Nigam *et al.*[32] have performed experiments in elastic–plastic behavior of an uni-directional fiber reinforced

composite. The present derivations can be simplified for unidirectional fiber composites. Micromechanic analysis of the composite will be performed and the calculated results will be compared with the experimental data.

ACKNOWLEDGEMENTS

The research was partially supported by US Air Force Office of Scientific Research (AFOSR). The authors are grateful for comments of the referees and very helpful discussions with N. J. Teng and K. Wong.

REFERENCES

1. Mura, T., *Micromechanics of Defects in Solids*. Martinus Nijhoff Publishers, The Hague, 1982.
2. Lin, T. H., Physical theory of plasticity. *Adv. Appl. Mech.*, 1971, **11**, 255–311.
3. Adams, D. F., Composite micromechanics. *Int. Encyclopedia of Composites*, 1990, **1**, 441.
4. Hashin, Z. and Shtrikman, S., A variational approach to the theory of elastic behavior of multiphase materials *J. Mech. Phys. Solids* 1963 **Mar–Apr.**, pp. 127–140.
5. Hashin, Z. and Rosen, B. W., The elastic noduli of fiber-reinforced material. *J. Appl. Mech.*, 1964, **31**, 223–232.
6. Hill, R., Elastic properties of reinforced solids: some theoretical principles. *J. Mech. Phys. Solids*, 1963, **12**, 199–212.
7. Budiansky, B., On the elastic moduli of some heterogeneous materials. *J. Mech. Phys. Solids*, 1965, **13**, 223–232.
8. Walpole, L. J., On the overall elastic moduli of composite materials. *J. Mech. Phys. Solids*, 1969, **17**, 235.
9. Willis, J. R., Bounds and self-consistent Estimates for the overall properties of anisotropic composites. *J. Mech. Phys. Solids*, 1977, **25**, 185.
10. Weng, G. J., Explicit evaluation of Willis Bounds in the ellipsoidal inclusions. *Int. J. Eng Sci.*, 1992, **30**(6), 83–92.
11. Teply, J. L. and Dvorak, G. J., Bounds on overall instantaneous properties of elastic–plastic composites. *J. Mech. Phys. Solids*, 1988, **36**(1), 29–58.
12. Drucker, D. C., A more funamental approach to plastic stress–strain measurements. In *Proc. First U.S. Natl. Congress Appl. Mech.*, 1951, p. 487.
13. Martin, J. B., *Plasticity: Fundamentals and General Results*. The MIT Press, Cambridge, MA, 1975.
14. Scheirer, S. T. and Toth, I. J., *The mechanical behavior of metal matrix composites*. AFML-TR-73-178 1973, p. 25.
15. Walker, K. P., Jordan, E. H. and Freed, A. D., Nonlinear mesomechanics of composites with periodic microstructure. Girst Report, NASA, Tech Memorandum 102051, 1989.
16. Nemat-Nasser, S. and Hori, M., *Micromechanics: Overall Properties of Heterogeneous Materials*. Elsevier Science Publishers, Amsterdam, 1993.
17. Dvorak, G. J. and Teply, J. L., Periodic hexagonal array models for plasticity analysis of composite materials. In *Modeling, Method and Applications*, ed. Sawzak and Bianchi. W. Olszak Memorial Volume, UK, 1985.
18. Dvorak, G. J., Bakei-El-Din, Y. A. and Wafa, A. M., The modeling of inelastic composite materials with the transformation field analysis. *Modeling Simulation Mat. Sci. Eng*, 1994, **2**, 571–586.
19. Sokolnikoff, I. S., *Mathematical Theory of Elasticity*. McGraw-Hill, 1965, p. 336.
20. Wu, X. Q., Development of the general theories and discrete methods of polycrystalline plasticity. Ph.D. Dissertation in Civil Engineering UCLA, 1989.
21. Hill, R., The mechanics of quasi-static plastic deformation in metals. In *Surveys in Mechanics*, G.L. Taylor 70th Anniversary Volume. Cambridge University Press, Cambridge, 1957, pp. 7–31.
22. Lin, T. H., *Theory of Inelastic Structures*. John Wiley, New York, 1968, pp. 32–54.
23. Lin, T. H. and Ribeiro, G. E., Development of a physical theory of plasticity. *Int. J. Solids Struct.*, 1981, **17**, 545–551.
24. Eshelby, J. D., The determination of elastic field of an ellipsoidal inclusion and related problems. *Proc. Roy. Soc. A*, 1957, **241**, 398.
25. Lin, T. H. and Ito, Y. M., Theoretical plastic stress-strain relationship of a polycrystal and comparison with von Mises' and Tresca's plasticity theories. *Int. J. Eng Sci.*, 1966, **4**, 543–561.
26. Gallagher, C. H., *Finite Element Analysis-Fundamentals*. Prentice Hall, Englewood Cliffs, NJ, 1975, p. 212.
27. Zhong, W., An elasto-plastic constitutive behavior of a cross-ply fiber reinforced composite. Ph.D. dissertation in Civil Engineering, UCLA 1995.
28. Guldenpfenning, J. and Clifton, R. J., On the computation of plastic stress-strain relations for polycrystalline metals. *Computer Methods Appl. Mech. Eng.*, 1977, **10**, 141–149.
29. Haftka, R. T. and Kamat, M. P., *Elements of structural optimization*. Martinus Nijhoff Publishers, The Hague, 1990, pp. 79–86.
30. Clyne, T. W. and Withers, P. J., *An Introduction to Metal Matrix Composites*. Cambridge University Press, Cambridge, 1993.
31. Bigelow, C. A., Thermal residual stresses in a silicon-carbide/titannium [0/90] laminate. *J. Compos. Technol. Res.*, 1993, **15**(4), 304–310.
32. Nigan, H., Dvorak, G. J. and Bahei-El-Din, V. A., An experimental investigation of elastic–plastic behavior of a fiberous boron-aluminum composite I and II. *Int. J. Plasticity*, 1994, **10**(1), 23–66.

Reprinted from

MATERIALS SCIENCE & ENGINEERING A

Materials Science and Engineering A246 (1998) 169–179

Micromechanic analysis of fatigue band crossing grain boundary

T.H. Lin [a,*], K.K.F. Wong [a], N.J. Teng [1,a], S.R. Lin [b]

[a] *Department of Civil and Environmental Engineering, University of California, Los Angeles, CA, USA*
[b] *The Aerospace Corporation, El Segundo, CA 90095 1593, USA*

Received 6 June 1997; received in revised form 5 September 1997

ELSEVIER

MATERIALS SCIENCE AND ENGINEERING A

The journal provides an international medium for the publication of theoretical and experimental studies and reviews of the properties and behavior of a wide range of materials, related both to their structure and to their engineering application. The varied topics comprising materials science and engineering are viewed as appropriate for publication: these include, but are not limited to, the properties and structure of crystalline and non-crystalline metals and ceramics, polymers and composite materials.

Types of contributions

Original research work not already published; plenary lectures and/or individual papers given at conferences; reviews of specialized topics within the scope of the journal; engineering studies; letters to the editor.

Subscription Information 1998

Volumes 239–255, each volume containing 2 issues, are scheduled for publication. Prices are available from the publishers upon request. Subscriptions are accepted on a prepaid basis only. Issues are sent by SAL (Surface Air Lifted) mail wherever this service is available. Airmail rates are available upon request.

Orders, claims, and product enquiries: please contact the Customer Support Department at the Regional Sales Office nearest you:

New York
Elsevier Science
P.O. Box 945
New York, NY 10159-0945, USA
Tel.: (+1) 212-633-3730
[Toll free number for North American customers: 1-888-4ES-INFO (437-4636)]
Fax: (+1) 212-633-3680
E-mail: usinfo-f@elsevier.com

Amsterdam
Elsevier Science
P.O. Box 211
1000 AE Amsterdam
The Netherlands
Tel.: (+31) 20-4853757
Fax: (+31) 20-4853432
E-mail: nlinfo-f@elsevier.nl

Tokyo
Elsevier Science
9–15 Higashi-Azabu 1-chome
Minato-ku, Tokyo 10600
Japan
Tel.: (+81) 3-5561-5033
Fax: (+81) 3-5561-5047
E-mail: info@elsevier.co.jp

Singapore
Elsevier Science
No. 1 Temasek Avenue
#17-01 Millenia Tower
Singapore 039192
Tel.: (65) 434-3727
Fax: (+65) 337-2230
E-mail: asiainfo@elsevier.com.sg

Abstracting and/or Indexing Services

American Ceramic Society; Cambridge Scientific Abstracts; Chemical Abstracts; Current Contents; Engineering Index; FIZ Karlsruhe; Fluid Abstracts; Fluidex; Glass Technology Abstracts; Inspec/Physics Abstracts; Metals Abstracts; Pascal (Centre National de la Recherche Scientifique); Physikalische Berichte; Research Alert™; Science Citation Index.

Advertising information: Advertising orders and enquiries may be sent to: **International**: Elsevier Science, Advertising Department, The Boulevard, Langford Lane, Kidlington, Oxford OX5 1GB, UK. Tel.: (+44)(0)1865 843565. Fax: (+44)(0)1865 843976. **USA and Canada**: Elsevier Science Inc., Mr. Tino DeCarlo, 655 Avenue of the Americas, New York, NY 10010-5107, USA. Tel.: +1 (212) 633 3815. Fax: +1 (212) 633 3820; E-mail: t.decarlo@elsevier.com. **Japan**: Elsevier Science Japan, Marketing Services, 1-9-15 Higashi-Azabu Minato-ku, Tokyo 10600, Tel: (+81)3-5561-5033; Fax: (+81)3-5561-5047.

ELSEVIER

Materials Science and Engineering A246 (1998) 169–179

MATERIALS SCIENCE & ENGINEERING A

Micromechanic analysis of fatigue band crossing grain boundary

T.H. Lin [a,*], K.K.F. Wong [a], N.J. Teng [1,a], S.R. Lin [b]

[a] *Department of Civil and Environmental Engineering, University of California, Los Angeles, CA, USA*
[b] *The Aerospace Corporation, El Segundo, CA 90095 1593, USA*

Received 6 June 1997; received in revised form 5 September 1997

Abstract

Displacement of dislocations in metals causes plastic strain which is often highly localized and produces fatigue bands under cyclic loadings. Inside these bands, highly concentrated dislocation pile-ups develop at the grain boundary, causing severe resolved shear stress exceeding the critical shearing stress. This excessive stress is relieved either by nucleation of crack at the grain boundary or by forming another fatigue band in the neighboring crystal. Micromechanic analyses were performed on a fatigue band in a most favorably oriented crystal and an adjacent crystal with a slightly different orientation. Two cases were analyzed: (1) The most favorably oriented crystal with a sliding direction making 45° with the free surface in an aluminum polycrystal; and (2) Two adjacent crystals with sliding directions parallel to the free surface of a copper polycrystal subject to variable loadings. Results show that the amount of slip that propagates across the grain boundary reduces rapidly with the difference in orientations between the two crystals. In (2), two sequences of loadings were calculated: one is a low-amplitude loading followed by a high-amplitude loading (LH) and the other is a high-amplitude loading followed by a low-amplitude loading (HL). The LH sequence shows that the low-amplitude loading has no significant effect on the deformation in the subsequent high-amplitude loading. On the other hand, in the HL sequence, the high-amplitude loading has significant effect on the deformation in the low-amplitude loading. All these analytical results agree well with experimental observations.

Keywords: Cyclic loading; Plastic strain; Misorientation of adjacent crystals; Crack initiation

1. Introduction

Single crystal tests show that under loading, slip occurs along certain directions on certain planes. This slip depends on the resolved shear stress and is independent of the normal stress on the sliding plane. The dependence of slip on the resolved shear stress, known as Schmid's law, had been shown by Parker [1] to hold also for cyclic loadings. When a cyclic loading is applied to a polycrystal, the individual grains begin to show fine slip markings. As the loading continues, some of these lines intensify, forming persistent slip bands (PSBs). The intense slip bands have been shown to be the source of subsequent fatigue cracks. Plastic strains are concentrated in these bands and the macroscopic plastic strain depends on the slip of all bands in all crystals. Ductility of the metal (i.e. the amount of deformation the metal can sustain before crack initiates) depends on the amount of all localized plastic strains and therefore the spread of plastic strain from one crystal to another has important effects on the ductility of metals.

Plastic strain in a slip band is due to displacement of dislocations. When a pile-up of dislocations pushes against a grain boundary, the leading dislocation is acted upon not only by the applied stress, but also by the interactive force produced by other dislocations in the pile-up. Thus a concentrated force (proportional to the applied stress and to the number of dislocations in the pile-up) develops at the leading dislocation. When the pile-up contains many dislocations, an extremely high resolved shear stress develops at the forefront of the pile-up at moderate applied stress. This high resolved shear stress can initiate yielding in the neighboring crystal or nucleate a crack at the grain boundary [2].

* Corresponding author. Tel.: +1 310 8251679; fax: +1 310 2062222.

[1] Current address: Universal Analytic Inc., Torrance, CA, USA.

0921-5093/98/$19.00
PII S0921-5093(97)00692-8

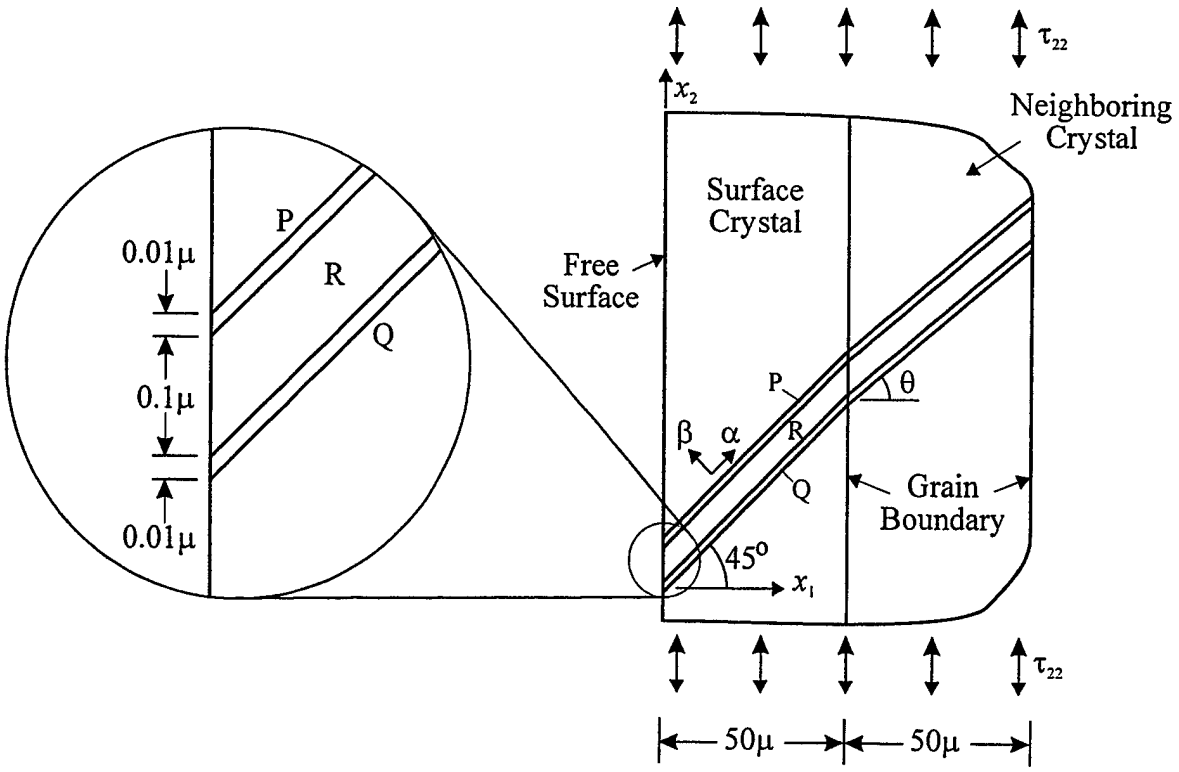

Fig. 1. Polycrystal with a fatigue band across grain boundary.

Surface grains are the most likely locations for fatigue crack initiation in metals and alloys of high purity. However, in engineering components made of commercial materials, fatigue cracks initiate both at the surface and in the interior [3]. Fatigue crack initiation in wavy slip single-phase materials was previously believed to occur transgranularly by slip-band cracking in PSBs at low amplitude of loadings and intergranularly at high amplitude of loadings [4]. However, Mughrabi's recent work [5–7] on copper polycrystal fatigued at constant plastic strain amplitudes at room temperature has shown that cracks also initiate at grain boundaries in high-cycle (low amplitude) range and were induced by PSB's impinging on the grain boundary. Figueroa and Laird [8] have shown in their copper polycrystals fatigue tests that grain boundaries provide the preferential sites for crack initiation in both high and low strain amplitude tests. They have also studied fatigue damage under variable loadings. They found that fatigue crack nucleation sites at low amplitudes are controlled by the localization of plastic strain during the fatigue process and thus no major difference is expected in the nucleation mechanism when the fatigue specimen is subjected to constant plastic strain or constant stress. Hence the analysis for constant stress is expected to be able to explain the crack nucleation occurring under constant plastic strain.

The micromechanic analysis using the ratchet mechanism developed by Lin [9] has successfully explained many experimental observations of fatigue crack initiation. The same analysis is used in the present study to analyze the propagation of fatigue band across the grain boundary. Three cases are considered:

(1) A fatigue band in the most favorably oriented crystal at a free surface of a pure aluminum polycrystal and an interior crystal adjacent to the surface crystal with a slightly different orientation, as shown in Fig. 1. Under this configuration, the sliding direction intersects the free surface.

(2) A fatigue band in a most favorably oriented crystal and an adjacent crystal of a slightly different orientation with slip directions parallel to the free surface of a copper polycrystal, as shown in Fig. 2. An initial strain $e^{i}_{\alpha\alpha}$ is assumed to exist in R of the fatigue band.

(3) Two sequences of variable-amplitude cyclic loadings: one is a low-amplitude loading followed by a high-amplitude loading (LH) and the other is a high-amplitude loading followed by a low-amplitude loading (HL).

2. Fatigue band in crystals with sliding direction intersecting the free surface

Extrusions and intrusions grow monotonically on fatigued specimens [10]. Kinematically, an extrusion forms when a positive shear strain occurs in a thin slice

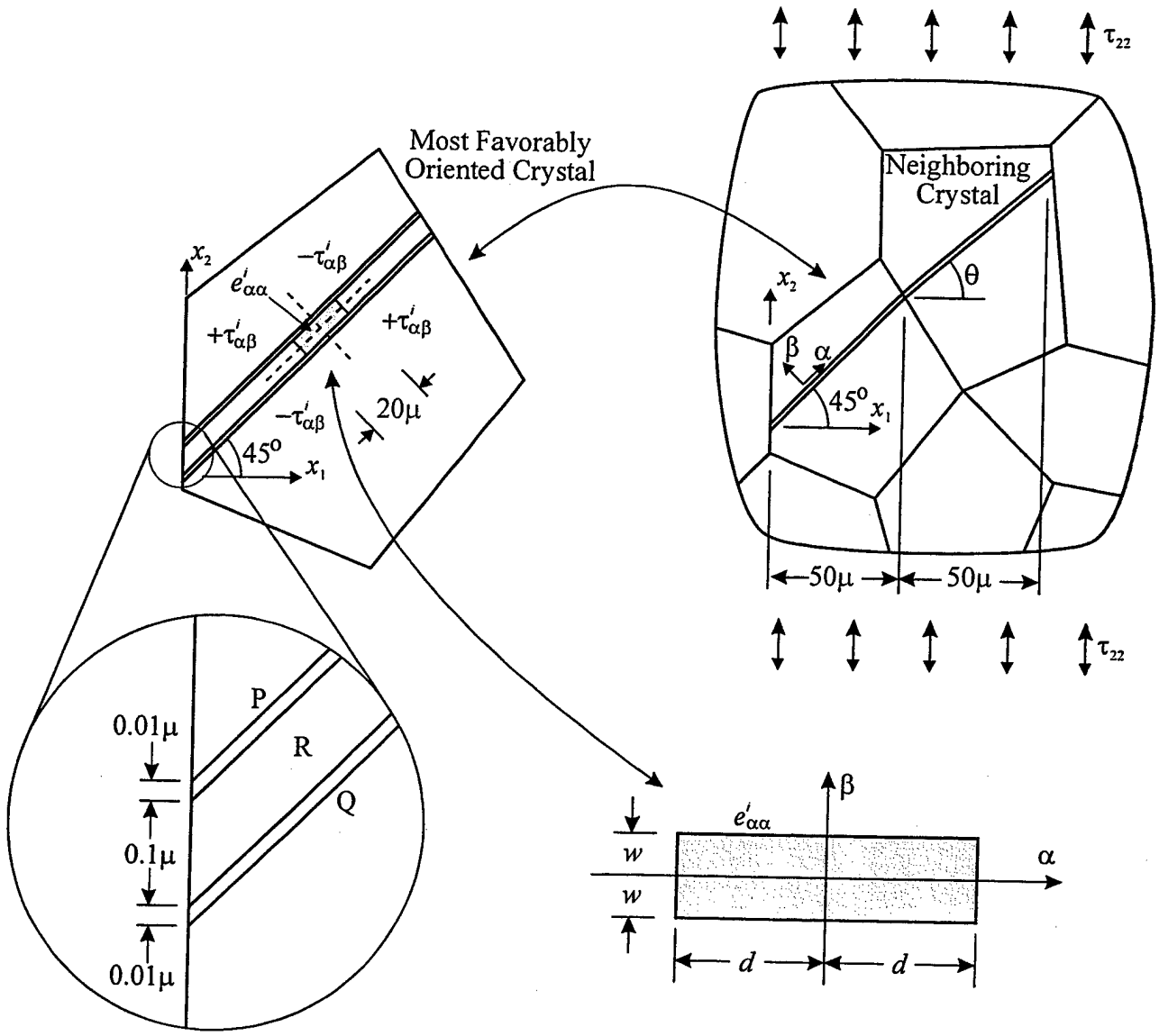

Fig. 2. Polycrystal with a fatigue band parallel to free surface.

P and a negative shear strain in a closely located thin slice Q (see Fig. 1). All metals have defects which cause an initial stress field. The initial stress field, τ^i, favorable to this mode of slip (i.e. positive shear strain in P and negative in Q) is one having positive shear stress in P and negative in Q. Such an initial stress field can be provided by an initial tensile strain, $e^i_{\alpha\alpha}$ in R along the slip direction α. Lin and Ito [10] suggested in 1967 that the tensile strain $e^i_{\alpha\alpha}$ in R may be provided by a row of interstitial dipoles.

During cyclic loading (Fig. 1), a tensile loading of σ_{22} on the polycrystal produces a positive applied stress τ^a in the whole crystal. For τ^i that is positive in P and negative in Q, the resolved shear stress, $\tau^i + \tau^a$, in P reaches the critical shear stress, τ^c, first and causes P to slide. This slip causes a residual shear stress τ^r. Assuming no strain hardening, the critical shear stress τ^c remains constant. The plastic strain resulting from this slip is taken to be constant along the x_3-direction (normal to the plane of Fig. 1) and therefore the deformation was considered to be of plane strain.

In the calculation of the residual stress, τ^r, the analogy between plastic strain and applied force was employed [11]. The body force per unit volume along the x_i-direction due to plastic strain e''_{ij} in an isotropic elastic body is

$$F_i = -(\lambda e''_{kk,i} + 2\mu e''_{ij,j}) \quad (1)$$

where λ and μ are Lame's constants. The repetition of an alphabetic subscript denotes summation and the subscript after a comma denotes differentiation with respect to the coordinate variable. The equivalent surface force per unit area along the x_i-direction due to plastic strain e''_{ij} is

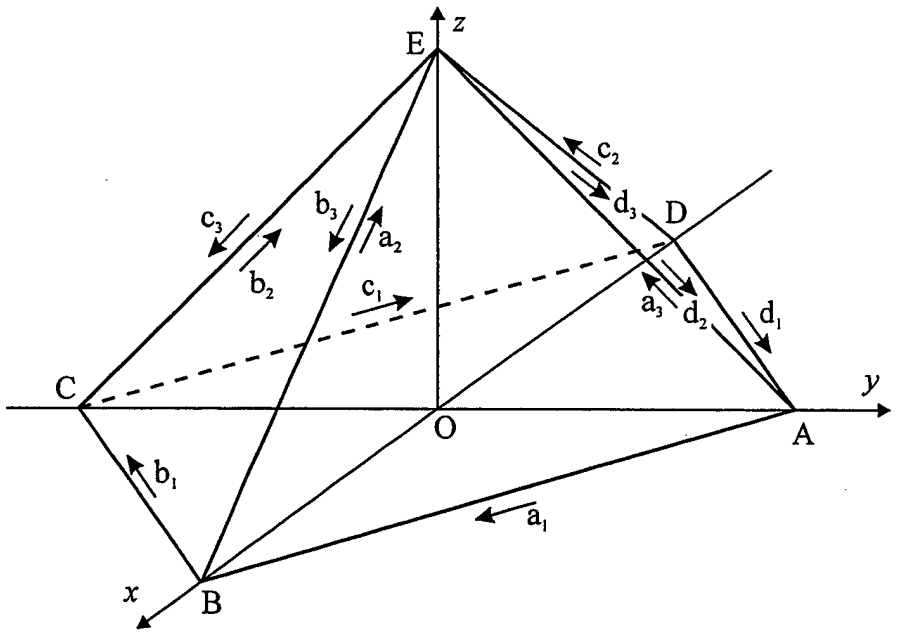

Fig. 3. Crystallographic direction of a f.c.c. crystal.

$$S_i = (\lambda\delta_{ij}e''_{kk} + 2\mu e''_{ij})\eta_j \tag{2}$$

where δ_{ij} is the Kronecker delta and η_j is the direction cosine of the angle between the exterior normal to the surface and the x_j-axis.

Since the fatigue band intersects the free surface and the polycrystal is assumed to be of fine grain, the equivalent forces are considered to act in a semi-infinite solid. Melan [12] had developed a plane stress solution of the stress field due to a point force applied in a semi-infinite plate and his solution was later modified by Tung and Tung and Lin [13] for plane strain. Let $\tau_{ij}(\boldsymbol{x}, \boldsymbol{x}'_k)$ be the stress at point x due to a unit force applied at point x' along the x_k-direction. The stress components are expressed in terms of the Airy stress functions, ϕ_k's, as

$$\tau_{11}(\boldsymbol{x}, \boldsymbol{x}'_k) = \frac{\partial^2\phi_k}{\partial x_2^2}, \qquad \tau_{22}(\boldsymbol{x}, \boldsymbol{x}'_k) = \frac{\partial^2\phi_k}{\partial x_1^2},$$

$$\tau_{12}(\boldsymbol{x}, \boldsymbol{x}'_k) = \frac{\partial^2\phi_k}{\partial x_1\partial x_2}, \quad k = 1, 2 \tag{3}$$

where

$$\phi_1(\boldsymbol{x}, \boldsymbol{x}') = -(p+q)(x_2 - x'_2)(\theta_1 + \theta_2) + \frac{1}{2}q(x_1 - x'_1)\ln\frac{X_1}{X_2} + 2p\frac{x_1x'_1(x_1 + x'_1)}{X_2}$$

$$\phi_2(\boldsymbol{x}, \boldsymbol{x}') = -(p+q)(x_2 - x'_2)(\theta_1 + \theta_2) + \frac{1}{2}q(x_2 - x'_2)\ln\frac{X_1}{X_2} - 2p\frac{x_1x'_1(x_2 - x'_2)}{X_2} \tag{4}$$

$$p = \frac{1}{4\pi(1-\upsilon)}, \qquad q = p(1-2\upsilon)$$

$$X_1 = (x_1 - x'_1)^2 + (x_2 - x'_2)^2,$$

$$X_2 = (x_1 + x'_1)^2 + (x_2 - x'_2)^2$$

$$\theta_1 = \arctan\left(\frac{x_2 - x'_2}{x_1 - x'_1}\right) \quad -\pi \le \theta_1 \le \pi,$$

$$\theta_2 = \arctan\left(\frac{x_2 - x'_2}{x_1 + x'_1}\right) \quad -\frac{\pi}{2} \le \theta_2 \le \frac{\pi}{2} \tag{5}$$

and υ is the Poisson's ratio. By dividing the fatigue band into N grids, the resolved shear stress, $\tau(m)$, in the mth grid due to a unit plastic strain, $e''(n)$, in the nth grid was obtained using the solution given in Eqs. (3)–(5). After the occurrence of slip in this band, the resolved shear stress is

$$\tau = \tau^{\mathrm{i}} + \tau^{\mathrm{a}} + \tau^{\mathrm{r}} \tag{6}$$

Let the resolved shear stress exceeding the critical stress be referred to as the excessive shear stress, τ^{E}, i.e.

$$\tau^{\mathrm{E}} = \tau - \tau^{\mathrm{c}} = \tau^{\mathrm{i}} + \tau^{\mathrm{a}} + \tau^{\mathrm{r}} - \tau^{\mathrm{c}}$$

This excessive resolved shear stress is relieved through sliding. Since the deformation is assumed to be of plane strain, $\partial\tau_{\alpha 3}/\partial x_3 = 0$. Applying the equilibrium condition $\tau_{ij,j} = 0$ in terms of the (α, β, x_3) coordinates gives $\partial\tau_{\alpha\alpha}/\partial x_\alpha + \partial\tau_{\alpha\beta}/\partial x_\beta = 0$. In this equation, the first term is small and thus the second term is also small. Hence, the change in $\tau^{\mathrm{r}}_{\alpha\beta}$ across the small band thickness (from P to Q) is negligible. As a result, the slip in P relieves the excessive positive shear stress not only in P, but also in the neighboring region including Q. This decrease of positive shear stress is the same as the increase of negative shear stress, thus causing Q to slide more readily during the reversed loading [14]. Similarly, dur-

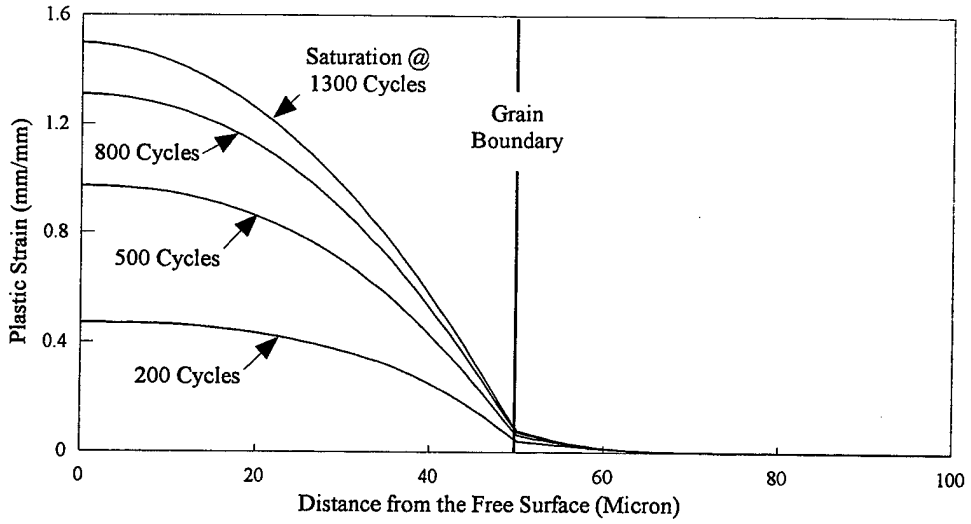

(a) Plastic Strain Distribution in Primary Slip System (P)

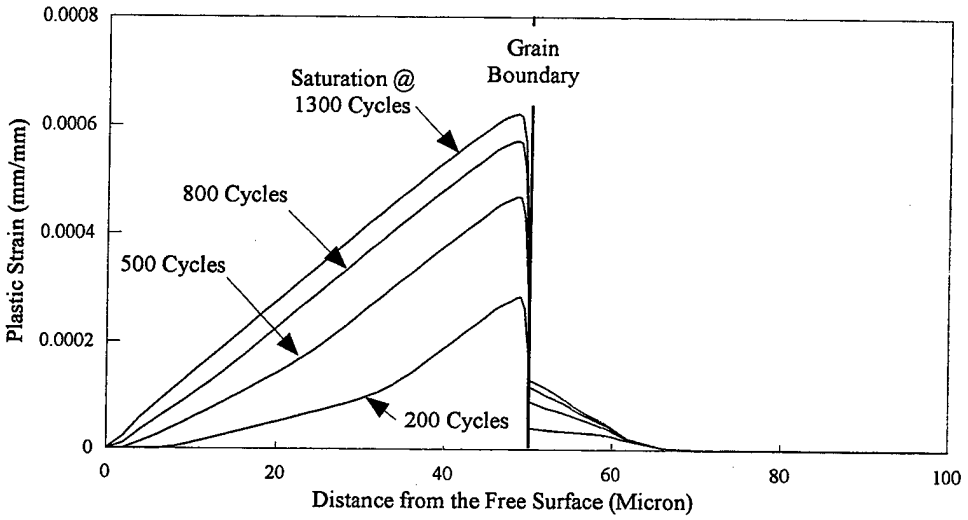

(b) Plastic Strain Distribution in Secondary Slip System (R)

Fig. 4. Plastic strain distribution under cyclic loadings of aluminium. The neighboring crystal is at 40° and the applied stress amplitude of cyclic loading is 0.740 MPa. The saturated plastic strain is at 1300 cycles.

ing the reversed loading, the negative slip in Q relieves not only the negative excessive shear stress in Q, but also increases the positive shear stress in P, thus causing P to slide more readily during the second forward loading. The process is repeated for every cycle and thus provides a natural gating mechanism to cause the alternate slip in P and Q resulting in monotonic growth of the extrusion, as observed in experiments. This gating mechanism does not require the crystal to have more than one slip plane such as a face-centered cubic (f.c.c.) crystal, hence is also applicable to other crystals such as hexagonal crystals.

Under cyclic loading, R increases in length as the extrusion grows and the elongation causes the initial compression in R to decrease. For a f.c.c. polycrystal there are 12 slip systems in each crystal. The change of direct stress $\tau_{\alpha\alpha}$ in R causes changes in resolved shear stress in all slip systems. When the decrease in compression in R becomes large, the applied stress can cause a second slip system to have a shear stress reaching the critical value and to slide. The plastic strain in the second slip system, $e''_{\xi\eta}$, caused by slip has a tensor component just like $e^{i}_{\alpha\alpha}$ in causing the positive $\tau^{i}_{\alpha\beta}$ in P and negative $\tau^{i}_{\alpha\beta}$ in Q. Therefore, the secondary slip system can greatly increase the extent of extrusion. The 12 slip systems of a f.c.c. crystal are shown in Fig. 3. The $\alpha\beta$ slip system in Fig. 1 is called the primary slip system, which is identified as a_2 (see Fig. 3). The secondary slip system due to the change of direct stress $\tau_{\alpha\alpha}$ under cyclic loading was found by Lin et al. [15] and

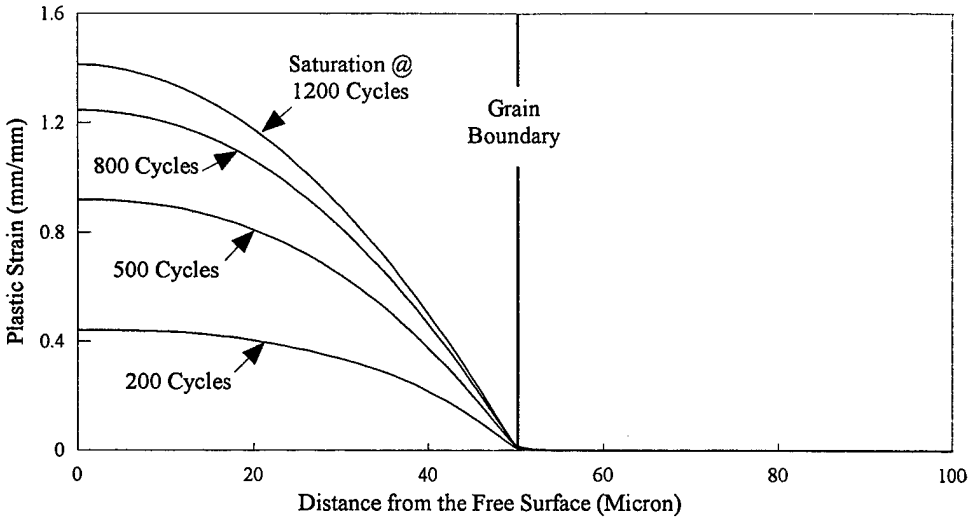

(a) Plastic Strain Distribution in Primary Slip System (P)

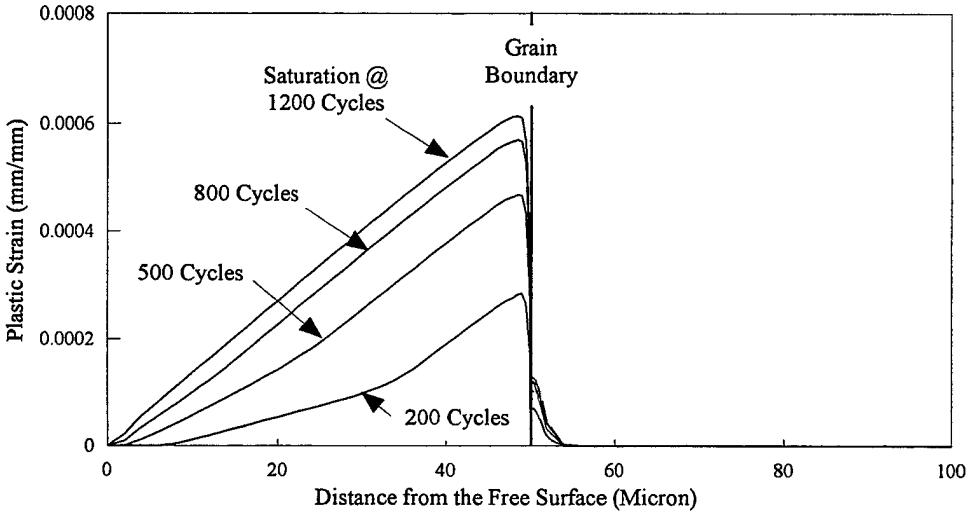

(b) Plastic Strain Distribution in Secondary Slip System (R)

Fig. 5. Plastic strain distribution under cyclic loadings of aluminium. The neighboring crystal is at 35° and the applied stress of cyclic loading is 0.740 MPa. The saturated plastic strain is at 1200 cycles.

Lin [9] to be c_3 (see Fig. 3). The secondary slip was later observed in the slip band in a recent paper by Zhai et al. [16]. The secondary slip can increase greatly the plastic shear strain in P and Q [15] and hence is considered in the present study. In the calculation, zero latent hardening is assumed.

To study the effect of the misorientation (i.e. the difference in orientation) between the surface crystal and its neighboring crystal on the propagation of a fatigue band across the grain boundary, an aluminum polycrystal is considered. It is composed of a surface crystal with a slip system inclined at 45° and a neighboring crystal with a slip system inclined at an angle θ with respect to the x_1-axis, as shown in Fig. 1. Many cyclic deformation data of aluminum single crystals have recently been reported by Vorren and Ryum [17,18] and Videm and Ryum [19]. For numerical calculations, the cyclic loading σ_{22} was ± 0.740 MPa, giving an applied shear stress, $\tau^{a}_{\alpha\alpha}$, of ± 0.370 MPa. The initial shear stress, $\tau^{i}_{\alpha\beta}$, was assumed to be 3.50×10^{-3} MPa in P and -3.50×10^{-3} MPa in Q of the surface crystal. No initial stress was assumed in the neighboring crystal. The critical shear stress was assumed to be constant and equal to 0.369 MPa. Poisson's ratio was 0.3 and the shear modulus μ was 2.65×10^4 MPa. P and Q were 0.01 micron thick and R was 0.1 micron thick. The numerical methods used to calculate the slip distributions in P, Q and R were similar to that given by Lin et al. [15]. The calculated plastic shear strain distribution $e''_{\alpha\beta}$ of the primary slip system at different

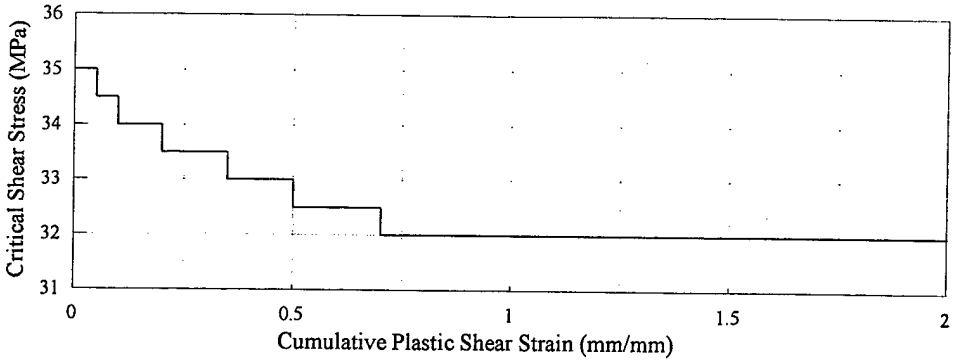

Fig. 6. Relationship between plastic shear strain and critical shear stress of copper.

cycles of loading for $\theta = 40°$ (i.e. misorientation of 5°) is shown in Fig. 4(a) and that of the secondary slip system in this single band is shown in Fig. 4(b). As the extrusion grows further with cycles of loading, the initial tensile strain in R decreases and eventually vanishes and then the plastic strain in P and Q ceases to grow. This plastic strain distribution is referred to as the saturated plastic strain. The saturated plastic strain occurs at 1300 cycles with the distribution shown in Fig. 4. It is seen that the slip strains in P and Q increase monotonically with the number of cycles.

A second case with the inclined angle in the neighboring crystal of $\theta = 35°$ (misorientation of 10°) was also analyzed under the same amplitude of applied load. The result is shown in Fig. 5, with the saturated plastic strain occurring at 1200 cycles. A comparison between Figs. 4 and 5 shows that the plastic strain distribution in the adjacent crystal oriented at $\theta = 35°$ is much smaller than that at $\theta = 40°$. These results indicate that the grain boundary blocks the propagation of the fatigue bands across the boundary.

3. Propagation of a fatigue band with slip direction parallel to free surface

Many experiments have been performed to study slips parallel to the free surface. Nabarro [20] discussed the crossing of a shear band from one grain to another. Mura [21,22] showed the relation between the plastic strain and dislocation displacements. Stroh [23] considered a dislocation pile-up to represent the shear band and used a two-dimensional analysis to study the crack initiation in brittle solid. Figueroa and Laird [8] performed an experiment to study the grain boundary effect on fatigue band growth of copper polycrystals. In the present study, a micromechanic two-dimensional analysis on two adjacent copper crystals with slip direction parallel to the free surface (see Fig. 2) was performed to explain the observed experimental results.

Hunsche and Neumann [24] have shown that the critical shear stress varies with the cumulative shear strain of a pure single copper crystal. They found that the critical shear stress increases from 32 to 35 MPa and then decreases to 32 MPa. To simplify the numerical calculation, each crystal in the copper polycrystal was assumed to be work hardened to 35 MPa before the analysis begins and the critical shear stress was dropped from 35 to 32 MPa in a step-wise manner. The characteristics are shown in Fig. 6 and applied to the following numerical calculations.

Mecke and Blochwitz [25] conducted an experimental study on nickel single crystals under cyclic loading. The experiment was performed at room temperature and at a constant plastic strain amplitude. The results showed that the PSB penetrated across the whole crystal and extruded from both sides. In order for the PSB to extrude, the slip band must be in compression near the extrusion. An initial tensile strain in the central part of the PSB will give this compression near both ends of the band. In the analysis, an initial tensile strain was assumed to vary linearly from a maximum value at the center to zero at the two ends of a 20 micron segment in the fatigue band (see Fig. 2). This segment was divided into a number of grids and each grid was approximated by a uniform initial tensile strain. Let $\tau^{i}_{\alpha\beta}(\boldsymbol{x}, e^{i}_{\alpha\alpha})$ be the resolved shear stress at point $\boldsymbol{x}$, in the α–β coordinate system, due to a uniform initial tensile strain in a rectangular area centered at the origin, as shown in Fig. 2. Consider again that the metal is of fine grain, using the analogy of inelastic strain and applied force in an infinite medium, the resolved shear stress due to $e^{i}_{\alpha\alpha}$ in the rectangular area is

$$\tau^{i}_{\alpha\beta}(\boldsymbol{x}, e^{i}_{\alpha\alpha}) = \frac{\mu e^{i}_{\alpha\alpha}}{2\pi(1-\upsilon)}$$
$$\left\{\frac{1}{2}\ln\left[\frac{((\alpha-d)^2+(\beta-w)^2)((\alpha+d)^2+(\beta+w)^2)}{((\alpha-d)^2+(\beta+w)^2)((\alpha+d)^2+(\beta-w)^2)}\right]\right.$$
$$+\frac{1}{1-2\upsilon}\left[\frac{(1-\upsilon)(\alpha-d)^2+\upsilon(\beta+w)^2}{(\alpha-d)^2+(\beta+w)^2}\right.$$
$$\left.\left.+\frac{(1-\upsilon)(\alpha+d)^2+\upsilon(\beta-w)^2}{(\alpha+d)^2+(\beta-w)^2}\right.\right.$$

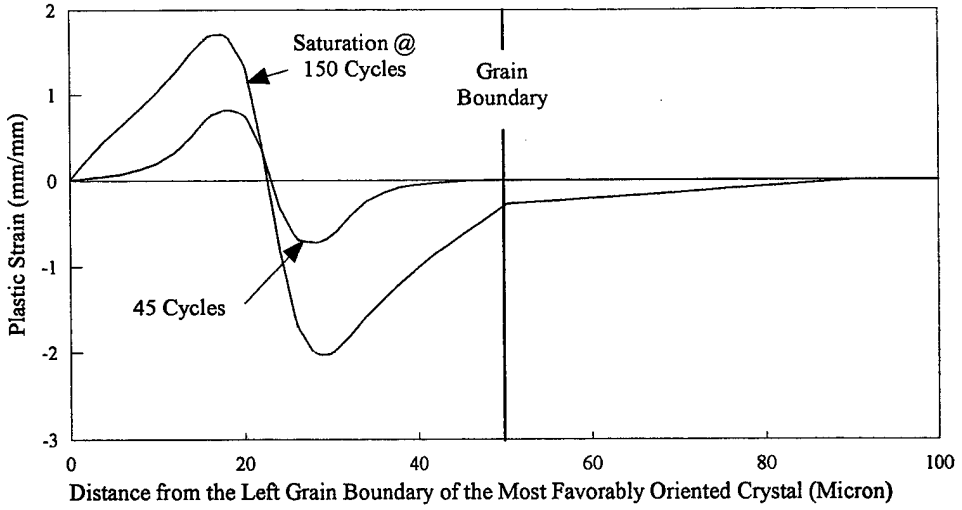

(a) Plastic Strain Distribution in Primary Slip System (P)

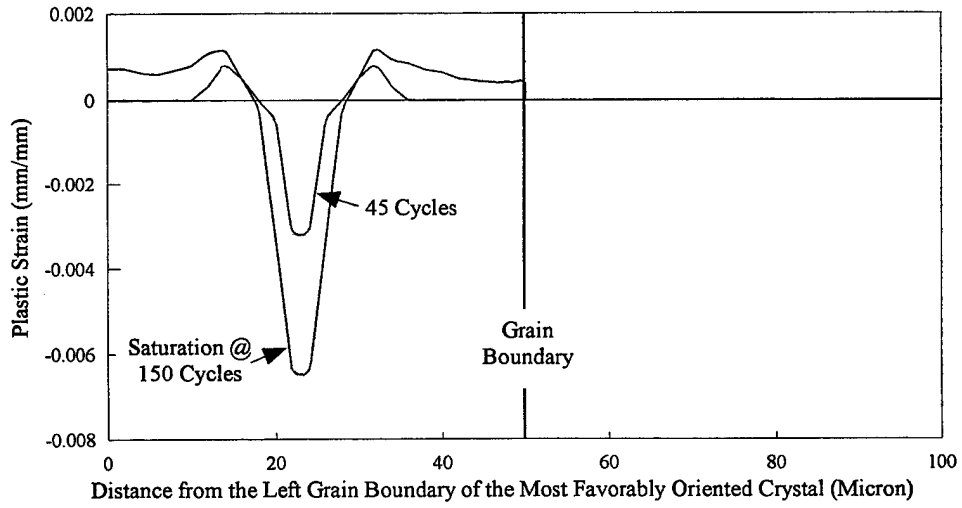

(b) Plastic Strain Distribution in Secondary Slip System (R)

Fig. 7. Plastic strain distribution under cyclic loadings of copper. The neighboring crystal is at 40° and the applied cyclic loading stress is 68.7 MPa. The saturated plastic strain is found after 150 cycles.

$$-\frac{(1-\upsilon)(\alpha-d)^2+\upsilon(\beta-w)^2}{(\alpha-d)^2+(\beta-w)^2}$$
$$+\frac{(1-\upsilon)(\alpha+d)^2+\upsilon(\beta+w)^2}{(\alpha+d)^2+(\beta+w)^2}\Bigg]\Bigg\} \quad (8)$$

The initial shear stress fields caused by a collection of uniform initial tensile strains were then obtained by the use of Eq. (8). The assumed initial tensile strain distribution causes nearly uniform initial resolved shear stress. Thus a uniform initial shear stress of 0.8 MPa was assumed in the present analysis.

Consider a crystal oriented at 45° from the loading axis with an adjacent crystal of a different orientation, θ, as shown in Fig. 2. The polycrystal was loaded under alternating tension and compression. Following the procedure discussed in Section 2, the plastic strain distributions in the fatigue bands of the two crystals are shown in Figs. 7 and 8. Fig. 7 presents the result when the neighboring crystal is oriented at $\theta = 40°$ (misorientation of 5°), and Fig. 8 presents the result when the neighboring crystal is oriented at $\theta = 35°$ (misorientation of 10°). These figures show that a small amount of the fatigue band propagated across the grain boundary when the misorientation is 5° and the fatigue band practically stopped at the grain boundary when the misorientation is 10°. The difference in crystal orientations is generally much greater than what was considered in the calculation, and the consideration of additional twisting of the boundary will further reduce the Schmid factors and thus the applied stress, τ^a. This

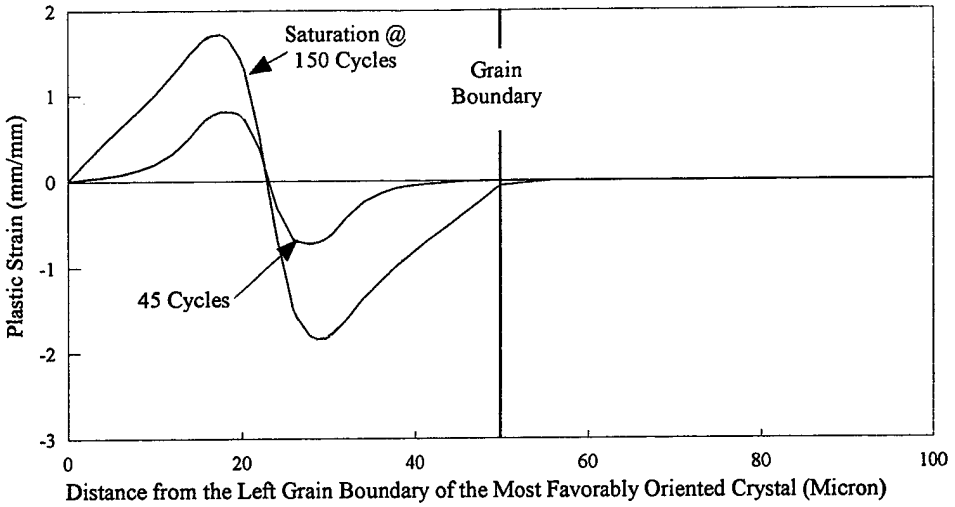

(a) Plastic Strain Distribution in Primary Slip System (P)

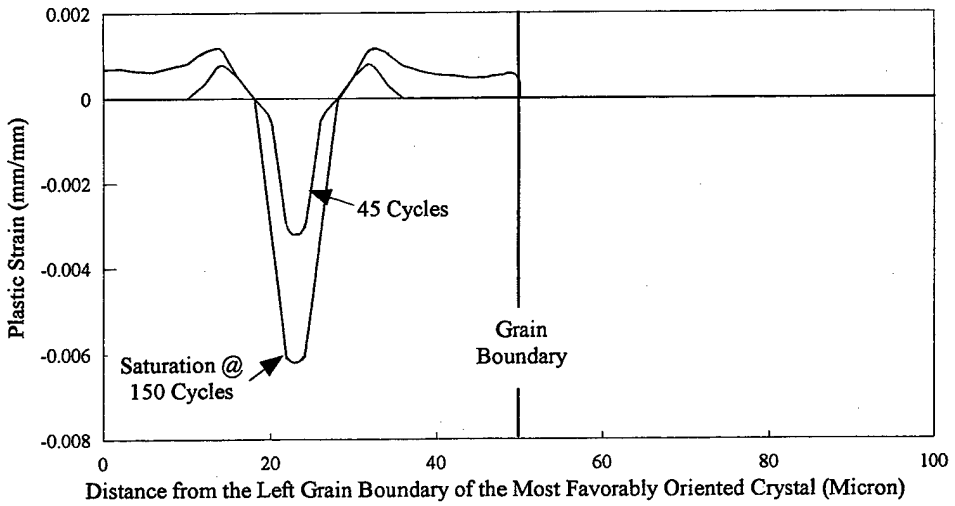

(b) Plastic Strain Distribution in Secondary Slip System (R)

Fig. 8. Plastic strain distribution under cyclic loadings of copper. The neighboring crystal is at 35° and the applied cyclic loading stress is 68.7 MPa. The saturated plastic strain is found after 150 cycles.

would increase the resistance to the propagation of the fatigue band across the grain boundary and thus tend to initiate intergranular crack. This seems to agree with the observations made by Figueroa and Laird [8].

4. Effect of sequence of variable fatigue loading

Figueroa and Laird [8] in their experimental study had shown, in the low-amplitude followed by high-amplitude fatigue loading (denoted by LH loading) on pure copper polycrystals, the subsequent cycles at the high-amplitude seem to ignore the damage produced first at the low-amplitude. Due to the variation of the critical shear stress with the cumulative plastic strain of copper, where the stress drops from 35 to 32 MPa, if a low-amplitude of loading < 35 MPa is first applied, this low-amplitude loading is expected to produce little plastic strain in the fatigue band. Hence, the present micromechanic analysis explains the experimental observation of the LH loading.

Besides the LH loading, Figueroa and Laird [8] also performed a high-low (HL) loading and they found that the high-amplitude loading has significant effect on the subsequent low-amplitude loading. From micromechanic analysis, if a high loading is applied first and if the stress has passed 35 MPa, the critical shear stress will drop to 32 MPa and hence a subsequent low amplitude loading will cause a further increase in plastic strain. To carry out this study, a numerical analysis

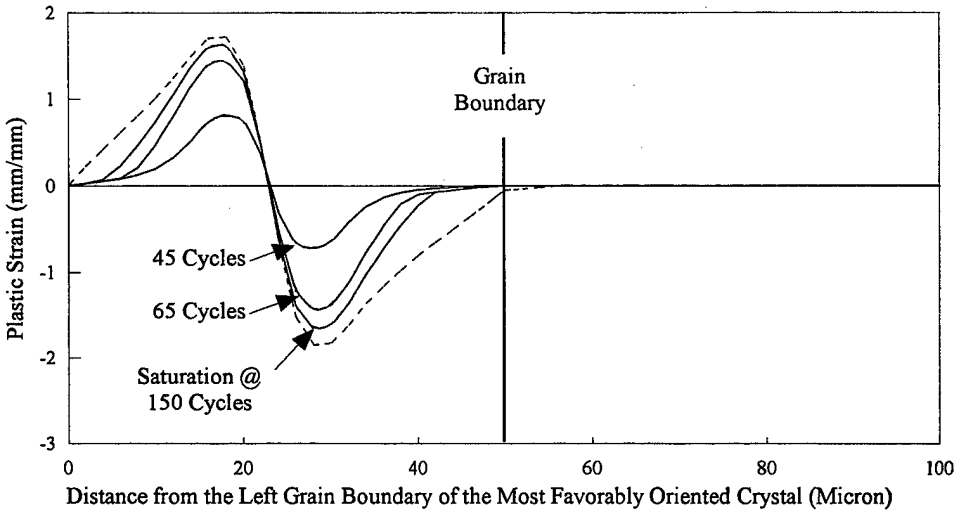

(a) Plastic Strain Distribution in Primary Slip System (P)

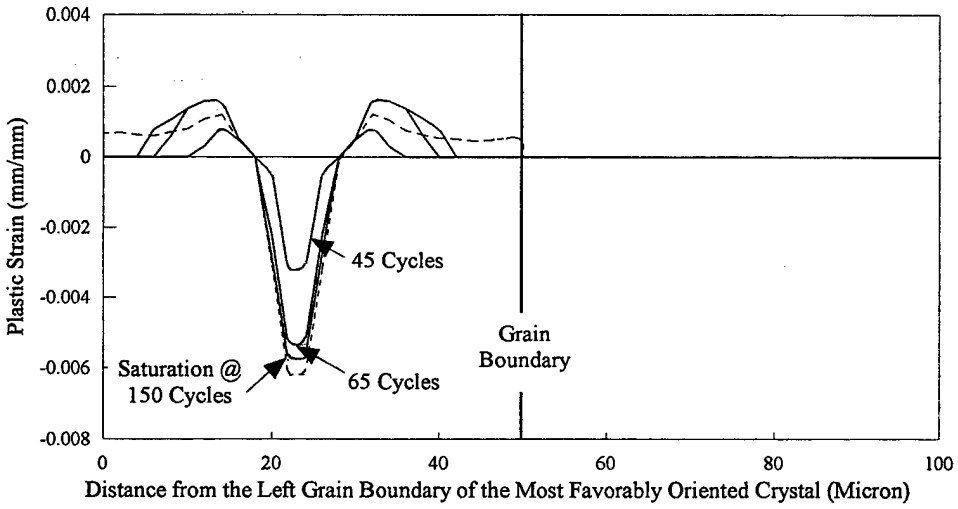

(b) Plastic Strain Distribution in Secondary Slip System (R)

Fig. 9. Plastic strain distribution under high-low cyclic loadings of copper. The neighboring crystal is at 35°, applied high-amplitude cyclic loadings is 68.7 MPa for 45 cycles, and subsequent low-amplitude is 65.7 MPa. The dotted line represents the saturated plastic strain at constant high-amplitude of 68.7 MPa (the same curves as those given in Fig. 8).

was performed on a HL cyclic loading of the copper polycrystal with a 10° misorientation in the neighboring crystal. A high-amplitude loading of 68.7 MPa was first applied. At 45 cycles, the loading was reduced to 65.7 MPa. The plastic strain distribution in the band is shown in Fig. 9. The subsequent low-amplitude loading is seen to cause considerable additional plastic strain in the fatigue band. This seems to explain the experimental observations of the HL loadings.

5. Conclusion

The resolved shear stress in a crystal is very much dependent on its Schmid's factor and hence on the crystal orientation. Taking the first sliding crystal at the free surface as the most favorably oriented crystal, the applied resolved shear stress in the adjacent crystal decreases rapidly with the misorientation between the two crystals. The resolved shear stress in the adjacent crystal is generally much less than that in the surface crystal. This tends to cause large resistance to the propagation of fatigue band across the grain boundary. On the other hand, the roughness of the free surface caused by the formation of extrusions and intrusions introduces stress concentrations, causing crack initiation in fatigue bands at the free surface before that occurring at the grain boundary.

For the cases of fatigue bands with the sliding direction parallel to the free surface, there is no free surface

roughness due to extrusions and intrusions. The misorientation remains to cause the decrease of the resolved shear stress in the adjacent crystal. This causes the difficulty of propagating the fatigue band across the grain boundary and thus develops intergranular cracks as observed in experiments.

The critical shear stress of a pure copper single crystal that contains a drop from 35 to 32 MPa with the cumulative cyclic plastic strain seems to have a large effect on the fatigue damage in low-high and high-low sequences of loadings. A low-amplitude loading of less than 35 MPa produces no plastic strain in the band and hence has no effect on the increase of plastic strain in the subsequent high-amplitude loading. On the other hand, after high-amplitude loading, the critical shear stress drops to 32 MPa and a subsequent low-amplitude loading can cause additional plastic strain in the fatigue band as shown in the analytical calculations. These micromechanic analysis results explain the experimental observations.

Acknowledgements

This research was supported by the Air Force Office of Scientific Research through Grant F49629-96-1-0350. The interest of Dr Brian Sanders and Dr James Chang are gratefully acknowledged.

References

[1] E.R. Parker, Micromechanic Behavior of Materials at Elevated Temperatures, in: J.E. Dorn (Ed.), McGraw-Hill, New York, 1961, pp. 129–148.
[2] J.P. Hirth, J. Lothe, Theory of Dislocations, McGraw-Hill, New York, 1968, pp. 694–710.
[3] S. Suresh, Fatigue of Materials, Cambridge University Press, New York, 1991, pp. 119–125.
[4] C. Laird, D.J. Duquette, Mechanism of Fatigue Crack Nucleation, Corrosion Fatigue, NACE-2, 1972, pp. 88–117.
[5] H. Mughrabi, Proceedings of the ICSMA 7, Montreal, Pergamon, Oxford, 1985, pp. 1917–1942.
[6] H. Mughrabi, R. Wang, K. Differt, V. Essmann, Fatigue Mechanism ASTM STP 811, 1983, pp. 5–45.
[7] U. Essmann, U. Gossel, H. Mughrabi, Phil. Mag. A44 (1981) 405–426.
[8] J.C. Figueroa, C. Laird, Mater. Sci. Eng. 60 (1983) 45–56.
[9] T.H. Lin, Adv. Appl. Mech. 29 (1992) 1–68.
[10] T.H. Lin, Y.M. Ito, J. Appl. Phys. 3 (1967) 775–780.
[11] T.H. Lin, Theory of Inelastic Structures, Chapter 2, Wiley, New York, 1968.
[12] E. Melan, Der spannugszustand der durch eine einzelkraft in innern beansprochten halbscheibe, Zeitschrift fur Angewandte Mathematik und Mechanik, 12 (1932) 343–346; Correction in vol. 20 (1940) 368.
[13] T.K. Tung, T.H. Lin, J. Appl. Mech. 33 (1966) 363–370.
[14] T.H. Lin, Y.M. Ito, Proc. Nat. Acad. Sci. USA 62 (1969) 631.
[15] T.H. Lin, S.R. Lin, X.Q. Wu, Phil. Mag. 59 (1989) 1263.
[16] T. Zhai, G.A.D. Briggs, J.W. Martin, Acta Mater. 44 (1996) 3489–3496.
[17] O. Vorren O, N. Ryum, Acta Metall. 35 (1987) 855–866.
[18] O. Vorren, N. Ryum, Acta Metall. 36 (1988) 1443–1453.
[19] M. Videm, N. Ryum, Mater. Sci. Eng. A219 (1996) 1–10.
[20] F.R.N. Nabarro, Theory of Crystal Dislocations, Dover, New York, 1987.
[21] T. Mura, Continuum Theory of Dislocations and Plasticity, Springer, Berlin, 1967.
[22] T. Mura, Micromechanics of Defects in Solids, Chapter 1, Martinus Nijhoff, Dordrecht, 1982.
[23] A.N. Stroh, Adv. Phys. 6 (1957) 418.
[24] A. Hunsche, P. Neumann, Acta Metall. 34 (2) (1986) 207–217.
[25] K. Mecke, C. Blochwitz, Phys. Stat. Sol. A64 (1980) K5–K7.

Instructions for Authors

SUBMISSION OF PAPERS

Manuscripts for the main part of the journal and for the Letters Section should be submitted as follows:

For authors in Europe

Professor Gernot Kostorz
ETH Zurich
Institut für Angewandte Physik
CH-8093 Zurich, Switzerland
Fax: +41 (1633) 1105

For authors in Japan

Professor Masahiro Koiwa
Department of Materials Science and Engineering
Faculty of Engineering
Kyoto University
Yoshida-Honmachi, Sakyo-ku
Kyoto 606-8501, Japan
Fax: +81 (75) 753 4861

For authors in North and South America and the rest of the world

Professor Carl C. Koch
North Carolina State University
Department of Materials Science and Engineering
233 Riddick Building
Yarbrough Drive
Raleigh, NC 27695-7907, USA
Fax: +1 (919) 515 7724
or
Professor Enrique J. Lavernia
Department of Chemical & Biochemical Engineering & Materials Science and Department of Mechanical & Aerospace Engineering
University of California Irvine
Irvine, CA 92697-2575, USA

Manuscripts

Three copies should be submitted to the Editor, in double-spaced typing on pages of A4 size and with wide margins (Letters should not exceed 2000 words and a maximum of 5 figures). All tables and illustrations should bear a title or legend.
An *abstract* should accompany reviews, original papers and Letters. It should present (preferably in 100–150 words; 50 words or less for Letters) a brief and factual account of the contents and conclusions of the paper, and an indication of the relevance of new material.

References should be indicated by numerals in square brackets, introduced consecutively and appropriately in the text.

References must be listed on separate sheet(s) at the end of the paper. Every reference appearing in the text should be quoted in the reference list, and *vice versa*. When reference is made to a publication written by more than two authors it is preferable to give only the first author's name in the text followed by "*et al.*" However, in the list of references the names and initials of all authors must be given.
Three sets of figures should be submitted. One set of line drawings should be in a form suitable for reproduction, drawn in Indian ink on drawing or tracing paper (letter height, 3–5 mm). Alternatively, such illustrations may be supplied as high contrast, black-and-white glossy prints. Duplicate original micrographs should be provided wherever possible to facilitate the refereeing process. Magnifications should be indicated by a ruled scale bar on the micrograph. Captions to illustrations should be typed in sequence on a separate page.
All abbreviated terms must be defined when first used (both in the abstract and in the text) and authors must express all quantities in SI units, with other units in parentheses if desired.
Authors in Japan please note that information about how to have the English of your paper checked, corrected and improved (before submission) is available from: Elsevier Science Japan
Higashi-Azabu 1-chome Building 4F, 1-9-15 Higashi-Azabu
Minato-ku, Tokyo 106, Japan
Tel: +81-3-5561-5032; Fax: +81-3-5561-5045.

Further information

All questions arising after the acceptance of manuscripts, especially those relating to proofs, should be directed to: Elsevier Science Ireland Ltd. Bay 15K, Shannon Industrial Estate
Shannon, Co. Clare, Ireland
Tel. +353 61 471944; Fax. +353 61 472144.

Submission of electronic text

The final text may be submitted on a 3.5 in or 5.25 in diskette (in addition to a hard copy with original figures). Double density (DD) or high density (HD) diskettes are acceptable, but must be formatted to their capacity before the files are copied on to them. The main text, list of references, tables and figure legends should be stored in separate text files with clearly identifiable file names. The format of these files depends on the word processor used. WordPerfect 5.1 is the most preferable but for other formats please refer to the Instructions to Authors booklet. It is *essential* that the name and version of the wordprocessing program, type of computer on which the text was prepared, and format of the text files are clearly indicated.
The final manuscript may contain last minute corrections which are not included in the electronic text but such corrections must be clearly marked on the hard copy.

0921-5093/98/$19.00

Damage Mechanics in Engineering Materials
G.Z. Voyiadjis, J.-W.W. Ju and J.-L. Chaboche (Editors)
1998 Elsevier Science B.V.

Micromechanics of Fatigue Crack Initiation of Single Crystal under Plane Strain

T.H. Lin[a], K. Wong[b], and N.J. Teng[c]

[a,b,c]Department of Civil & Environmental Engineering, University of California, Los Angeles
P.O. Box 951593, Los Angeles, CA 90095-1593

The micromechanic analysis of a fatigue band in the most favorably oriented crystal at the free surface of a polycrystal is extended to the analysis of a single crystal under plane strain. The boundary tractions on the boundaries of the crystal embedded in the polycrystal are removed by applying equal and opposite tractions. The stress field caused by these opposite tractions is analyzed using finite element method. Extrusions on both sides the of single crystals as commonly observed is shown in the analytical calculations.

1. INTRODUCTION

Single crystals have been used in component parts of turbine engines. These parts are subject to repeated mechanical and thermal loadings. It has been found that about 90% of the catastrophic failures of these parts are due to fatigue of materials [1]. Hence, understanding the mechanism of these failures is essential to their reductions. The present study attempts to give a method to analyze the fatigue crack initiation of these single crystals.

Lin [2] and Lin et al. [3] have developed a physical model to analyze the high-cycle fatigue crack initiation of a face-centered cubic (f.c.c.) polycrystal. This model is amended to analyze the fatigue crack initiation of f.c.c. single crystals.

Single crystal tests show that under loading, slip occurs along certain directions on certain planes. This slip depends on the resolved shear stress and is independent of the normal stress on the sliding plane. The dependence of slip on the resolved shear stress, known as Schmid's law, has been shown by Parker [4] to hold also for cyclic loadings. Initial defects exist in all metals and cause an initial stress field, which gives an initial resolved shear stress field τ^i in the metal. The shear stress due to applied load is denoted by τ^a. When this τ^a combined with τ^i reaches the critical shear stress τ^c in some region, slip occurs to keep the resolved shear stress from exceeding the critical. After unloading, the slip remains and causes a residual resolved shear stress field τ^r. The total resolved shear stress is then

$$\tau = \tau^a + \tau^i + \tau^r \tag{1}$$

The governing condition to initiate or continue slip in a region is to have this resolved shear stress τ equal to τ^c.

To calculate the residual stress, the analogy between plastic strain and applied force is used [5]. It has been shown that the equivalent body force per unit volume along x_i-axis due to plastic strain e''_{ij} is

$$F_i = -C_{ijkl} e''_{kl,j} \tag{2}$$

where C_{ijkl} is the elastic constants of the metal. The repetition of alphabetic subscripts denotes summation and the subscript after a comma denotes differentiation with respect to the coordinate variable. The equivalent surface force per unit area along x_i-axis has been shown as

$$S_i = C_{ijkl} e''_{kl} \eta_j \tag{3}$$

where η_j is the cosine of the angle between the exterior normal to the surface and the x_j-axis. In the following analysis, the slip plane and the slip direction of the crystal is taken to form a 45° angle with the specimen axis.

Extrusions and intrusions have been observed to grow monotonically on fatigued specimens [6]. Kinematically, an extrusion forms when a positive shear strain occurs in a thin slice P and a negative shear strain in a closely located thin slice Q (see Figure 1). The initial stress field τ^i favorable to this mode of slip is one having positive shear stress in P and negative in Q. Such an initial stress field can be provided by an initial tensile strain $e^i_{\alpha\alpha}$ in R (the repetition of Greek subscript does not denote summation). Lin and Ito [7] suggested that the tensile strain $e^i_{\alpha\alpha}$ in R along the slip direction α may be provided by a row of interstitial dipoles. Antonopoulos et al. [8] and Mughrabi et al. [9] have indicated that the ladder structure in a persistent slip band (PSB) can be described by an array of edge dislocation dipoles. A tensile loading τ_{22} on the polycrystal produces a positive τ^a in the whole crystal. Taking τ^i to be positive in P and negative in Q, then $\tau^i + \tau^a$ in P will first reach τ^c, prompting P to slide. This slip causes a residual shear stress $\tau^r_{\alpha\beta}$. The length of the crystal (along x_3-axis, normal to the plane of Figure 1) is assumed to be much longer than the band thickness. In the center length portion of the crystal, the slip and hence the plastic strain distributions along the band is assumed to be constant along the x_3-axis. This causes the deformation to be plane strain, and hence $\partial\tau_{\alpha 3}/\partial x_3 = 0$. Applying the equilibrium condition $\tau_{ij,j} = 0$ in terms of the (α, β, x_3) coordinates gives $\partial\tau_{\alpha\alpha}/\partial x_\alpha + \partial\tau_{\alpha\beta}/\partial x_\beta = 0$. The first term is generally small, so the second term is also small. Hence the change in $\tau^r_{\alpha\beta}$ across the small

band thickness (from P to Q) is very small. As a result, the slip in P reduces not only the positive shear stress in P, but also reduces the same amount of positive shear stress in Q. This decrease of positive shear stress is the same as increase of negative shear stress, causing Q to slide more readily during the reversed loading [7]. Similarly, the negative slip in Q reduces the negative shear stress not only in Q but also in P, thus causing P to slide more readily during the second forward loading. This process is repeated for every cycle and thus provides a natural gating mechanism to cause the alternate slip in P and Q, resulting in monotonic growth of the extrusion. Interchanging the signs of the initial stresses will produce an intrusion instead of an extrusion. This gating mechanism does not require the crystal to have more than one slip plane such as a f.c.c. crystal, hence is also applicable to hexagonal crystals.

The build-up of the slip strain $e''_{\alpha\beta}$ in P and Q is caused by $e^i_{\alpha\alpha}$ in R. This $e^i_{\alpha\alpha}$ causes an initial compression in R, which in turn causes positive $\tau'_{\alpha\beta}$ in P and negative $\tau'_{\alpha\beta}$ in Q. Under cyclic loading, the extrusion grows and R increases in length. This elongation causes the compression in R to decrease. There are 12 slip systems in a f.c.c. crystal. The change of direct stress $\tau_{\alpha\alpha}$ in R causes changes in resolved shear stress in all slip systems. When the decrease in compression in R becomes large, the applied stress can cause a second slip system to have shear stress reaching the critical value and slide. The plastic strain $e''_{\xi\eta}$ caused by slip in this secondary slip system has a tensor component just like $e^i_{\alpha\alpha}$ in causing the positive and negative $\tau'_{\alpha\beta}$ in P and Q, respectively. The occurrence of the secondary slip system was recently clearly observed by Zhai et al. [10]. The 12 slip systems of a f.c.c. crystal are shown in Figure 2. The $\alpha\beta$ slip system in Figure 1 is called the primary slip system, which is identified as a_2 system in Figure 2. The secondary slip system due to the change of direct stress $\tau_{\alpha\alpha}$ under cyclic loading was found by Lin et al. [3] to be c_3. The plastic strain $e''_{\xi\eta}$ due to the slip has a tensor component $e''_{\alpha 3}$, which induces an equivalent force component F_3. The presence of F_3 requires the modification of the plane strain solution. A similar problem was shown in the analysis of prismatic bars by Lekhnitski [11] and is referred to as the generalized plane strain problem. This problem is defined as

$$u_i = u_i(x_1, x_2) \quad , \quad i = 1,2,3 \tag{4}$$

The stress in an isotropic elastic body is given as

$$\tau_{ij} = 2\mu\left[\frac{\upsilon}{1+2\upsilon}\delta_{ij}\Theta + \frac{1}{2}\left(u_{i,j} + u_{j,i}\right)\right] \tag{5}$$

where $\Theta = u_{1,1} + u_{2,2}$, μ is the shear modulus, and υ is the Poisson's ratio.

2. METHOD OF ANALYSIS

To analyze the fatigue band in a single crystal under generalized plane strain, consider a crystal embedded at a free surface of a polycrystal under alternate tension and compression. The sliding direction and the slip plane make 45° with the free surface and the loading axis (see Figure 1). The solutions of the plastic strain distributions in the fatigue band of the polycrystal have been shown by Lin et al. [3]. Melan [12] has given a plane stress solution of the stress field due to a given loading on a semi-infinite plate. His solution has been modified by Tung and Lin [13] for plane strain. This plane strain solution is then generalized to include the generalized plane strain deformation. Let $\tau_{ij}(\mathbf{x},\mathbf{x}'_k)$ be the stress at point $\mathbf{x}$ due to a unit force applied at point $\mathbf{x}'$ along the x_k-direction. The stress components are expressed in terms of the Airy stress functions, ϕ_k's, as

$$\tau_{11}(\mathbf{x},\mathbf{x}'_k)=\frac{\partial^2\phi_k}{\partial x_2^2}\ ,\quad \tau_{22}(\mathbf{x},\mathbf{x}'_k)=\frac{\partial^2\phi_k}{\partial x_1^2}\ ,\quad \tau_{12}(\mathbf{x},\mathbf{x}'_k)=\frac{\partial^2\phi_k}{\partial x_1\partial x_2}\ ,$$
$$\tau_{13}(\mathbf{x},\mathbf{x}'_k)=\tau_{23}(\mathbf{x},\mathbf{x}'_k)=0\ ,\quad \tau_{33}(\mathbf{x},\mathbf{x}'_k)=-\upsilon\left(\tau_{11}(\mathbf{x},\mathbf{x}'_k)+\tau_{22}(\mathbf{x},\mathbf{x}'_k)\right)\ ,\quad k=1,2 \tag{6}$$

$$\tau_{11}(\mathbf{x},\mathbf{x}'_k)=\tau_{22}(\mathbf{x},\mathbf{x}'_k)=\tau_{33}(\mathbf{x},\mathbf{x}'_k)=\tau_{12}(\mathbf{x},\mathbf{x}'_k)=0\ ,$$
$$\tau_{13}(\mathbf{x},\mathbf{x}'_k)=\frac{\partial\phi_k}{\partial x_1}\ ,\quad \tau_{23}(\mathbf{x},\mathbf{x}'_k)=\frac{\partial\phi_k}{\partial x_2}\ ,\qquad k=3 \tag{7}$$

where

$$\phi_1(\mathbf{x},\mathbf{x}')=-(p+q)(x_2-x'_2)(\theta_1+\theta_2)+\frac{1}{2}q(x_1-x'_1)\ln\frac{X_1}{X_2}+2p\frac{x_1x'_1(x_1+x'_1)}{X_2} \tag{8}$$

$$\phi_2(\mathbf{x},\mathbf{x}')=-(p+q)(x_2-x'_2)(\theta_1+\theta_2)+\frac{1}{2}q(x_2-x'_2)\ln\frac{X_1}{X_2}-2p\frac{x_1x'_1(x_2-x'_2)}{X_2} \tag{9}$$

$$\phi_3(\mathbf{x},\mathbf{x}')=-\frac{\ln X_1+\ln X_2}{4\pi} \tag{10}$$

and

$$p=\frac{1}{4\pi(1-\upsilon)}\ ,\quad q=p(1-2\upsilon)\ ,$$
$$X_1=(x_1-x'_1)^2+(x_2-x'_2)^2\ ,\quad X_2=(x_1+x'_1)^2+(x_2-x'_2)^2 \tag{11}$$

$$\theta_1=\arctan\left(\frac{x_2-x'_2}{x_1-x'_1}\right)\ -\pi\le\theta_1\le\pi\ ,\quad \theta_2=\arctan\left(\frac{x_2-x'_2}{x_1+x'_1}\right)\ -\frac{\pi}{2}\le\theta_2\le\frac{\pi}{2} \tag{12}$$

Equations (6) and (7) give the residual stress field, τ^r, in the surface crystal embedded in the polycrystal. This analysis also gives surface tractions on the grain boundaries (see

Figure 1). In a single crystal, the surface tractions are zero, and hence must be removed by applying equal and opposite tractions on the boundary. The stress field caused by the equal and opposite tractions is here solved by finite element method (FEM). Plastic strain occurs only in the fatigue band. The fatigue band is divided into a number of grids. The plastic strain in a grid in the left half of the crystal is denoted by $e_{ij}^{p(L)}$ and in the right half by $e_{ij}^{p(R)}$. The solution of the stress field in Figure 3(a) is the sum of the solution of Figures 3(b), (c), and (d). Figure 3(b) gives uniform stress. The stress field caused by plastic strain, $e_{ij}^{p(L)}$, is solved by the semi-infinite solid solution with the free surface at the left, as shown in Figure 4. This solution satisfies the condition of zero traction at the free surface and gives surface tractions on the right, top, and bottom planes (see Figure 4(b)). These tractions are removed by applying equal and opposite tractions as shown in Figure 4(c). The stress field due to the loading in Figure 4(c) is solved by FEM. With the plastic strain grid in the left half of the crystal, the equivalent forces induced by the plastic strain is relatively far from the considered crystal boundaries, and hence the variation of surface traction along the boundary is small, and the grids of the FEM does not need to be very fine. This will facilitate the FEM solution. Similarly, for the solution of Figure 3(d), the slid grid is in the right half. The free surface of the semi-infinite solid is taken to be at the right side. The initial strain e_{ij}^{i} has the same effect as the plastic strain, so the procedure for solving the residual stress field can be applied for solving the initial stress caused by initial strain in the fatigue band. This gives a method to calculate the influence coefficient of the stress in the mth grid due to a unit inelastic strain (plastic strain and initial strain) in the nth grid. The resolved shear stress τ is the sum of the initial stress τ^{i}, the applied stress τ^{a}, and the residual stresses, $\tau^{r(L)}$ and $\tau^{r(R)}$. This sum is equated to the critical shear stress, τ^{c}, and the incremental plastic strain distributions at different stages of loading are obtained.

3. EXPERIMENTAL OBSERVATIONS

Mecke and Blochwitz [14] observed the subgrain displacement in single nickel crystal under cyclic loading. These experiments were carried out under constant plastic strain amplitudes at room temperature. It is shown that the PSBs have penetrated across the whole crystal and extruded out on both sides as shown in figure 5. The case with extrusion protruding on one side and intrusion on the other side was not observed. Basinski et al. [15,16] tested copper single crystals at a constant plastic strain amplitude at room temperature under cyclic loadings. In these tests, both extrusions and intrusions are observed. Zhai et al. [17,18] performed fatigue experiments on aluminum single crystals under constant cyclic stress amplitude. Again, both extrusions and intrusions were observed on the free surfaces.

A PHYSICAL METHOD OF FATIGUE CRACK INITIATION IN SINGLE CRYSTAL

T.H.Lin*, N.G.Liang*, K.K.F.Wong** & N.J.Teng*

Single crystal superalloys have been developed to eliminate grain boundaries, which are susceptible to cause grain corrosion, cracking and large creep deformation. These single crystals are used in turbine blades. The predicting fatigue life of the crystals is needed. Large amount of single crystal test data are available, but there seems to lack a general sound theory to correlate them. The present paper attempts to take these test data as guide to develop a physical mechanism of this crack formation.

LOCALIZATION OF PLASTIC STRAIN AND FATIGUE RATCHET MECHANISM CAUSED BY STRESS FIELD

Consider a thin slice of metal of a uniform rectangular cross-section experiencing a uniform plastic shear strain $e_{12}^{"}$ in an infinite isotropic elastic medium as shown in Figure 1(a). Imagine that we cut this slice out, see Figure 1(b), and apply a uniform shear stress $-2G\,e_{12}^{"}$, where G is the shear modulus, to restore the slice back to the original shape and size before the occurrence of the plastic strain and then welded back to the medium. Since there is no such stress applied, it is relaxed by applying an equal and opposite force of $2G\,e_{12}^{"}$ per unit area of the boundary of the slice as shown in Figure 1(c). Denoting the stress field caused by the boundary force as τ_{ij}^{s}, the stress field due to the uniform plastic strain is then

$$\tau_{ij}^{r} = \tau_{ij}^{s} - 2Ge_{12}^{"} \qquad (1)$$

The stress field caused by $e_{12}^{"}$ in this slice is readily calculated. The resolved shear

* *University of California, Los Angeles*
** *Nanyang University, Singapore*

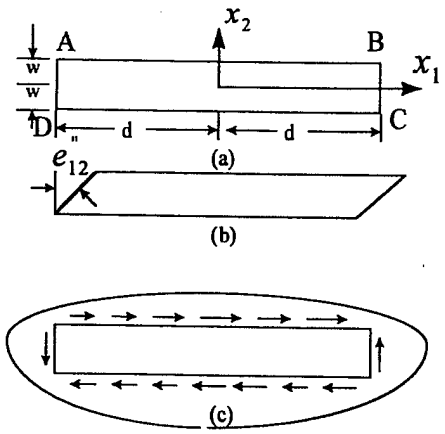

Figure 1 Shear Band Model

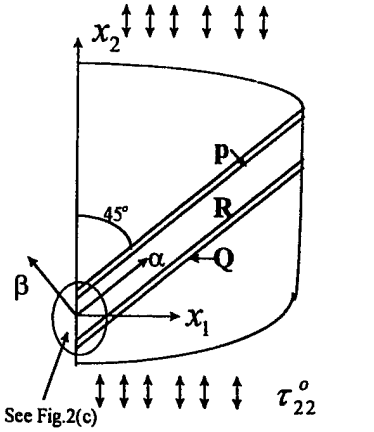

(a) Most Favorable Oriented Crystal

Figure 2 Fatigue Band Model (a)

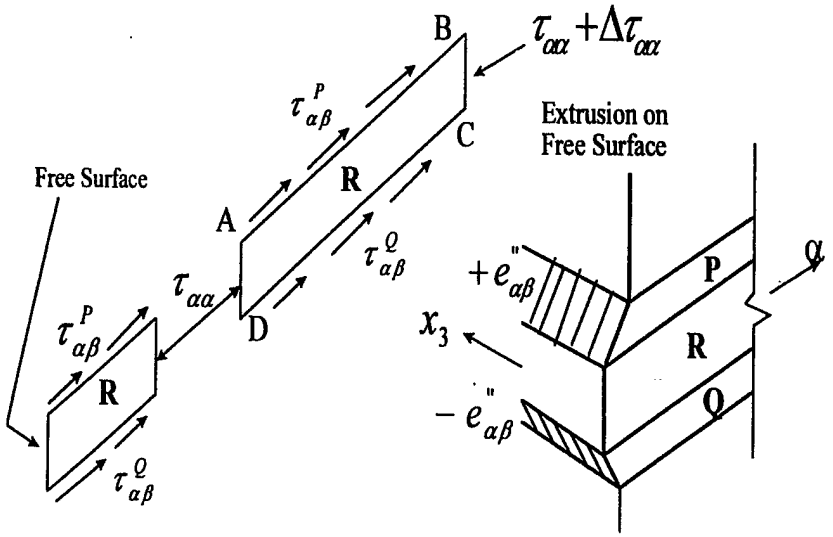

(b) Compressive Stress in R to Cause $+\tau_{\alpha\beta}^{P}$ and $-\tau_{\alpha\beta}^{Q}$

(c) Three-Dimansional View of Extrusion

Figure 2 Fatigue Band Model (b) and (c)

stress along x_2-axis has been found (Lin, 1991 and Lin et al, 1989) to be

$$\tau^r = \frac{4Ge^*_{12}w}{\pi(1-\nu)d}\left\{\frac{\left(\frac{x_2}{d}\right)^2 - 1}{\left[\left(\frac{x_2}{d}\right)^2 + 1\right]^2}\right\} \tag{2}$$

The relief of shear stress τ^s_{ij} is propotional to $e^*_{12}\left(\frac{w}{d}\right)$. For a finite value of τ^r_{ij}, e^*_{12} has to be very large since $\left(\frac{w}{d}\right)$ is very small. This explains the formation of the localized plastic strain to give a shear band under a monotonic loading. The above equation also gives a negligible variation of this residual stress across the thickness. This provides a natural fatigue gating mechanism as explained later.

Forsyth and Stubbington(1955) discovered that thin ribbons protruding out of the surface of fatigue specimens. These protruding ribbons are known as extrusion. Negative extrusion, called intrusion were also observed. Based on these observations, a physical model of fatigue crack initiation was proposed. This model is shown in Figure 2. The formation of an extrusion requires a positive shear strain $e^*_{\alpha\beta}$ in P on the top and a negative shear strain in Q on the bottom of the extrusion R, Figure 2(c). This can be caused by a positive initial resolved shear stress τ^i in P and a negative initial stress in Q. This system of initial resolved shear stress in a segment can be caused by a variation of compressive stress in R, as shown in Figure 2(b).

Consider the segment ABCD in Figure 2(b) having an initial tensile strain $e^i_{\alpha\alpha}$; i.e., this segment has an initial length longer than the slot. Imagine that this segment were cut out and compressed to the same length as the slot, and then welded back to the slot under this imaginary compression. Since there is no such compression, this compression must be relieved by applying an equal and opposite force. This produces a compressive stress $\tau_{\alpha\alpha}$ on the segment at the free surface, which pushes the segment out of the free surface, creating an extrusion. Hence a set of positive shear stress in P and negative in Q is produced by an initial tensile strain in R. This initial tensile strain can be provided by a row of interstitial dipoles (Lin, 1992; Mughrabi, 1981).

RATCHET MECHANISM

With an initial tension in R (Figure 2), the initial shear stress in P, τ^i_P, is positive and that of Q, τ^i_Q, is negative. The shear stress due to the applied load σ_{22} is the same in the whole crystal, thus $\tau^\alpha_P = \tau^\alpha_Q = \tau^\alpha$. Due to the negligible variation of shear stress across the thickness, $\tau^r_P = \tau^r_Q = \tau^r$. Consider the following sequence of loadings :

1. First Cyclic Forward Loading ($\tau^a > 0$): P slides, $\tau^r_{1f} < 0$. Therefore,

$$\tau_P = \tau^i_p + \tau^a + \tau^r_{1f} = \tau^c \quad (3a)$$

$$\tau_Q = \tau^i_Q + \tau^a + \tau^r_{1f} > -\tau^c \quad (3b)$$

2. First Cyclic Reverse Loading ($\tau^a < 0$): Q slides, $\tau^r_{1r} > 0$. Therefore,

$$\tau_P = \tau^i_p + \tau^a + \tau^r_{1f} + \tau^r_{1r} < \tau^c \quad (4a)$$

$$\tau_Q = \tau^i_Q + \tau^a + \tau^r_{1f} + \tau^r_{1r} = -\tau^c \quad (4b)$$

3. Second Cyclic Forward Loading ($\tau^a > 0$): P slides, $\tau^r_{2f} < 0$. Therefore,

$$\tau_P = \tau^i_p + \tau^a + \tau^r_{1f} + \tau^r_{1r} + \tau^r_{2f} = \tau^c \quad (5a)$$

$$\tau_Q = \tau^i_Q + \tau^a + \tau^r_{1f} + \tau^r_{1r} + \tau^r_{2f} > -\tau^c \quad (5b)$$

4. Second Cyclic Reverse Loading ($\tau^a < 0$): Q slides, $\tau^r_{1r} > 0$. Therefore,

$$\tau_P = \tau^i_p + \tau^a + \tau^r_{1f} + \tau^r_{1r} + \tau^r_{2f} + \tau^r_{2r} < \tau^c \quad (6a)$$

$$\tau_Q = \tau^i_Q + \tau^a + \tau^r_{1f} + \tau^r_{1r} + \tau^r_{2f} + \tau^r_{2r} = -\tau^c \quad (6b)$$

This process is repeated.

This model has extensive metallurgical supports. An informative experiment on slip band formation was made by Wood and Bender(1992). They tested copper circular specimens subject to torsion. The deformation in a typical slip band AB of a specimen subject to single twist is shown in Figure 3; a,b,c are typical scratches which were

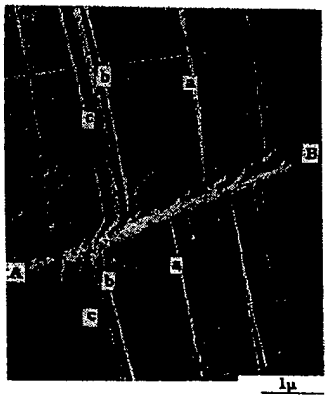

a,b,c are displaced by a shear band under monotonical loading.

Figure 3 Initial straight scratches.

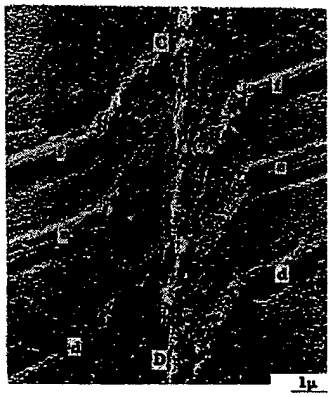

Cyclic slip band causes scratches to displace equally forward and backward

Figure 4 Cyclic slip band causes

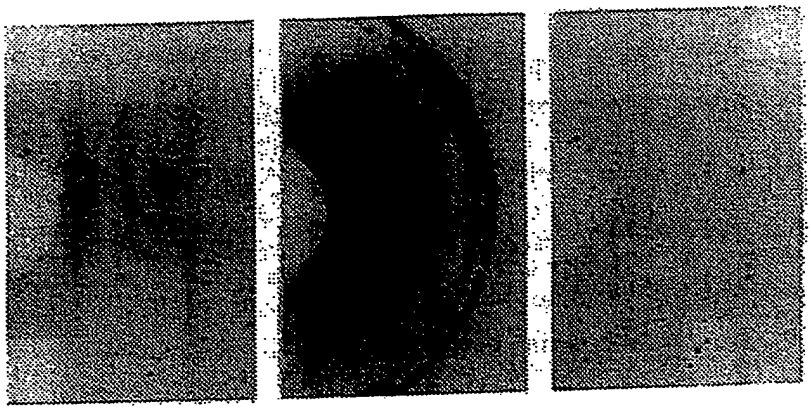

(a) (b) (c)

(a)Sharp X-ray reflection from annealed α-brass. (b)From same specimen as (a) after a unidirectional strain 150×0.5^{o} twist. (c)From same specimen as (a) after 1500 reversals of plastic strain 0.5^{o} twist and showing same reflections as (a). Reproduced from the book "Fracture", 1959, courtesy of Technological Press, Massachusetts Institute of Technology.

Figure 5 X-ray diffraction-patterns

initially straight and continuous. It is seen that the single twist causes the scratches above AB to displace relatively to those below. Figure 4 shows the deformation under cyclic torsion with scratched d,e,f and a typical fatigue band DC. It is seen that the cyclic deformation causes no relative displacement of the scratches left and right of the fatigue bands, but within the band, the scratches have displaced equally up and down producing a zigzag. A severely slid line with positive shear such as P is sandwiched by two less severely slid lines with negative shear such as Q. This clearly agrees with the theory proposed.

X-ray reflection patterns of cyclically loaded specimens retain the discrete spots like those of annealed metals(ssee Figure 5). This is because the positive slip in P is balanced by the negative slip in Q. The stress field and lattice strain is small in the bulk of this metal. Under monotonic loadings, the slip in all slip lines are of the same sign and causes a significant average plastic strain and hence an appreciable lattice strain in the bulk of the metal. This clearly agrees with the proposed theory.

Single crystals are traction-free on all transverse surfaces as shown in Figure 6. The stress caused by a fatigue band varies along three axes. The analysis requires three dimension analysis. To reduce the large amount of computation, boundary element method has been used. Calculated hysteresis loops for stress-controlled loadings are shown in Figure 7.

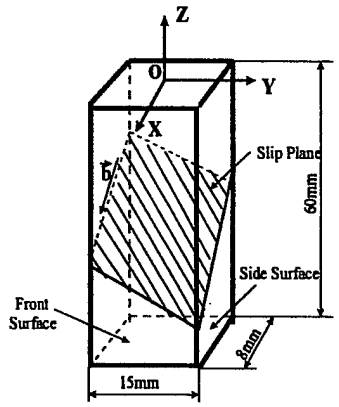

Figure 6 Geometry of the Single Crystal

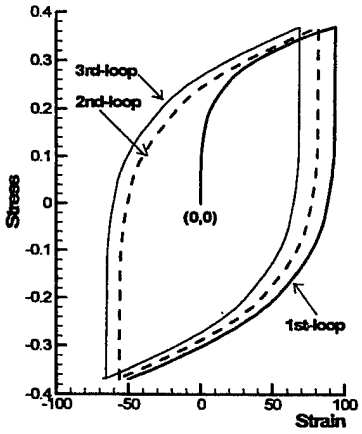

Figure 7 Hysteresis Loops of Stress-Strain

This model has been found to be able to explain many other metallurgical observations such as the secondary slip(Zhai et al, 1996), the effect of grain size, mean stress etc(Lin,1995). It is hoped to develop this model to give a more general fatigue theory for metals.

Acknowledgements: This research was sponsored by AFOSR through grant F49629-96-1-0350. The view and conclusions contained herein are those of the authors and should not be interpreted as necessarily representing the official polices of the sponsoring agency.

REFERENCES

1. Lin T.H.,"Micromechanics of Crack Initiation in high-cyclic Fatigue," Adv. in Applied Mechanics, Vol 29, 1991, pp1-68.

2. Lin T.H., Lin S.R. and Wu X.Q.,"Micromechanics of an Extrusion in High-Cyclic Fatigue," Phil. Mag. A, 59, 1989, pp1263-1276.

3. Forsyth P.J.E. and Stubbington C.A., The Slip Band Extrusion Effect Observed in Some Aluminum Alloys Subject to Cyclic Stress", J.Inst. Metals, Vol 83,1955,pp395.

4. Wood W.A. & Bender, A.M., The Fatigue Progress in Copper as Studies by Electron Metallography, Trans. Metalurgical society AIME 244, 1962, pp180-186.

5. Wood W.A., Mechanism of Fatigue, in "Fatigue in Aircraft Structures" Edited by A,M,Freundenthal Academic Press, New York, 1956 pp1-19.

6. Zhai T., Briggs G.A.D. and Martin J.W.,"Fatigue Damage at Room Temperature in Aluminum Single Crystals IV:Secondary Slip," Acta Metall., 44, 1996, pp3489-3496.

To be published in Journal of Applied Mechanics.

MICROMECHANICS OF HYSTERESIS LOOPS OF FATIGUE IN SINGLE CRYSTAL

T. H. Lin
Department of Civil and Environmental Engineering
University of California, Los Angeles
Los Angeles, CA 90095-1593

K. K. F. Wong
Department of Civil and Environmental Engineering
University of California, Los Angeles
Los Angeles, CA 90095-1593

N. J. Teng
Universal Analytics, Inc.,
Torrance, CA 90503

Grain boundaries are susceptible to cause boundary corrosion, cracking, and creep deformation. Single crystals are presently used in turbine engines. A micromechanic analysis is shown to explain the occurrence of highly localized plastic strain in the slip band known as the shear band in metals under a monotonic loading. Based on the prior analyses of fatigue bands in polycrystals, a micromechanic analysis of a single crystal under plane deformation is developed. Bauschinger effect and hysteresis loops of these single crystals were calculated and shown. The calculated results agree generally with experimental observations.

1 Introduction

Single crystal nickel based superalloys have been developed to eliminate the grain boundaries which are susceptible to cause grain boundary corrosion, cracking, and creep

deformation (Walker and Jordan, 1989). These single crystals are presently used in turbine engine parts. The prediction of fatigue life of these single crystals is of both scientific interest and practical need. This paper, based on the extension of the micromechanic high-cycle fatigue analysis of a face-centered-cubic (f.c.c.) polycrystal, gives a method to analyze single crystals under cyclic loading in plane deformation. This analysis is first shown to explain the formation of shear band under a monotonic loading, then to explain the growth of fatigue band in a polycrystal under a cyclic loading, and finally gives the analysis of fatigue band in high-cycle fatigue (HCF) of a single crystal under plane deformation.

2 A Micromechanic Theory of Fatigue Crack Initiation

Initial defects always exist in metals and cause an initial stress field τ^i. During loading, when the resolved shear stress in some region reaches the critical shear stress τ^c, slip occurs. After unloading, this slip remains and induces a residual shear stress τ^r. Denoting the resolve shear stress caused by loading by τ^a, the total resolved shear stress is then

$$\tau = \tau^i + \tau^a + \tau^r \tag{1}$$

The governing condition to initiate or continue sliding is to have the resolved shear stress equal to the critical shear stress, i.e.,

$$\tau = \tau^c \quad , \quad \text{slip occurs} \tag{2a}$$

$$\tau < \tau^c \quad , \quad \text{no slip} \tag{2b}$$

(i) *Role of Microstress Field on the Formation of Fatigue Band*

When a piece of metal is uniformly loaded, slip lines appear on the surface. These slip lines are the results of highly localized plastic deformation. This raises the question of why the

plastic strain is so heterogeneous. To explain this highly heterogeneous plastic deformation, the micromechanic shear stress field due to a uniform plastic strain e_{12}'' in a thin slice (see Figure 1) in an isotropic infinite medium is analyzed. This analysis gives the residual shear stress (Lin, 1992) along x_1-axis as

$$\tau^r = \frac{4\mu e_{12}'' wd}{\pi(1-\upsilon)} \frac{x_1^2 - d^2 - w^2}{\left(w^2 + (x_1 + d)^2\right)\left(w^2 + (x_1 - d)^2\right)} \tag{3}$$

This τ^r is positive outside the slice. Hence the width $2d$ of this slice tends to increase. This explains why in general, a slip band rapidly widens, covering the whole crystal. Along the x_2-axis, this analysis gives a residual shear stress as

$$\tau^r = \frac{4\mu e_{12}'' wd}{\pi(1-\upsilon)}\left[1 - \left(\frac{x_2}{d}\right)^2\right] \tag{4}$$

The thickness $2w$ is generally very small and approaches zero. The plastic strain e_{12}'' required to yield a finite value of τ^r has to be very large. This explains why the highly localized plastic strain occurs in thin slip bands in single phase metal under uniform loading. Hence, the combination of Eqs. (3) and (4) explains the formation of shear band under a monotonic loading. Equation (4) not only shows the large plastic strain in the shear band, but also gives the negligible variation of the residual shear stress across the thickness. This is referred to as the continuity of the resolved shear stress field. This is important in explaining the ratchet mechanism in fatigue band, which will be explained later.

(ii) *Fatigue Band Model*

Under cyclic loadings, slip lines appear on the surface (see Figure 2). After removing these slip lines by electro-polishing and recycling, original lines reappear. These slip lines are

known as persistent slip bands (PSBs), which are the favorable sites of crack initiation. In 1950's, thin ribbons protruding out of fatigue specimen surface were discovered (Forsyth and Stubbingtion, 1955). These ribbons are known as extrusions. Negative extrusion, called intrusions, were also observed (see Figure 3). Based on the hints supplied by these observations, a physical model was developed for HCF crack initiation.

The physical model of fatigue crack initiation is shown in Figure 4(a). The extrusion or intrusion is represented by R in this figure. The formation of an extrusion requires a positive shear strain $e''_{\alpha\beta}$ in P on the top and a negative shear strain in Q on the bottom of the extrusion R. This can be caused by a positive initial shear stress τ^i in P and a negative initial shear stress $-\tau^i$ in Q. This system of initial resolved shear stress in a segment can be caused by a change of compressive stress in R, as shown in Figure 4(b).

Consider the segment *ABCD* in Figure 4(b) having an initial tensile strain $e^i_{\alpha\alpha}$; i.e., this segment has an initial length longer than the slot. Imagine that this segment is cut out and compresses to the same length as the slot, and then is welded back to the slot under this imaginary compression. Since there is no such compression, this compression must be relieved by applying an equal and opposite force. This produces a compressive stress $\tau_{\alpha\alpha}$ on the segment at the free surface, which pushes the segment out of the free surface, creating extrusion. Hence a set of positive shear stress in P and negative in Q is produced by an initial tensile strain in R. This initial tensile strain can be provided by a row of interstitial dipoles (Lin, 1992; Essmann *et al.*, 1981).

(iii) *Ratchet Mechanism*

With an initial tensile strain $e^i_{\alpha\alpha}$ in R (see Figure 4), the initial shear stress in P, τ^i_P, is positive and that of Q, τ^i_Q, is negative. The shear stress due to the applied load σ_{22} is the same in the whole crystal, thus $\tau^a_P = \tau^a_Q = \tau^a$. Due to the continuity of the residual shear stress field as given by Eq. (4), $\tau^r_P = \tau^r_Q = \tau^r$. The relief of the resolved shear stress is practically constant across the thickness of the slice. The regions outside the slice did not slide when the slice did. This indicates the initial stress in these regions was less than that in the slice. After the slice slides, the resolved shear stress would be still less than that in the slice and hence is still less than the critical shear stress and remains unslid (Lin, 1991). Consider the following sequence of loadings:

1. *First Cycle Forward Loading* ($\tau^a > 0$): P slides, $\tau^r_{1f} < 0$, where the subscript "1*f*" denotes the first forward loading. Therefore,

$$\tau_P = \tau^i_P + \tau^a + \tau^r_{1f} = \tau^c \tag{5a}$$

$$\tau_Q = \tau^i_Q + \tau^a + \tau^r_{1f} > -\tau^c \tag{5b}$$

2. *First Cycle Reversed Loading* ($\tau^a < 0$): Q slides, $\tau^r_{1r} > 0$. Therefore,

$$\tau_P = \tau^i_P + \tau^a + \tau^r_{1f} + \tau^r_{1r} < \tau^c \tag{6a}$$

$$\tau_Q = \tau^i_Q + \tau^a + \tau^r_{1f} + \tau^r_{1r} = -\tau^c \tag{6b}$$

3. *Second Cycle Forward Loading* ($\tau^a > 0$): P slides, $\tau^r_{2f} < 0$. Therefore,

$$\tau_P = \tau^i_P + \tau^a + \tau^r_{1f} + \tau^r_{1r} + \tau^r_{2f} = \tau^c \tag{7a}$$

$$\tau_Q = \tau^i_Q + \tau^a + \tau^r_{1f} + \tau^r_{1r} + \tau^r_{2f} > -\tau^c \tag{7b}$$

4. *Second Cycle Reversed Loading* ($\tau^a < 0$): Q slides, $\tau^r_{2r} > 0$. Therefore,

$$\tau_P = \tau_P^i + \tau^a + \tau_{1f}^r + \tau_{1r}^r + \tau_{2f}^r + \tau_{2r}^r < \tau^c \tag{8a}$$

$$\tau_Q = \tau_Q^i + \tau^a + \tau_{1f}^r + \tau_{1r}^r + \tau_{2f}^r + \tau_{2r}^r = -\tau^c \tag{8b}$$

This process is repeated. A typical numerical result of the plastic strain distributions in P at different cycles of loading of the surface crystal is shown in Figure 5. It is seen that P always slides in the positive direction and Q in the negative direction. The magnitudes of these slips and hence the extrusions are monotonically increasing.

(iv) *Secondary Slip*

The build-up of the slip strain $e_{\alpha\beta}''$ in P and Q is caused by $e_{\alpha\alpha}^i$ in R. If R were cut out, the free length of R would be longer than the slot by an amount known as the static extrusion (Mughrabi *et al.*, 1983). The $e_{\alpha\alpha}^i$ causes an initial compression in R, which in turn causes positive $\tau_{\alpha\beta}^i$ in P and negative $\tau_{\alpha\beta}^i$ in Q. Under cyclic loading, the extrusion grows and R increases in length. This elongation causes the compression in R to decrease. There are 12 slip systems in a f.c.c. crystal. The change of direct stress $\tau_{\alpha\alpha}$ in R causes changes in resolved shear stress in all slip systems. When the decrease in compression in R becomes large, the applied stress can cause a second slip system to have shear stress reaching the critical value and slide. The plastic strain $e_{\xi\eta}''$ caused by slip in this secondary slip system has a <u>tensor</u> component $e_{\alpha\alpha}''$, just like the initial tensile strain $e_{\alpha\alpha}^i$ in causing the positive and negative $\tau_{\alpha\beta}^i$ in P and Q, respectively (Lin *et al.*, 1989). Hence with secondary slip, the extrusion can grow considerably beyond the static extrusion. The occurrence of the secondary slip system was recently clearly observed (Zhai *et al.*, 1996).

3 Experimental Verifications

This model has extensive metallurgical supports (Lin, 1992), and two of these supports are discussed as follows:

(i) *Slip Band Formation*

An informative experiment on slip band formation was made be Wood and Bender (1962). They tested copper circular rod specimens subject to torsion. The specimens were electro-polished and then scratched as markers with a pad carrying 0.5μ diamond dust. Some specimens were subject to alternate torsion and some subject to single twist through large angles. The deformation in a typical slip band AB of a specimen subject to single twist is shown in Figure 6; a, b, c are typical scratches which were initially straight and continuous. It is seen that the single twist causes the scratches above AB to displace relative to those below. Figure 7 shows the deformation under cyclic torsion with scratches d, e, f and a typical fatigue band DC. It is seen that the cycle deformation caused no relative displacement of the scratches left and right of the fatigue band, but within the band the scratches have displaced equally up and down producing a zig-zag. A severely slid line with positive shear as P is sandwiched in two less severely slid lines with negative shear such as Q. This clearly verifies with the theory proposed.

(ii) *Lattice Straining*

X-ray reflection patterns of monotonically and cyclically loaded specimens are very different (Wood, 1956). The later retain the discrete spots like that of annealed metals while the former do not (Figure 8). This shows that slip occurrence in alternate loadings

does not cause lattice straining in the bulk of the metal. Under cyclic loading, the positive shear slip lines (like P) are closely located with the negative one (like Q). At some distance from the slip lines, the stress field caused by positive slip in P is balanced by that caused by negative slip in Q. Hence the stress field and the lattice strain is small in the bulk of the metal. Under monotonic loadings, the slip in all slip lines tends to be all of the same sign and causes a significant average plastic strain, which causes an appreciable stress field and a lattice strain in the bulk of the metal. The above theory accounts for the different X-ray reflection patterns of the monotonically deformed and cyclically deformed metals.

4 Single Crystals

The single crystal nickel-based superalloys have been developed to eliminate the grain boundaries, which are susceptible to grain boundary corrosion, cracking, and creep deformation (Walker and Jordan, 1989). These single crystals are presently used in turbine engines. The prediction of HCF life of these single crystals is of practical need. The following shows the analysis of fatigue bands of single crystals.

(i) *Method of Analysis*

A crystal embedded at the free surface of the polycrystal under alternated tension and compression is first analyzed, as shown in Figure 4(a). This solution gives surface tractions on the grain boundary. In a single crystal, the surface tractions are zero and hence must be removed by applying equal and opposite tractions on the boundary. The stress field caused by this equal and opposite tractions is analyzed by finite element method (FEM).

Plastic strain is taken to occur only in the fatigue band. The band is divided into a number of grids. The plastic strain in the left half of the crystal is denoted by $e_{ij}''^{(L)}$ and in the right half by $e_{ij}''^{(R)}$. The solution of the stress field in Figure 9(a) is the sum of the solutions of Figures 9(b), (c), and (d). Figure 9(d) gives uniform stress. The stress field due to $e_{ij}''^{(L)}$ is solved by the semi-infinite solid analysis with the free surface at the left, as shown in Figure 10. This solution yields the condition of zero traction at the free surface and gives surface tractions on the right, top, and bottom planes (see Figure 10(b)). These tractions are removed by applying equal and opposite tractions, as shown in Figure 10(c). The plastic strain in the grid is replaced by the equivalent forces (Lin, 1968) and the stress field caused by these equivalent forces is solved by FEM. This equivalent force due to $e_{ij}''^{(L)}$ is relatively far from the considered crystal boundaries and hence the variation of the surface traction on the boundary is small, and thus the grids of the FEM do not need to be very fine. This facilitates the FEM solution. Similarly, for the grid in the right half of the crystal, the free surface of the semi-infinite solution is taken to be at the right side.

The initial strain e_{ij}^{i} has the same effect as plastic strain e_{ij}'' in causing a stress field, so the initial strain can be analyzed in the same way as the plastic strain. This gives a method to calculate the stress influence coefficient in the mth grid caused by a unit inelastic strain (either plastic strain or initial strain) in the nth grid. The resolved shear stress τ equals the sum of the initial stress τ^{i}, the applied stress τ^{a}, and the residual stresses $\tau^{r(L)} + \tau^{r(R)}$. Equating the resolve shear stress τ to the critical shear stress τ^{c} gives the incremental plastic strain distributions at different stages of loading.

(ii) *Experimental Observations of Fatigue Bands in Single Crystals*

Mecke and Blochwitz (1980) observed the subgrain displacement in single nickel crystal under cyclic loading. These experiments were carried out under constant plastic strain amplitudes at room temperature. It is shown that the PSBs have penetrated across the whole crystal and extruded out on both sides as shown in Figure 11. The case with extrusion protruding on one side and intrusion on the other side was not observed. Basinski *et al.* (1983 and 1985) tested copper single crystals at constant plastic strain amplitudes at room temperature under cyclic loadings. In these tests, both extrusions and intrusions are observed. Zhai *et al.* (1990 and 1995) performed fatigue experiments on aluminum single crystals under constant cyclic stress amplitude. Again, both extrusions and intrusions were observed on the free surfaces.

(iii) *Numerical Calculations*

The analytical solution developed in previous sections is here applied to analyze the single crystal tests. To simplify the calculation, a single fatigue band in the single crystal is considered (the grain boundary shown in Figure 4(a) is now a free surface). The analytical method can readily be used to analyze multiple fatigue bands in the crystal. Referring to Figure 4(a), both P and Q are assumed to be 0.05 μm in thickness, and R to be 1.0 μm. The crystal is f.c.c. and is assumed to be elastically isotropic with shear modulus $\mu = 50\ GPa$ and the Poisson ratio $\upsilon = 0.3$. The critical shear stress, τ^c, is taken to be 200 *MPa*, and cyclic loading $\tau_{22} = 399.55\ MPa$. An initial tensile strain was assumed to vary linearly from a maximum value at the center to zero at the two ends of a 1.4 mm segment in the fatigue band. This segment was divided into a number of grids, and each grid was approximated by a uniform initial tensile strain. This assumed initial tensile strain distribution was found to give an initial resolved shear

stress, τ^i, quite uniform over each half of the fatigue band. Thus a uniform τ^i of 0.5 *MPa* was used in the present analysis. The variations of the plastic strain in P and Q along the length of the fatigue band at different cycles of loading are shown in Figure 12.

The widening of a slip band, i.e., the increase of "2*d*," has been explained in the micromechanic analysis (see Eq. (3)). This gives the spread of the fatigue band toward the two free surfaces, causing the protruding of extrusion on two sides. If the initial tensile strain in the above is replaced by an initial compression strain, intrusions instead of extrusions will occur on both sides. The present model seems to explain the observed extrusions and intrusions.

(iv) *Hysteresis Loops*

This analytical model is used to calculate hysteresis loops of aluminum single crystals, with shear modulus $\mu = 26.5$ *GPa* and Poisson ratio $\upsilon = 0.3$. The critical shear stress, τ^c, is taken to be 0.369 *MPa*. A calculated hysteresis loop is shown in Figure 13. In the initial loading and unloading curve, the elastic limit in unloading occurs at a positive normal stress, i.e., at positive resolved shear stress. This indicates a large Bauschinger effect. The widths of the hysteresis loops have been found to decrease with the number of cycles and approaches zero reaching the saturation stage of cyclic loading. This agrees with the experimental hysteresis loops of aluminum single crystals shown in Figure 14 (Thompson and Wadsworth, 1958).

5 Conclusions

For an extrusion to protrude, the shear strain in P has to be positive and that in Q has to be negative near the occurrence of extrusion. This requires positive resolved shear stress in P and negative in Q. In turn, this requires a compressive stress in R to push the extrusion out. The

occurrence of extrusion on both sides of the single crystal implies compression in R on both faces. Similarly, for an intrusion to occur on the left side, the shear strain in P must be negative and that in Q must be positive. This requires a tensile stress in R to pull the intrusion in. A segment in R with an initial compressive strain tends to increase the length of the tensile stress in R under cyclic loadings. The spread of the tension in R over the length of the fatigue band will result in intrusions on both faces. Initial compression and initial tension may occur in the specimens. Hence extrusions on both faces and intrusions on both faces have been observed.

This single crystal fatigue band analysis is for plane strain, which gives an approximate solution for the central length portion of the crystal. To calculate the slip in the second slip system near the side faces that was clearly observed, a three-dimensional model is required and is being developed. This study is essential to improve the representation of the constitutive relation of single crystals and single crystal superalloys, which is important to the design of engine parts made of single crystals.

Acknowledgment

This work was sponsored by the Air Force Office of Scientific Research (AFOSR), USAF, under grant number F49629-96-1-350. The views and conclusions contained herein are those of the authors and should not be interpreted as necessarily representing the official policies or endorsements, either expressed or implied, of the AFOSR or the U.S. Government.

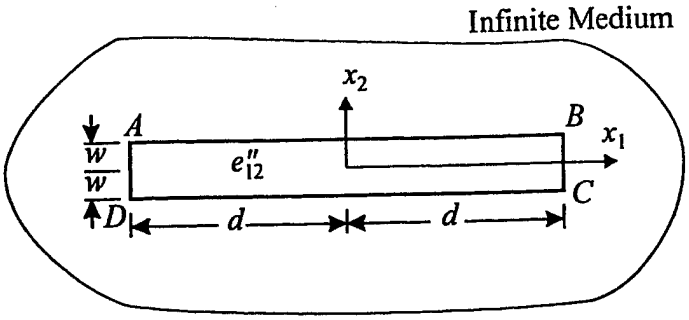

Fig. 1 Shear band model.

(a) after 10^4 cycles

(b) after $5x10^4$ cycles

Fig. 2 Slip lines in polycrystalline nickel during two stages of cyclic loading (Kennedy, 1963).

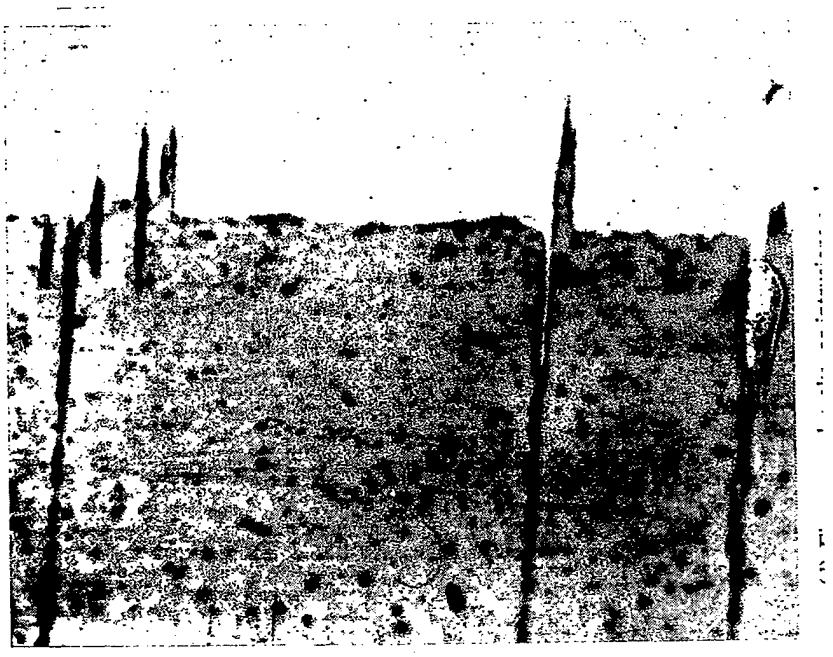

Fig. 3 Intrusions and extrusions in copper during fatigue.

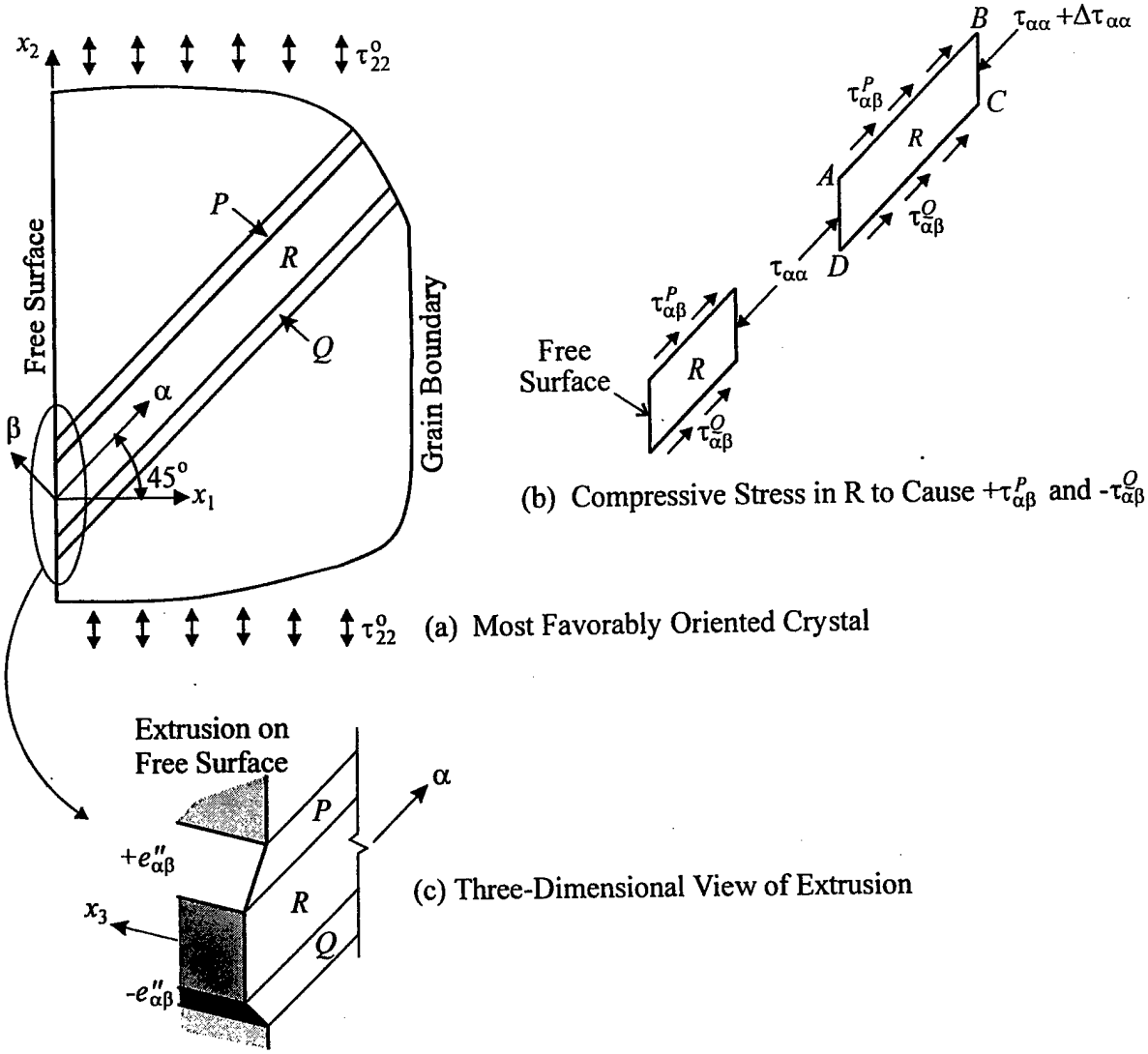

Fig. 4 Fatigue band model.

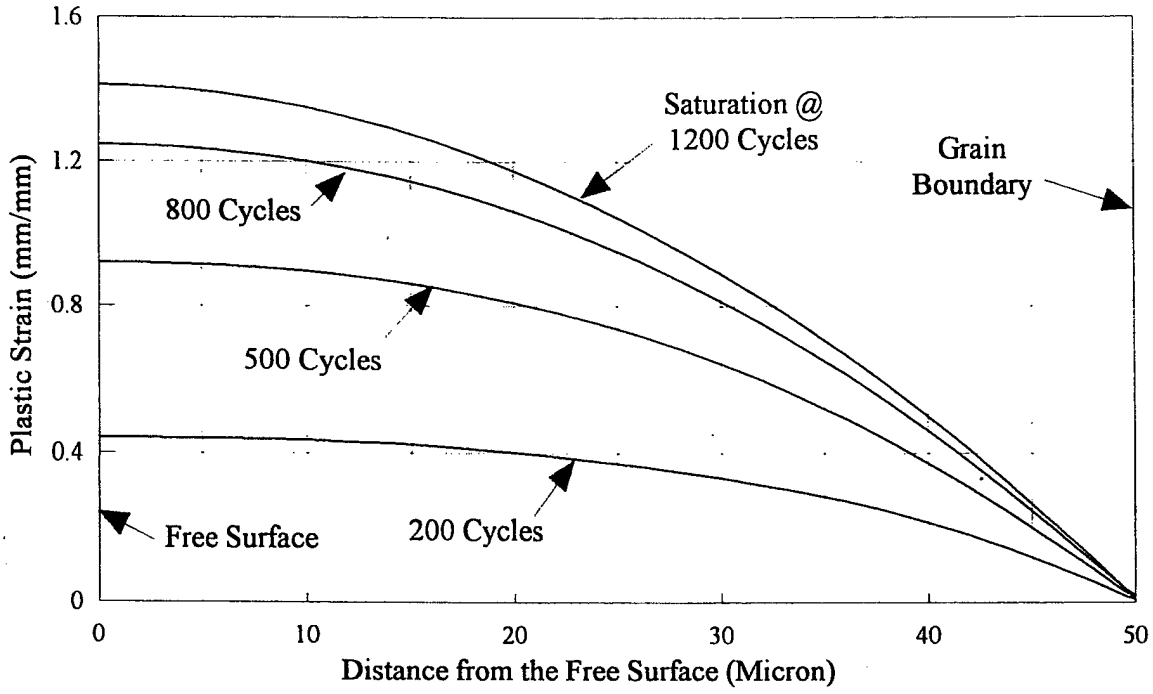

Fig. 5 Typical plastic strain distribution under cyclic loadings of aluminum.

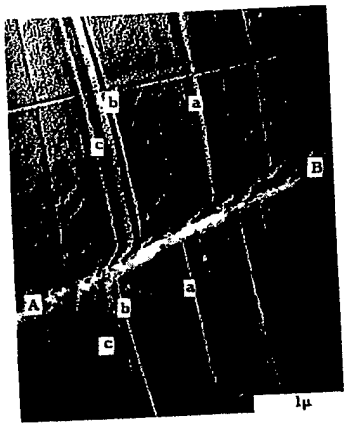

Fig. 6 Initially straight scratches a, b, c are displaced unidirectionally by static slip band AB.

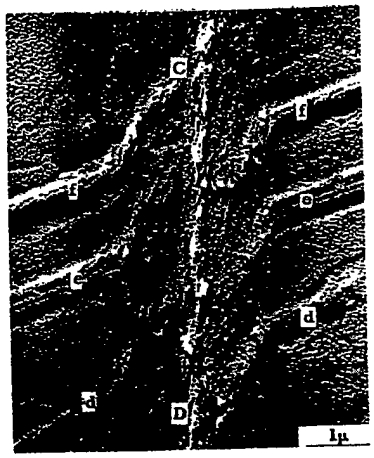

Fig. 7 Cyclic slip band CD produces no overall displacement of scratches d, e, and f. Within the slip band, the scratches are displaced equally backward and forward.

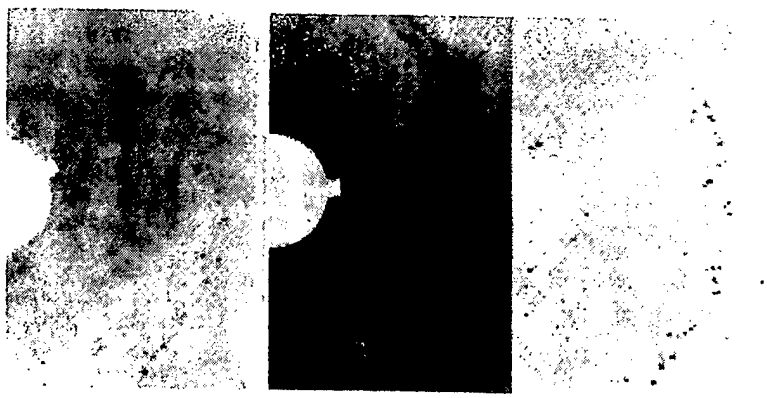

(a) (b) (c)

Fig. 8 X-ray reflection patterns: (a) Sharp X-ray from annealed α-brass, (b) from same specimen as (a) after a unidirectional strain 50 x 0.5° twist, (c) from same specimen as (a) after 1500 reversals of plastic strain 0.5° twist and showing same direction as (a).

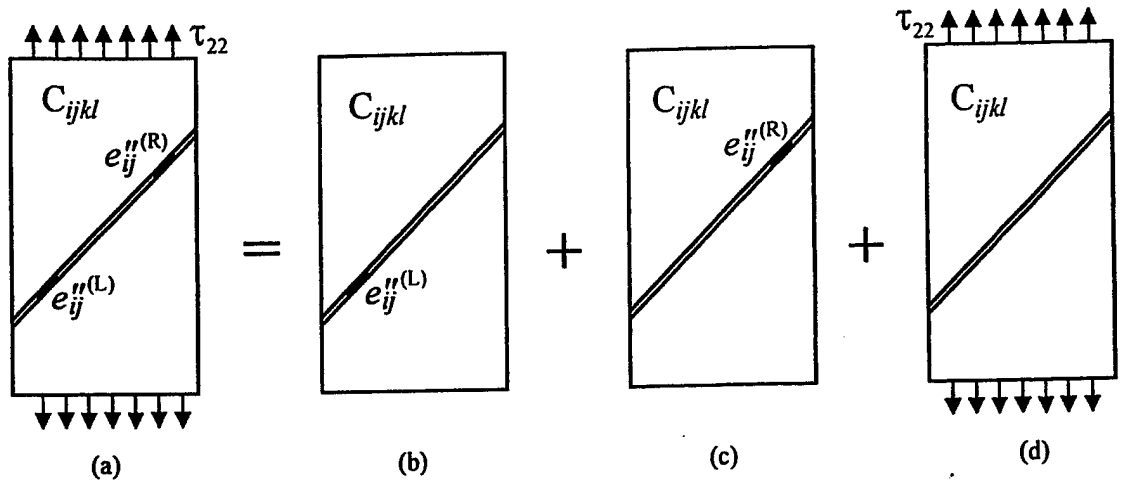

Fig. 9 Procedure for decoupling the single crystal problem.

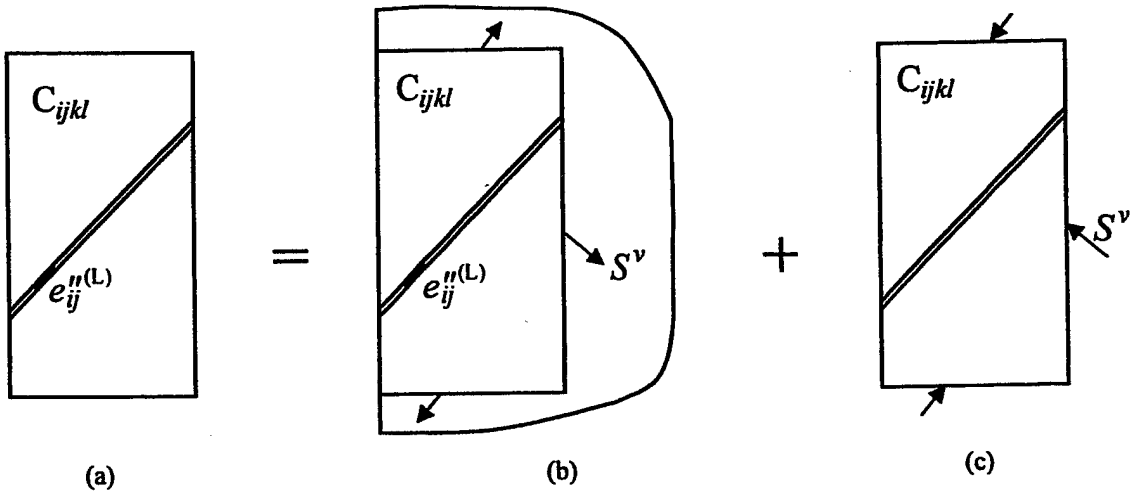

Fig. 10 Removal of boundary tractions for a single crystal.

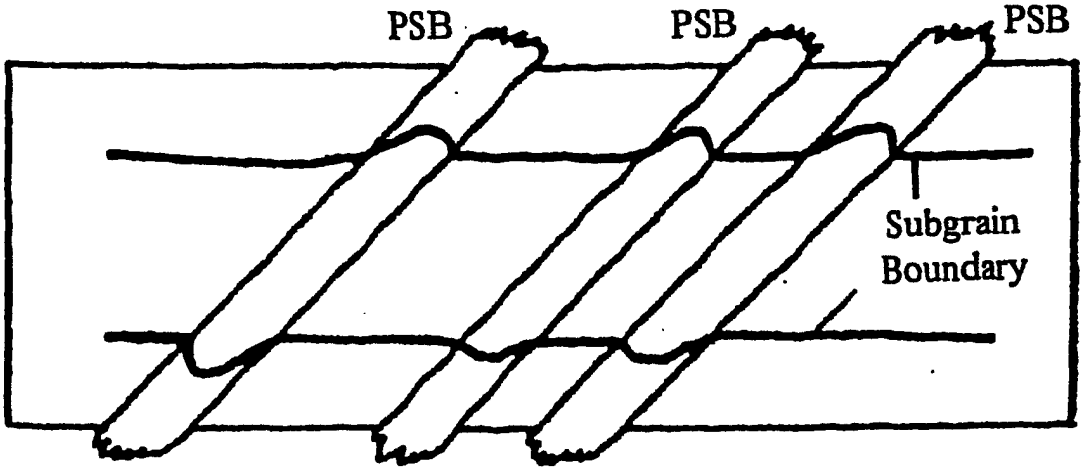

Fig. 11 Extrusions observed in single crystal.

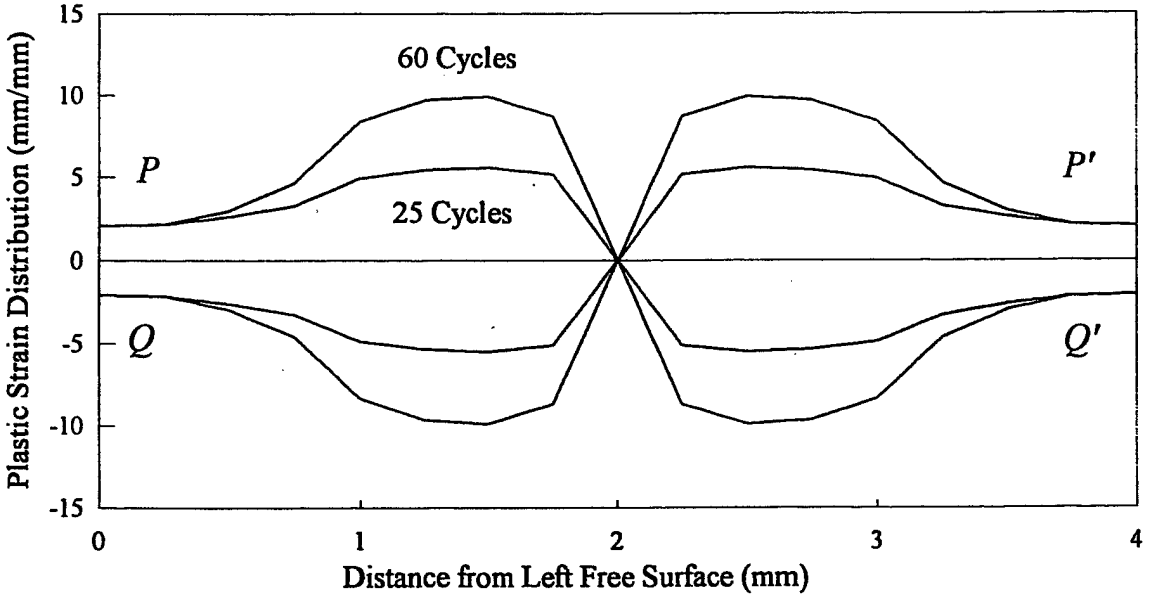

Fig. 12 Plastic strain distribution with initial strain at center. P & Q' and Q & P' are symmetrically located. Extrusions protruding out on both faces.

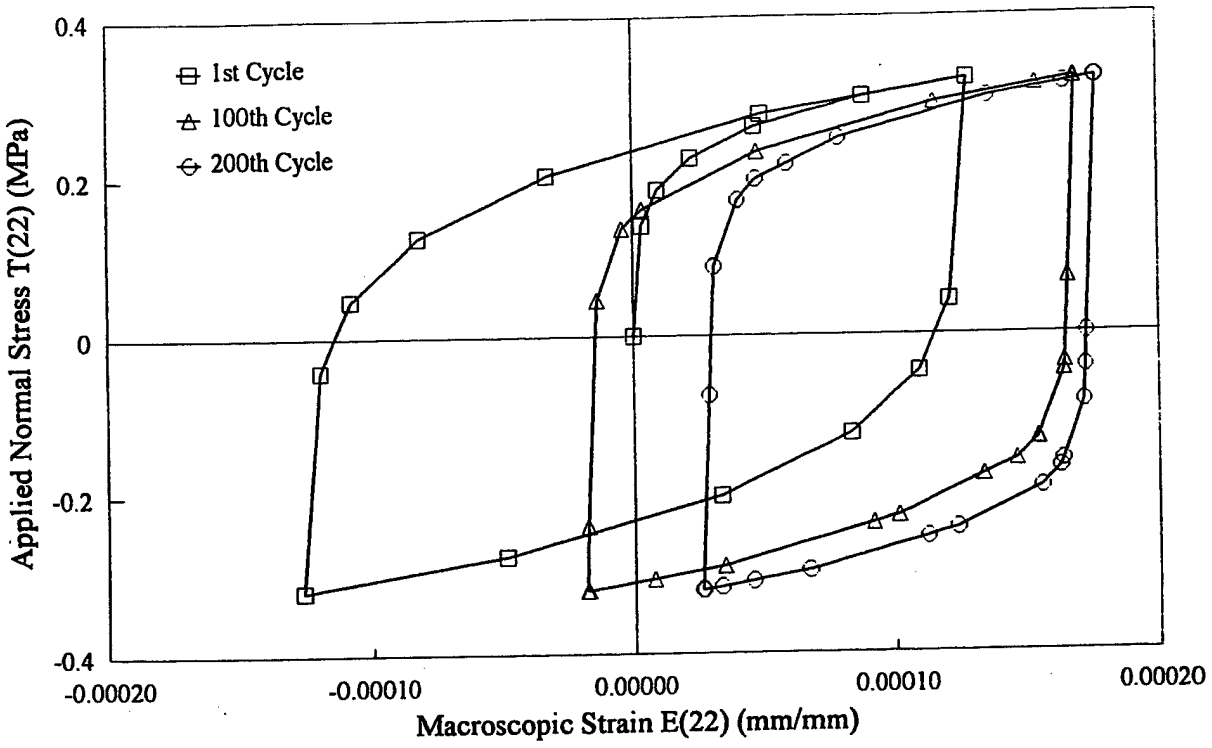

Fig. 13 Hysteresis loops of an aluminum single crystal.

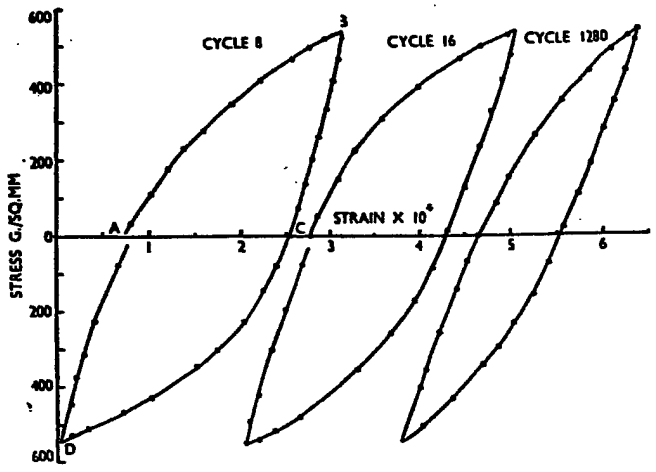

Fig. 14 Experimental observation of hysteresis loops in aluminum single crystal.

References

Basinski, Z. S., Pascual, R., and Basinski, S. J., 1983, "Low Amplitude Fatigue of Copper Single Crystals I – The Role of the Surface in Fatigue Failure," *Acta Metall.*, Vol. 31, pp. 591-602.

Basinski, Z. S. and Basinski, S. J., 1985, "Low Amplitude Fatigue of Copper Single Crystals II – PSB Sections," *Acta Metall.*, Vol. 33, pp.1319-1327.

Forsyth, P. J. E. and Stubbington, C. A., 1955, "The Slip Band Extrusion Effect Observed in Some Aluminum alloys Subject to Cyclic Stresses," *J. Inst. Metals*, Vol. 83, p. 395.

Essmann, V., Gossel, V, and Mughrabi, H., 1981, "A Model of Extrusions and Intrusions in Fatigued Metals I – Point Defect Production and the Growth of Extrusions," *Phil. Mag. A*, Vol. 44, pp. 405-426.

Kennedy, A.J., 1963, *Process of Creep and Fatigue of Metals*, John Wiley & Sons, NY.

Lin, T. H., 1968, *Theory of Inelastic Structures*, John Wiley & Sons.

Lin, T. H., Lin, S. R., and Wu, X. Q., 1989, "Micromechanics of an Extrusion in High-Cycle Fatigue," *Phil. Mag. A*, Vol. 59, pp. 1263-1276.

Lin, T. H., 1992, "Micromechanics of Crack Initiation in High-Cycle Fatigue," *Adv. in Applied Mechanics*, Vol. 29, pp. 1-62.

Mecke, K. and Blochwitz, C., 1980, "Internal Displacement of Persistent Slip Bands in Cyclically Deformed Nickel Single Crystals," *Phys. Stat. Sol. (A)*, Vol. 64, p. K5-K7.

Mughrabi H., Wang, R., Differt, K., and Essmann, V., 1983, "Fatigue Crack Initiation by Cyclic Slip Irreversibilities in High-Cycle Fatigue," *Fatigue Mechanism*, STM STP 811, pp. 5-45.

Thompson, N. and Wadsworth, N. J., 1958, "Metal Fatigue," *Advances in Physics*, Vol. 7, pp. 72-170.

Walker, K. P. and Jordan, E. M., 1989, "Biaxial Constitutive Modeling and Testing of a Single Crystal Superalloy at Elevated temperatures", *Biaxial and Multiaxial Mechanical Engineering Publication*, London, pp. 145-170.

Wood, W. A., 1956, "Mechanisms of Fatigue," Fatigue in Aircraft Structures, A. M. Freudenthal (Ed.), Academic Press, New York, pp. 1-19.

Wood, W. A. and Bendler, H. M., 1962, "The Fatigue Process in Copper as Studies by Electron Metallography," *Trans. Metallurgical Society AIME*, Vol. 224, pp. 180-186.

Zhai, T., Lin, S., and Xiao, J. M., 1990, "Influence on Non-Geometric Effect of PSB on Crack Initiation in Aluminum Single Crystal," *Acta Metall. Mater.*, Vol. 38, pp. 3813-3825.

Zhai, T., Martin, J. W., and Briggs, G. A. D., 1995, "Fatigue Damage at Room Temperature in Aluminum Single Crystals I: On the Surface Containing the Slip Burger's Vector," *Acta Metall. Mater.*, Vol. 43, pp. 3813-3825.

Zhai, T., Briggs, G. A. D., and Martin, J. W., 1996, "Fatigue Damage at Room Temperature in Aluminum Single Crystals IV: Secondary Slip," *Acta Mater.*, Vol. 44, pp. 3489-3496.

To be published in Philosophical Magazine A.

Micromechanic Analysis of Crack Initiation and Hysteresis Loops of Aluminum Single Crystals under High-Cycle Fatigue

By T. H. Lin, N. G. Liang†, K.F.F.Wong‡ and N. J. Teng §

Department of Civil and Environmental Engineering

University of California, Los Angeles, California 90095

ABSTRACT

The micromechanic model of an extrusion formation in a polycrystal under high-cycle fatigue is briefly reviewed. Following the same general approach, and guided by the observations on the subgrain boundary displacement in a single crystal (Mecke and Blochwitz, 1981), a micromechanic model of extrusions and intrusions in an aluminum single crystal with multiple fatigue bands under stress-controlled loadings is presented. The microstress and strain fields in the crystal are calculated by the boundary element method for the three-dimensional elasto-plastic solids. From these micro fields, the macroscopic stress and strain of the crystal at different stages of loading are calculated. The numerical analysis gives the changes of hysteresis loop shape with loading cycles. The incremental plastic strain distribution and the incremental residual stress in each cycle depend on the initial shear stresses. Two sets of initial stresses are taken to calculate the hysteresis loops. It shows the dependence of the shape and size of the hysteresis loops on the distribution of initial shear stresses. The size and distribution of persistent slip bands (PSBs) on the front-surface of the present model are the same as those on the side-surface. This agrees with experiments (Zhai, et al.,1995 and 1996). Both the calculated and the experimental

PSBs on the side-surfaces are concave. The calculated extrusion height and intrusion depth at stress saturation seem to agree with the experimental values. This model seems to provide an explanation for a number of observations in a fatigued single crystal oriented for single slip.

---

† Present address: Institute of Mechanics, Academy of Sciences, Beijing, China

‡ Present address: Department of Civil Engineering, Nanyang Techological University, Singapore 639798.

§ Also with MSC.Software Corporation, Los Angeles, California, U.S.A.

1. INTRODUCTION

It is estimated that nearly 90% of catastrophic failures of structural parts are due to material fatigue (Puskar and Golovin, 1985). The fatigue process of ductile metals may be roughly divided into two stages, i.e., fatigue crack initiation and crack propagation. In high-cycle fatigue (HCF), fatigue crack initiation takes about 80% of the fatigue life, while in low-cycle fatigue (LCF), the fatigue process is dominated by crack propagation. Fatigue crack initiation always precedes fatigue crack propagation. The objective of this paper is to study the phenomenon of fatigue crack initiation in aluminum single crystals under HCF, from the consideration of the microscopic mechanism and macroscopic responses including hysteresis loops.

Numerous fatigue tests have indicated that persistent slip bands (PSBs) are the most frequently observed fatigue crack nucleation sites in ductile single crystals (Basinski and Basinski, 1992). Cyclic plastic strains are highly localized in PSBs while the matrix between PSBs is almost free from plastic deformation. The concentrated cyclic plastic strains in PSBs are induced by the intensive generation, movement and interaction of dislocations at the microscopic level. Extrusions and intrusions on the free surface of fatigued metals are the most striking feature of the formation of PSBs.

A micromechanic theory of fatigue crack initiation (Lin, 1991) has been proposed to model the physical mechanism of both extrusions and intrusions of PSBs in polycrystalline metals of face-centered cubic structure. A PSB in a surface crystal is represented by three thin slices of P, Q and R, where P and Q are two intensively plastically deformed layers between R and the matrix and R is sandwiched by P and Q. The plastic shear strains in P and Q, caused by the local cyclic microstress field, either push the material in R out of the free surface to form an

extrusion or suck it in to create an intrusion. This theory is supported by many experimental observations and has been applied to analyze the HCF of polycrystals.

Mecke and Blochwitz (1980) observed the subgrain displacement in a nickle single crystal fatigued under constant plastic strain amplitude at room temperature. It is found that the PSBs have penetrated across the whole crystal and extruded out on both sides. Recently, Zhai et al. (Zhai, Martin and Briggs 1995 and 1996, Zhai, Martin, Briggs and Wilkinson 1996, Zhai, Briggs and Martin 1996) have shown a set of very interesting fatigue tests of aluminum single crystals under stress-controlled cyclic loadings. The specimen has two special surfaces. One is the side-surface containing the active Burgers vector. The other is the front-surface perpendicular to the side-surface and has the largest slip steps under fatigue loading. The specimen is loaded in equal cyclic tension and compression. The preferred slip system is $[0\,\bar{1}\,1](111)$. The PSBs on the front-surface are of the same size and distribution as those on the side-surface. It is found that many PSBs on the side-surface are concave.

In this paper, we extend the model of polycrystal fatigue crack initiation (Lin, 1991) to the case of an aluminum single crystal under a stress-controlled cyclic loadings of equal amplitudes of tension and compression. The microscopic deformations of PSBs on both front and side surfaces are quantitatively analyzed. The correlation of hysteresis loops with the microstress field in the PSBs is presented. In the following, we first briefly review the theory of fatigue crack initiation. Then, the numerical calculation of microstress field by the boundary element method for an elasto-plastic three-dimensional body is presented. The gating mechanism of P, Q and R is applied to the single crystal. Finally, the numerical results of surface profiles of PSBs on both front and side surfaces are compared with the test observations, and hysteresis loops are computed and presented.

2. MICROMECHANIC THEORY OF FATIGUE CRACK INITIATION

In this section, we will briefly review the fundamentals of micromechanic theory of fatigue crack initiation (Lin, 1991), which constitute the basis of the present study.

2.1. Gating mechanism provided by microstress field

The extrusions and intrusions observed on the free surface of a fatigued metal specimen are driven by the alternate microstress fields in the PSBs. To illustrate the mechanism, a PSB is modelled as a thin slice R sandwiched by two PSB-matrix interface layers P and Q, as shown in Fig. 1. A favorable distribution of initial shear stresses is positive in P and negative in Q. Under the cyclic loading, plastic shear strains are built up in both P and Q and induce an alternate residual stress field in the PSB. Since the resolved shear stress τ^a in the primary slip system due to the applied load σ_{22} is the same all over the specimen, we have

$$\tau_P^a = \tau_Q^a = \tau^a$$

where τ_P^a and τ_Q^a are the resolved shear stresses in P and Q, respectively, due to the applied load σ_{22}. The sequence of alternate microstress field, which promotes the extrusion at the free surface, is further explained as follows:

1. First Cyclic Forward Loading $(\tau^a > 0)$: P slides. The residual shear stress in P during the first forward loading $\tau_{1f}^r < 0$, where the subscript f stands for the forward loading. We have

$$\tau_P = \tau_p^i + \tau^a + \tau_{1fP}^r = \tau^c \qquad (1a)$$

$$\tau_Q = \tau_Q^i + \tau^a + \tau_{1fQ}^r > -\tau^c \tag{1b}$$

2. First Cyclic Reversed Loading ($\tau^a < 0$): Q slides and $\tau_{1rQ}^r > 0$, where the subscript r stands for the reversed loading. We have

$$\tau_P = \tau_p^i + \tau^a + \tau_{1fP}^r + \tau_{1rP}^r < \tau^c \tag{2a}$$

$$\tau_Q = \tau_Q^i + \tau^a + \tau_{1fQ}^r + \tau_{1rQ}^r = -\tau^c \tag{2b}$$

3. Second Cyclic Forward Loading ($\tau^a > 0$): P slides and $\tau_{2fP}^r < 0$. We have

$$\tau_P = \tau_p^i + \tau^a + \tau_{1fP}^r + \tau_{1rP}^r + \tau_{2fP}^r = \tau^c \tag{3a}$$

$$\tau_Q = \tau_Q^i + \tau^a + \tau_{1fQ}^r + \tau_{1rQ}^r + \tau_{2fQ}^r > -\tau^c \tag{3b}$$

4. Second Cyclic Reverse Loading ($\tau^a < 0$): Q slides and $\tau_{1rQ}^r > 0$. We have

$$\tau_P = \tau_p^i + \tau^a + \tau_{1fP}^r + \tau_{1rQ}^r + \tau_{2fP}^r + \tau_{2rQ}^r < \tau^c \tag{4a}$$

$$\tau_Q = \tau_Q^i + \tau^a + \tau_{1fP}^r + \tau_{1rQ}^r + \tau_{2fP}^r + \tau_{2rQ}^r = -\tau^c \tag{4b}$$

The critical shear stress τ^c is here assumed to be constant, i.e., there is no strain hardening or softening involved. This process is repeated for each loading cycle, and consequently provides a natural gating mechanism.

As the number of loading cycles increases, the growth of extrusion causes a tensile strain and stress in R. This tensile stress combined with other stresses may activate a secondary slip system in R. It has been demonstrated that this secondary slip significantly increases the extent of both extrusions and intrusions (Lin, Lin and Wu, 1989).

2.2. Residual stress influence coefficients

The calculation of the residual stress field induced by plastic shear strain in the most favorably oriented slip systems is essential to quantify the theory of gating mechanism. The analogy between inelastic strain and applied forces (Lin, 1968) is used to calculate the stress field caused by plastic strain in a semi-infinite solid undergoing a generalized plane strain deformation. In computation, the three slices P, Q and R are discretized into a number of elements. In each element, the plastic strain is taken either uniformly or linearly distributed. The residual stress influence coefficients, which represent the residual stress in an element caused by a unit plastic strain distribution in another element or the element itself, are derived analytically based on the close-form stress functions (Lin and Lin, 1974).

3. NUMERICAL ANALYSIS OF A FATIGUED ALUMINUM SINGLE CRYSTAL

3.1. Computational procedure

An aluminum single crystal is treated as a three-dimensional finite body in the present study. The previous approach for calculating the residual stress influence coefficients (Lin,1991) is no longer suitable. We use the boundary element method to numerically compute these coefficients. The rationale of using the boundary element method instead of the widely used finite element method is that the stress components at an interior point of the body are solely determined by the boundary displacement and traction, and the plastic strains in the PSBs. Since the thickness of a PSB is extremely thin in comparison with the dimension of the single crystal, the computation of stresses at points in a PSB by the finite element method either requires excessive refinement of the finite element mesh in both the band and its neighboring area, or

sacrifices the numerical accuracy by using the interpolation and extrapolation based on a coarse mesh.

From the Maxwell-Betti reciprocity theorem or Somigliana equation (Brebbia and Dominguez, 1989), we can derive the boundary integral equations allowing plastic strains as follows

$$C_{ij}u_j(\mathbf{x}) = \int_\Gamma u_{ij}^*(\mathbf{x},\mathbf{x}')S_j(\mathbf{x}')d\Gamma - \int_\Gamma S_{ij}^*(\mathbf{x},\mathbf{x}')u_j(\mathbf{x}')d\Gamma + \int_\Omega \sigma_{ikj}^*(\mathbf{x},\mathbf{x}')\varepsilon_{kj}^p(\mathbf{x}')d\Omega$$

where Γ is the boundary of domain Ω, ε_{kj}^p the plastic strains, the constant

$$C_{ij} = \begin{cases} \delta_{ij}, & \mathbf{x} \in \Omega \\ \delta_{ij}/2, & \mathbf{x} \in \Gamma \text{ and the boundary is smooth} \end{cases}$$

and S_j and u_j are the boundary traction and displacement, respectively. Kelvin solution u_{ij}^* and its derivatives, S_{ij}^* and σ_{ikj}^* are readily found in test books (Brebbia and Dominguez, 1989).

To compute the residual stress influence coefficients, we divide the thin slices of P, Q and R of a PSB into a number of elements in which the plastic shear strains are taken to be constant. The surfaces of the single crystal are also divided into a set of boundary elements. For a unit plastic shear strain in an element of the PSB, the algebraic equations of the discretized boundary integral equations are solved for the displacements in the boundary elements. The stresses in the elements of the PSB can be directly computed from these boundary displacements and the prescribed boundary traction.

3.2. Results of numerical analysis

The geometry of a single crystal to be analyzed is shown in Fig. 2. The specimen is taken to be of pure aluminum with a critical shear stress τ^c of 0.369 MPa (53 psi) and is loaded alternately under uniform tensile and compressive stress with magnitude of 0.9x0.369 MPa.

In the present analysis, the multiple PSBs are assumed to be 1 μm in thickness and have 5 μm spacing. The layout of these PSBs is similar to what was observed in the tests by Zhai, et al. (1995 and 1996). The average of microscopic plastic strains in the PSBs is taken as the macroscopic plastic strain. By this way, we compute the hysteresis loops.

From Eqns. (1) - (4), the development of residual stresses τ^r in a PSB depends on the distribution of the initial stresses τ^i in P and Q. Two sets of initial stresses with the same average value in each of four segments P, P', Q and Q' (Fig. 1) are considered under the same cyclic loading: one with a linearly distributed initial stress, giving the hysteresis loops as shown in Fig. 3, and the other with a uniformly distributed one, giving the hysteresis loops as shown in Fig. 4. It is seen that the one with uniform initial shear stress reaches the saturation value of cumulative plastic strain much sooner than the one with linear initial stress. The distribution of initial stresses in a specimen is generally heterogeneous. Let τ^i_{max} denote the maximum value of initial stress in a PSB. During the forward loading, when the summation of τ^i_{max} and τ^a reaches the critical shear stress τ^c in some region, this region slides and yields the plastic strain. The loading amplitude gives the microscopic elastic limit of the specimen. As the forward loading increases, more region in the PSBs slides. This gradual spreading of the sliding area makes the curved part of the stress-strain curve as shown in Fig. 3. The residual stresses in P and Q are negative, thus relieve the shear stress in P while increase the negative shear stress in Q. The negative shear stress causes Q to slide more easily in the reversed loading. This is known as the

Bauschinger effect. Further reversed loading gives the curved part of the negative stress-strain curve until the maximum reversed loading is reached. Then the forward loading gives the linear stress-strain curve followed by a curved part of the hysteresis loop until the maximum forward loading is reached. As explained before, the negative residual stress τ_P^r is built up in P and the positive residual stress τ_Q^r in Q. These residual stresses induced by the accumulated plastic shear strains tend to cancel the initial shear stresses τ^i in P and Q. As the fatigue cycles increase, the area of the hysteresis loop, which represents the strain energy dissipated in one cycle, decreases. The changes of hysteresis loop shape proceed along with the decreasing of the growth rate of extrusions at the free surface. This process continues until it reaches the saturation state where extrusion ceases to grow A similar process occurs when the uniformly distributed initial stresses are assumed. In this case, the plastic sliding spreads along the PSB more readily than the case of linear distribution. Thus it gives the sharp corners in the hysteresis loops and causes the earlier occurrence of the saturation state (Fig. 4).

The extrusion in a PSB induces a tensile stress $\tau_{\alpha\alpha}$ in R. This tensile stress, combined with the applied cyclic axial stress $\pm\sigma_{22}$, may activate a secondary slip in R. This causes R to subject to a cyclic stress with a mean static stress, thus creating extrusions and intrusions on the side-surface of the single crystal. These extrusions and intrusions have been observed on the side-surface of the fatigued aluminum single crystals at the later stage of loading cycles (Fig. 5) by Zhai, Briggs and Martin (1996). The fatigue tests also indicate that a PSB with an extrusion or intrusion on the front-surface continuously extends to the side-surface across the edge of the specimen. The present numerical analysis shows that the secondary slip in R causes the displacement on the side-surface to be inward. This may explain why the experimentally

observed PSBs on the side-surface are concave (Zhai, Briggs and Martin, 1996). In the present model, both the inward movement of a PSB on the side-surface and the extrusion on the front-surface are induced by the displacement in R. Hence, the PSBs on the side-surface are of the same size and distribution as the PSBs on the front-surface. The calculated extrusion height on the front-surface at saturation exceeds 0.7μm, which is favorably comparable with that observed by Zhai, et al. (1995 and 1996). The present theory seems to be able to explain a number of experimental observations.

4. CONCLUSIONS

The micromechanic theory of polycrystal crack initiation has been applied to the analysis of a fatigued aluminum single crystal undergoing three-dimensional elasto-plastic deformation. The microstress field due to plastic slip in the PSBs is computed by the boundary element method. The quantative modelling of extrusions on the front-surface and inward displacement on the side-surface agree with the experimental observations. The secondary slip plays an important role in the formation of PSBs. This has been proved not only by fatigue tests but also by the present analysis. The hysteresis loops of an aluminum single crystal are computed in the presence of PSBs in the specimen. It is found that both the shape of hysteresis loops and the number of cycles to reach the saturation are affected by the distribution of initial stresses in the PSBs. The linear distribution of initial stresses in PSBs gives the shape of hysteresis loops more similar to the test results than the uniform one.

ACKNOWLEDGEMENT

This research was supported by the U. S. Air Force Office of Scientific Research under Grant F49629-96-1-350.

REFERENCES

Basinski, Z. S., and Basinski, S. T., 1992, *Progress in Materials Science*, **36**, 89.

Brebbia, C. A., and Dominguez, J., 1989, *Boundary Elements, An Introduction Course* (New York: McGrawn-Hall Book Company).

Lin, T. H., 1968, *Theory of Inelastic Structures* (New York: John Wiley and Sons, Inc.).

Lin, T. H., 1991, *Advances in Applied Mechanics*, **29**, 1.

Lin, T. H., and Lin, S. R., 1974, *J. Mech. and Phys. Solids*, **22**, 177.

Lin, T. H., Lin, S. R., and Wu, X. Q., 1989, *Phil. Mag.* A, **59**, 1263.

Mecke, K., and Blochwitz, C., 1980, *Phys. Stat. Sol.*, A, **64**, K5.

Puskar, A., and Golovin, S. A., 1985, *Fatigue in Materials: Cumulative Damage Processes* (Amsterdam: Elsevier Science Publishing Company, Inc.).

Zhai, T., Martin, J. W., and Briggs, G. A. D., 1995, *Acta. Metall. Mater.* **43**, 3813.

Zhai, T., Martin, J. W., and Briggs, G. A. D., 1996, *Acta. Metall.* **44**, 1729.

Zhai, T., Martin, J. W., Briggs, G. A. D., and Wilkinson, A. J., 1996, *Acta. Metall.* **44**, 3477.

Zhai, T., Briggs, G. A. D., and Martin, J. W., 1996, *Acta. Metall.* **44**, 3489.

Fig. 1

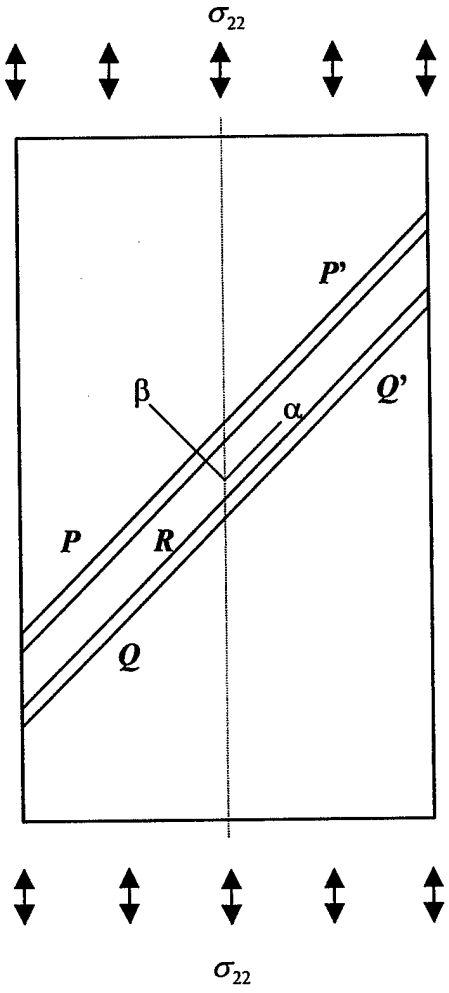

A Persistent Slip Band in a Single Crystal

Fig. 2

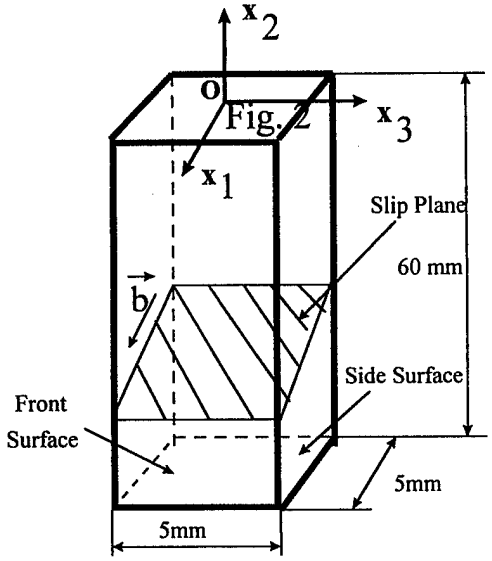

Geometry of the specimen to be analyzed

Fig. 3

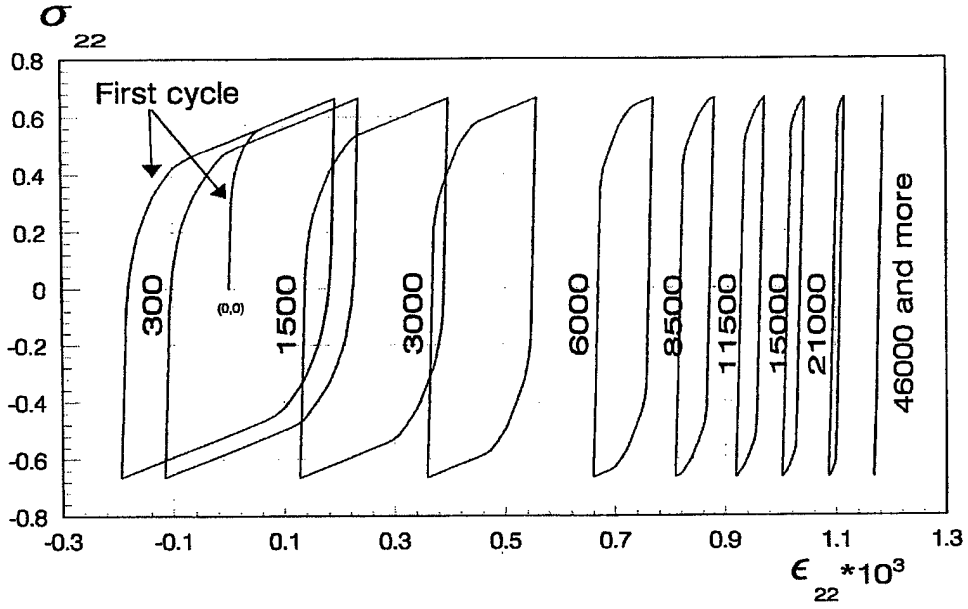

Hysteresis loops of a crystal with linearly distributed initial shear stress

Fig. 4

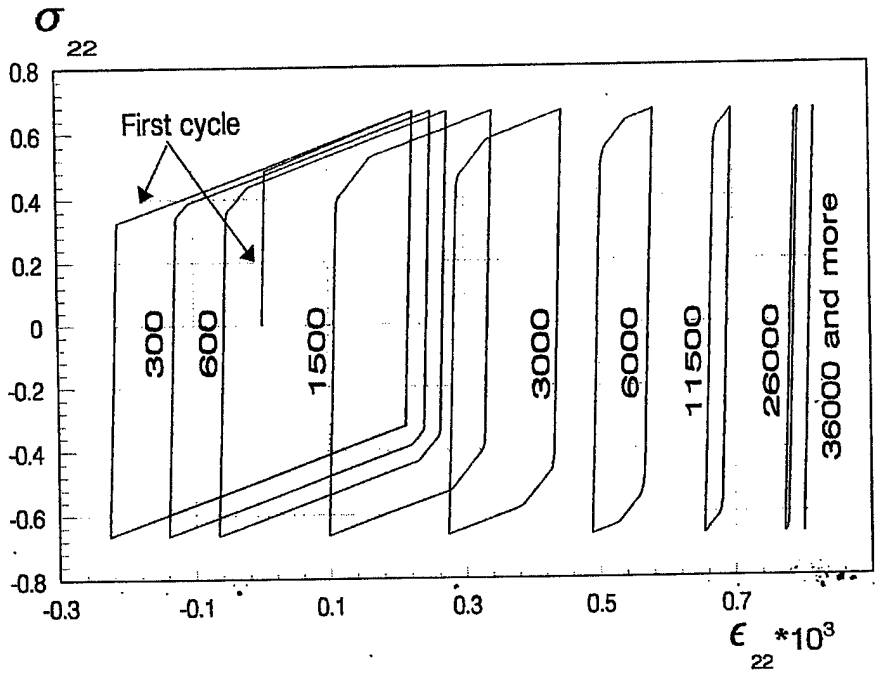

Hysteresis loops of a crystal with uniform initial shear stress

Fig. 5

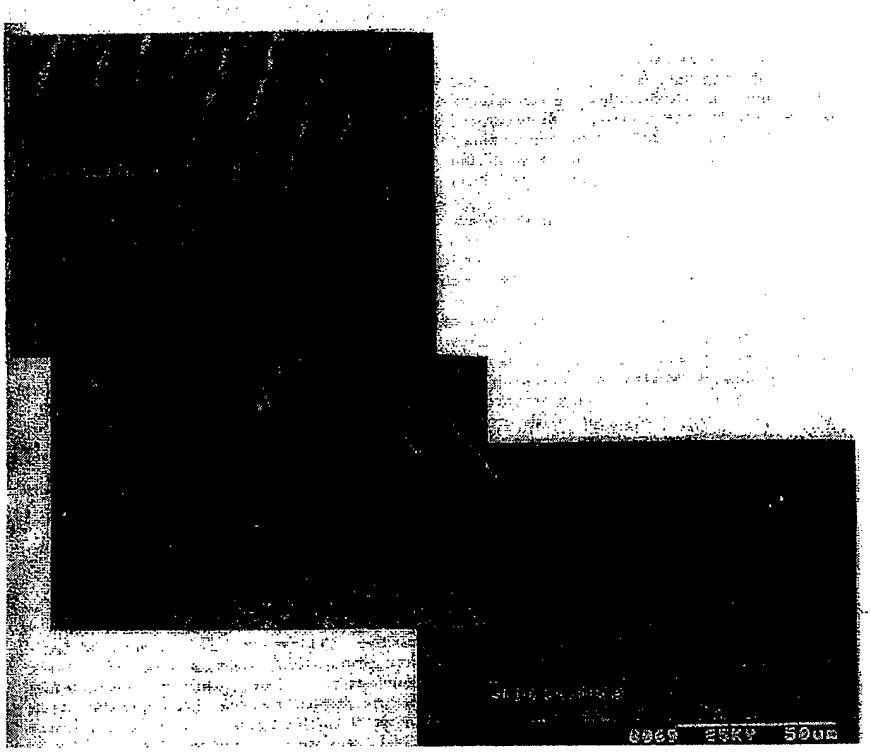

SEM micrograph showing PSBs on the front-surface and side-surface and PSBs meeting at the edge (Zhai, Briggs and Martin, 1996); reproduced from ACTA mater Vol. 44 No.9, 1996. Courtesy of Elsevier Science Ltd.